



Ruben Arnaiz Merino

Development of Railway Wheels with Alternative Materials and Production Processes

Masterarbeit zur Erlangung des akademischen Grades

Diplom-Ingenieur

Technische Universität Graz

Fakultät für Maschinenbau und Wirtschaftswissenschaften

Studienrichtung: Wirtschaftsingenieurwesen-Maschinenbau

Institut für Leichtbau



Graz, im März 2015



In Kooperation mit

Siemens AG Österreich

SIEMENS

Title

Development of Railway Wheels with Alternative Materials and Production Processes

Date

März, 2015

Author

Name: Ruben Arnaiz Merino

Registration Nr.: 1231751

Language

English

A 30 ECTS Master Thesis submitted to the completion of the degree of

Master of Science (Diplom-Ingenieur)

Production Science and Management

Educational Institution

Graz University of Technology

Faculty of Mechanical Engineering and Economic Sciences

Institute

Institute of Lightweight Structures

Thesis Supervisors:

Ass.Prof. Dipl.-Ing. Dr. techn.

Christian Moser

Graz University of Technology

DI Rubén De La Prida Caballero

Siemens AG Österreich

Division Rail Systems

**SIEMENS**

Beschluss der Curricula-Kommission für Bachelor-, Master-, und Diplomstudien vom 10.11.2008.

Genehmigung des Senates am 01.12.2008.

Deutsche Fassung:

EIDESSTATTLICHE ERKLÄRUNG

Ich erkläre an Eides statt, dass ich die vorliegende Arbeit selbstständig verfasst, andere als die angegebenen Quellen/Hilfsmittel nicht benutzt und die den benutzten Quellen wörtlich und inhaltlich entnommene Stellen als solche kenntlich gemacht habe.

Graz,

.....

(Unterschrift)

Englische Fassung:

STATUTORY DECLARATION

I declare that I have authored this thesis independently, that I have not used other than the declared sources / resources, and that I have explicitly marked all material which has been quoted either literally or by content from the used sources.

Graz,

.....

(signature)

Dedicado a mis padres, por su trabajo y confianza en mí todos estos años, y a quienes con este logro espero devolver un poco de todo lo que me han dado.

Abstract

Austempered Ductile Iron (ADI), also known as Ausferritic Ductile Iron, is the most recent addition to the ductile iron family. ADI is produced by giving conventional ductile iron a special heat treatment known as Austempering, which provides it with an excellent combination of strength and ductility, together with good fatigue and wear properties. This great combination of properties has therefore opened new horizons for cast irons to replace steel castings and forgings in many engineering applications with important cost benefits. ADI is stronger per unit weight than aluminum, as wear resistant as steel and has the potential for up to 50% cost savings.

This Thesis focuses in the railway sector, and more concretely in the underground rapid transit system of Nürnberg (Germany), where the particular properties of ADI are able to meet the demands for quieter and lighter wheels while at the same time reducing life-cycle costs. When compared to steel, ADI shows three times more damping capacity, promising in consequence a remarkable decrease in travelling noise. Regarding its maintenance, ADI is also superior to steel due to its self-lubricating behavior on the rail to wheel contact. An additional important advantage of ADI over steel is its 10% lower density, allowing this for a substantial weight reduction due to the presence of graphite nodules in the matrix structure.

Within the vehicle/bogie design, wheels play an important role in terms of carrying varying amount of loads while maintaining its dynamics, stability and noise aggravation. Over the last years, different kind of materials including ADI have been explored for wheelsets while a variety of production processes have been examined as well. This project aims to continue the optimization process by analyzing the relevance of ADI as alternative material for wheels together with production processes for the optimum safe performance of the vehicle in real service operation.

Table of Contents

1. INTRODUCTION	1
1.1. Problem Formulation.....	1
1.2. Objectives	2
1.3. Theoretical Background	2
1.4. Organization of the Thesis.....	3
1.5. Glossary	4

PART I

THE MATERIAL – LITERATURE REVIEW

2. OVERVIEW TO CAST IRONS	6
2.1. Introduction to Cast Irons	6
2.2. Microstructural Constituents.....	9
2.3. Types of Cast Iron.....	11
2.3.1. Grey Iron.....	11
2.3.2. White Iron.....	12
2.3.3. Mottled Iron	13
2.3.4. Malleable Iron.....	13
2.3.5. Ductile Iron.....	14
2.3.6. Compacted Graphite Iron	16
3. AUSTEMPERED DUCTILE IRON (ADI)	17
3.1. Introduction.....	17
3.2. Standards of ADI.....	18
3.3. Performance Properties of ADI	21
4. THE PRODUCTION OF ADI	23
4.1. Introduction.....	23
4.2. Previous Considerations	23
4.2.1. Nodule Count and Nodularity	24

4.2.2. Casting Quality	24
4.2.3. Carbon Equivalent.....	25
4.2.4. Chemical Composition	25
4.3. The Austempering Process	25
4.3.1. Austenitizing Temperature and Time.....	26
4.3.2. Cooling to the Austempering Temperature (Quenching).....	27
4.3.3. Choice of Austempering temperature and Time	28
5. DYNAMIC PROPERTIES OF ADI.....	29
5.1. Wear Resistance.....	29
5.1.1. Introduction to Wear	29
5.1.2. Background.....	30
5.1.3. Wear Behavior of ADI	31
5.1.4. Improving ADI Wear	32
5.1.5. Galling in ADI	33
5.2. Fatigue Strength.....	34
5.2.1. Introduction to Fatigue	34
5.2.2. High Cycle Fatigue (HCF) versus Low Cycle Fatigue (LCF).....	41
5.2.3. High Cycle Fatigue of ADI.....	42
5.2.4. Fatigue crack growth in ADI	47
5.3. Fracture Toughness	49
5.3.1. Introduction to Fracture Toughness	49
5.3.2. ADI Toughness	49
6. OTHER PROPERTIES OF ADI.....	51
6.1. Damping and Noise Reduction	51
6.1.1. Introduction.....	51
6.1.2. Damping Capacity of ADI.....	52
6.1.3. Noise evaluation in ADI.....	53
6.1.4 Damping evaluation in ADI.....	53
6.2. Density.....	55
6.3. Corrosion Resistance.....	56
6.3.1. Introduction.....	56
6.3.2. Corrosion in ADI	56

6.4. Environmental Assisted Embrittlement (EAE).....	57
6.4.1. Introduction.....	57
6.4.2. Background.....	57
6.4.3. Environmental Assisted Embrittlement process	58
6.4.4. Protection against EAE.....	59
6.5. Operating Temperature.....	60
6.5.1. Introduction.....	60
6.5.2. Temperatures in Service	60
6.5.3. Coefficient of thermal expansion.....	61
7. MANUFACTURABILITY OF ADI AND COSTS	62
7.1. Introduction.....	62
7.2. Cost Advantages of ADI.....	62
7.3. Machinability	64
7.3.1. Introduction.....	64
7.3.2. Machining characteristics of ADI.....	64
7.3.3. Machining in North America and Europe	65
7.3.4. High volume machining	65

PART II

EXPERIMENTAL APPROACH

8. INTRODUCTION TO WHEELSETS.....	67
8.1. Introduction.....	67
8.2. Developments in the Railway Context.....	68
8.3. Design.....	68
8.3.1. Current calculation of wheels	69
8.3.2. Loads	70
8.3.3. Fatigue criteria	70
8.4. Manufacture	71
8.4.1. Wheel materials.....	71
8.5. Maintenance.....	72

9. THE MEAN STRESS EFFECT.....	74
9.1. Introduction.....	74
9.2. General description of Mean Stress Effect	75
9.3. Mean Stress Sensitivity Factor.....	77
10. NON DESTRUCTIVE TESTING OF WHEELS (NDT).....	79
10.1. Introduction.....	79
10.2. Non-destructive testing of ADI castings	79
10.3. Inspection of Rolling Surface and Tread.....	80
10.3.1. In-motion inspection of the rolling surface of the wheel	80
10.3.2. Detection and sizing of crack like defects in the tread.....	82
10.4. Wheel spoke inspection	84
10.4.1. Potential Drop Methods.....	85
11. FACTOR OF SAFETY AS DESIGN VARIABLE	89
11.1 Introduction.....	89
11.2 The Statistical Reliability-Based Factor of Safety	90
11.3 Conclusion	94
12. SUMMARY AND CONCLUSIONS	95
12.1. ADI as general alternative engineering material.....	95
12.2. ADI as potential rail wheel material.....	96
12.3. Possible problems in the ADI wheel	97
12.4. Important calculations for the ADI wheel	98
12.5. NDT In-Service inspection of the wheels.....	99
12.6. Future work.....	100

LIST OF FIGURES

LIST OF TABLES

REFERENCES

Chapter 1

1. INTRODUCTION

This Master Thesis describes the work executed at the Siemens Division of Rail Systems in Graz, Austria. This chapter provides the reader with a brief introduction of the entire thesis. Section 1.1 starts with the formulation of the problem, and after that the objectives of the thesis are defined in section 1.2. Section 1.3 continues with a theoretical background gathering some previous work on the field. Following section 1.4 presents the structure of the whole thesis and section 1.5 finally closes this introductory chapter with the glossary of terms.

1.1. Problem Formulation

Noise, is still today one of the main problems to face in all kind of railway operations. Railway noise is caused by different sources and depends directly on the operating conditions. The importance of traction noise, which includes noise from the power unit and auxiliaries, takes place when stopping, accelerating and when speeds are usually below 60 km/h ^[1]. For higher speeds above 350 km/h, aerodynamic noise, which is generated by unsteady airflow over the train, becomes dominant ^[2]. In the wide range of speeds in between, the interaction between wheel and rail induced at the wheel/rail contact is the predominant source of noise emission. This wheel/rail noise consists mainly of rolling noise, but other important types of wheel/rail noise such impact noise and curve squeal must be noted.

Nürnberg's underground in Germany, despite of being the newest underground in the country, faces at the moment serious problems regarding noise travelling. Impact noise, which is caused by irregularities of the wheel and rail running surfaces, seems to be the main cause of the noise aggravation. The most common irregularities in this case seem to be the so-called wheel flats, which basically are flat spots on the rolling surface of the wheel that have been caused by its unintentional sliding on the rail. Reasons behind such sliding may be poorly adjusted, frozen or defect brakes, or too high braking forces in relation to the available wheel/rail adhesion.

The problem of a flat spot on the wheel tread is that once formed, it triggers the so-called polygonization of the wheel. This polygonal phenomenon, which is also known as wheel corrugation or wheel periodic out-of-roundness (OOR), is nowadays still not perfectly understood and in that way further investigations are still underway ^[3].

Therefore, due to the non-homogeneous wear of the tread, wheels don't stay circular, becoming regularly or irregularly polyhedral. After this, although a wheel may continue to function even carrying a small flat or polygonal shape, it will be subjected to a cyclic impact load every time it rotates and it will generate in consequence an evident increase in noise induced by the wheel/rail interaction.

1.2. Objectives

The objectives of this Master Thesis are derived from the need of solving the current problems of noise and wheel unroundness described in previous section 1.1.

In this way, the Siemens Division of Rail Systems in Graz has been working in an especial spoke wheel design to be casted and heat treated in order to benefit from the outstanding properties of Austempered ductile iron (ADI). The lack of experience of Siemens in this material together with the particular geometry of the new wheel represents a tremendous challenge for the successful in-service operation with an optimum safe performance. In consequence, with the problem situation to face in mind, the main objectives of this Master Thesis can be summarized as follows:

- a) Conducting a depth investigation of Austempered ductile iron as a potential material for railway wheels contributing to understand the material regarding to its mechanical and major properties under different conditions.
- b) Determination of the minimum fatigue strength of the casted wheels for a safe track service according to the current standards.
- c) Definition of Non Destructive Testing methods (NDT) for the inspection of the most critical parts of the wheel once in service.

1.3. Theoretical Background

Austempered ductile cast iron (ADI) has emerged as a major engineering material in the last decade. Although the material was originally discovered in the late 1950's it has not been exploited to its full potential due to the relative slow commercialization of the Austempering process. Today, nearly 70 years after its discovery, ADI is still widely considered as a new material in most mechanical engineering designs. However, due to the extensive research made over the last years around the world, new processing techniques have shown even more opportunities for ADI to achieve superior combinations regarding strength, ductility, wear resistance, and machinability between others.

ADI offers interesting attributes for the railway industry which promise to meet the demands for quieter and lighter components, while at the same time reduce life-cycle costs. In fact rail to wheel contacts with high normal loads and a contact area of approximately 1cm^2 represent one of the highest loaded roll and slide contact conditions encountered in steel ^[4]. When compared to steel, ADI shows three times more damping capacity, 10% lower density, and a particular "self-lubricating" capability that makes it suitable as a potential new material for wheels on rolling stock.

Nevertheless, ADI as an alternative material for rail wheels is not a new topic. The National Railway from Finland (VR) already made an attempt in the application of ADI as alternative material for railway wheels ^[5]. In their experiments, they used ADI with 980N/mm^2 of minimum tensile strength and 5 % elongation for passenger train car wheels, demonstrating a remarkable 30 % reduction in life-cycle cost approximately. However, and despite of their pioneer experiments, no practical advance in ADI wheels came out from them afterwards. Main reason for that was the origination of failures in the wheel tread, as a consequence in their own opinion of a deficient manufacturing and not because of the material itself.

In view of this, the Deutsche Bahn AG in Germany through their research and technology center, conducted different rolling-wear tests with different loads on ADI wheels for their later comparison with other tests already published for conventional wheel/rail steel pairings under the same conditions ^[4].

It was clear that an ADI/steel pairing for wheel and rail had the most beneficial wear characteristics. Mass loss at higher contact forces was reduced remarkably with the ADI wheel. It was clear then that both ADI wheel and the steel track wore considerably less, concluding in this way that the lubricating effect of the graphite was missing between normal steel pairing contacts.

1.4. Organization of the Thesis

This thesis is divided into two major parts. Following this first introductory chapter starts Part I, which comprises chapters from 2 until 7, and represents the researching and literature review part for a better understanding of the material ADI as well as its major properties. Part II on the other hand comprises chapters from 8 until 11, with a primary focus on the wheel and its experimental aspects. Finally chapter 12 closes the thesis with several conclusions and insights derived from both Parts I and II. Following lists of figures, tables and references complete the report.

1.5. Glossary

ACPD	Alternative Current Potential Drop
ADI	Austempered Ductile Iron
ALC	Amplitude Locus Curve
ASTM	American Society for Testing and Materials
ATC	Automatic Train Control
BWE	Reflected Backwall Echo
CADI	Carbide Austempered Ductile Iron
CE	Carbon Content
CEN	European Committee for Standardization
CGI	Compacted Graphite Iron
DCPD	Direct Current Potential Drop
DI	Ductile Iron
DIN	German Institute for Standardization
EAE	Environmental Assisted Embrittlement
EMAT	Electromagnetic Acoustic Transducer
EN	European Standard
ERRI	European Rail Research Institute
FCC	Face Centered Cubic
FKM	Forschungskuratorium Maschinenbau
FS	Factor of Safety
GJL	Grey Cast Iron
GJM	Malleable Cast Iron
GJS	Spheroidal graphite Cast Iron
GS	Cast Steel

HBN	Hardness Brinell Number
HBW	Hardness Brinell
HCF	High Cycle Fatigue
HRC	Hardness Rockwell
HV	Hardness Vickers
IADI	Intercritically Austenitized Ductile Iron
ISI	In Service Inspection
IZFP	Fraunhofer Institute for Non destructive Testing
LCF	Low Cycle Fatigue
LCT	Low Critical Temperature
LEFM	Linear Elastic Fracture Mechanics
MADI	Machinable Austenitized Ductile Iron
NDT	Non destructive Testing
PD	Potential Drop
PF	Probability of Failure
SAE	Society of Automotive Engineers
SGI	Spheroidal Graphite Cast Iron
UCT	Upper Critical Temperature
UIC	International Union of Railways

Note

There exists mixed convention regarding the capitalization of the various forms of the words *Austenite* and *Austemper*. The *A* is rightly capitalized as the pre-fix *Aus* is a formal derivation from the name of the metallic phase *Austenite* and its principal discoverer, the British metallurgist Sir William Chandler Roberts Austen.

The same fundament applies for the various conjugations of *Bainite*, the metallurgical mixture of phases named after its discoverer, Edgar Bain, and *Martensite*, a mixture of phases which was named after the German investigator Adolph Martens.

PART I

THE MATERIAL

LITERATURE REVIEW

Chapter 2

2. OVERVIEW TO CAST IRONS

2.1. Introduction to Cast Irons

Although the focus of this work is on Austempered Ductile Iron (ADI) as a potential material for railway wheels, a brief introduction to the Cast Iron family may be useful for a better understanding of this material since ADI has directly emerged as a new member of them. Then, when we are talking about cast iron or simply just “iron” we do not refer to a single specific material, but to a family of materials whose major constituent is iron in combination with carbon and silicon (Fe-C-Si alloy) in different proportions as shown in Figure 2.1. This Fe-C-Si alloy often contains other alloying elements that confere better qualities and it can be used in the as-cast condition as well as after a proper heat treatment.

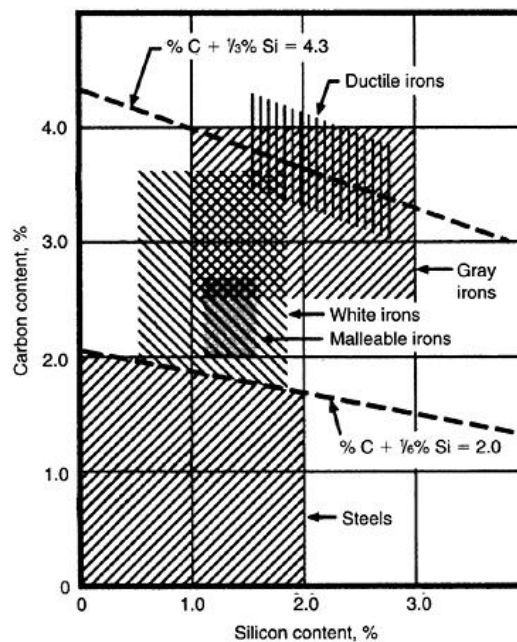


Figure 2.1– The approximate ranges of carbon and silicon for steel and various common cast irons^[6].

Main disadvantages of cast irons are their low ductility (high brittleness), and that they cannot be mechanically worked at room temperature. Furthermore, most of the cast irons are not malleable at any temperature. However, they melt easily and they can be casted into a variety of complicated shapes, being then usually machined to final dimensions. The term cast irons covers therefore a wide range of iron base materials, whose principal common feature is a relatively low melting point compared to steels. Main reason of calling them cast irons is because casting is the only suitable process for shaping such a group of alloys.

Cast irons are natural composite materials whose properties are determined by their microstructures, the stable and metastable phases formed during solidification or subsequent heat treatment ^[6]. The microstructure that a cast iron will have on solidification will be determined by two factors: *cooling rate* and *chemical composition*. An increase in the cooling rate for example decreases the tendency to form graphite while an increase in the carbon or silicon concentration in the other hand increases graphite formation. These two statements will bring us to the definition of the equivalent carbon content (*CE*) which is basically an index that indicates the combined effect of elements such as silicon and phosphorus in terms of the influence of carbon ^[7].

$$CE(\text{wt}\%) = C + \frac{(Si + P)}{3}$$

For a given cooling rate, the carbon equivalent value (*CE*) determines how close a given composition of iron is to the eutectic in the Fe-C phase diagram and in consequence how much free graphite is likely to be present ^[8].

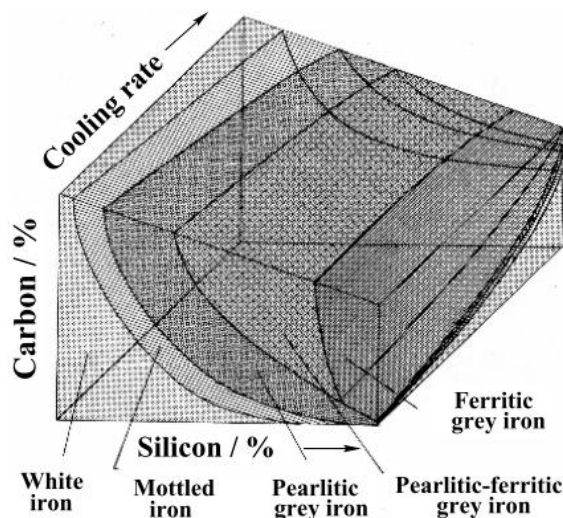


Figure 2.2 – The effect of cooling rate and chemical composition on the microstructure of cast iron ^[8].

According to this, if a cast iron has a CE sufficiently below the eutectic value, (corresponding with the point E with 4.30 wt % C on Figure 2.3) then graphite is suppressed. This can happen because of low silicon content, because of noticeable quantities of carbide-stabilizing elements, or simply if cooling rate is sufficiently rapid.

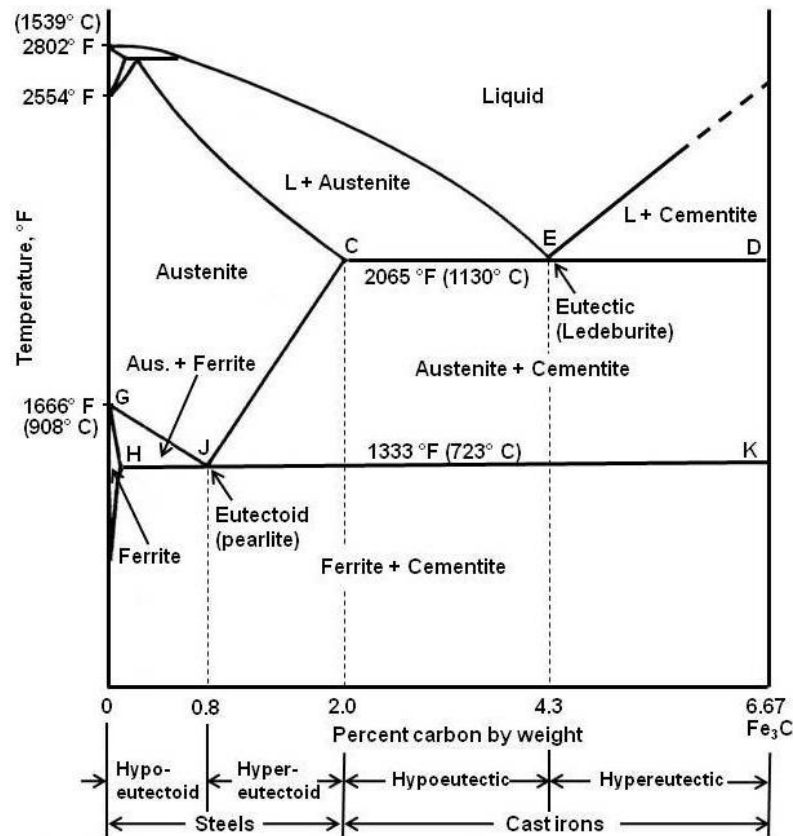


Figure 2.3 – The Iron-Carbon phase diagram. The Eutectic point indicated with “E” corresponds with a content of 4.3 wt % Carbon. (Courtesy of K.P Saha, *Practicalmaintenance*)

Plain Iron carbon alloys with carbon up to 2.11 wt % in iron are commonly known as steels and beyond that point the alloys are already considered as cast irons. As shown in Figure 1.3 before, the carbon content of cast irons can lie in between 2.11 to 6.67 wt % being the cast iron more brittle as higher the carbon content is. Nevertheless, industrial cast irons have usually carbon content in the range of 2.11% to 4.0%.

Although common cast irons are brittle as said and with lower strength in comparison with steels yet they are cheap and easy to cast. Also, by proper alloying, good foundry control, and appropriate heat treatment, their properties may vary over a wide range making them suitable for multiple applications.

2.2. Microstructural Constituents

The microstructural constituents of cast irons are basically two. Firstly the chemical and morphological forms taken by carbon, and secondly the continuous metal matrix in which the carbon and/or carbide are dispersed. The following important microstructural components are found in cast irons and must be well understood in order to fully understand microstructures ^[6]:

Graphite — this is the stable form of pure carbon in cast iron. Important physical properties of graphite are low density, low hardness and high thermal conductivity and lubricity. Graphite shape, which can range from flake to spherical, plays a significant role in determining the mechanical properties of cast irons. Figure 2.4 shows that the interconnected network of graphite flakes makes the alloy more brittle and acting like *cracks* in the iron matrix. On the other hand, Figure 2.5 shows that with the addition of inoculants, the graphite grows in spherical shapes that act like *crack arresters*, increasing the toughness of the alloy because graphite is no longer interconnected.

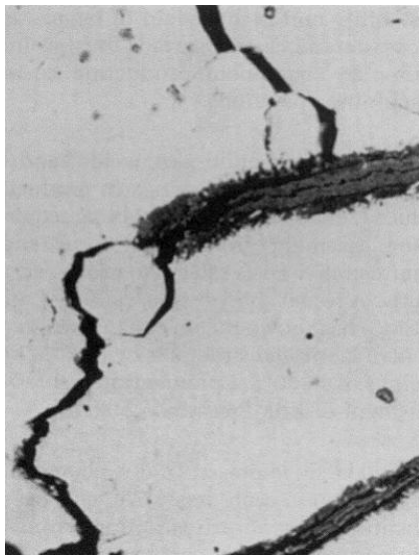


Figure 2.4 - Micrograph of Grey Iron showing the crack-like behavior of the graphite flakes ^[6].

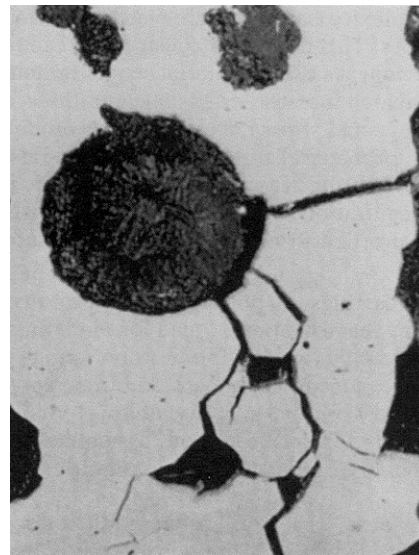


Figure 2.5 - Micrograph of a ductile iron showing the graphite spheroids acting as "crack-arresters" ^[6].

Carbide — iron carbide, also known as cementite (Fe_3C), is an extremely hard, brittle compound of carbon with either iron or strong carbide forming elements, such as chromium, vanadium or molybdenum. Massive carbides increase the wear resistance of cast iron, but make it brittle and very difficult to machine. Dispersed carbides in either lamellar or spherical forms play an important role in providing strength and wear resistance in as-cast pearlitic and heat-treated irons.

Ferrite — this is the purest iron phase in a cast iron. In conventional Ductile iron ferrite produces lower strength and hardness, but high ductility and toughness. In Austempered Ductile Iron (ADI), extremely fine-grained acicular ferrite provides an exceptional combination of high strength with good ductility and toughness. Acicular ferrite is formed in the interior of the original Austenitic grains by direct nucleation on the inclusions, resulting in randomly oriented short ferrite needles with a 'basket weave' appearance. Acicular ferrite is also characterized by high angle boundaries between the ferrite grains. This further reduces the chance of cleavage, because these boundaries impede crack propagation.

Pearlite — produced by a eutectoid reaction, is an intimate mixture of lamellar cementite in a matrix of ferrite. It is a common constituent of cast irons providing a combination of higher strength with a corresponding reduction in ductility. Bainite is a similar structure with lamellae much smaller than the wavelength of visible light and thus lacks this pearlescent appearance. It is prepared by more rapid cooling.

Martensite — it is a supersaturated solid solution of carbon in iron produced by rapid cooling. In the untempered condition it is very hard and brittle. Martensite is normally "tempered" (heat treated to reduce its carbon content by the precipitation of carbides) to provide a controlled combination of high strength and wear resistance. Martensite is not shown in the equilibrium phase diagram of the iron-carbon system because it is not an equilibrium phase. Equilibrium phases form by slow cooling rates that allow sufficient time for diffusion, whereas Martensite is usually formed by very high cooling rates

Austenite — normally a high temperature phase consisting of carbon dissolved in iron, it can exist at room temperature in Austenitic and Austempered cast irons. In Austenitic irons, Austenite is stabilized by nickel in the range 18-36%. In Austempered irons, Austenite is produced by a combination of rapid cooling which suppresses the formation of pearlite and the supersaturation of carbon during Austempering, which depresses the start of the Austenite-to-Martensite transformation far below room temperature.

In Austenitic irons, the Austenite matrix provides ductility and toughness at all temperatures, corrosion resistance and good high temperature properties, especially under thermal cycling conditions. In Austempered Ductile Iron stabilized Austenite, in volume fractions up to 40% in lower strength grades, improves toughness and ductility and response to surface treatments such as fillet rolling.

Bainite — Bainite is a mixture of ferrite and carbide, which is produced by alloying or heat treatment. The microstructures of Martensite and bainite at first seem quite similar, which is a consequence of the two microstructures sharing many aspects of their transformation mechanisms. Bainite is an intermediate of pearlite and Martensite in terms of hardness.

2.3. Types of Cast Iron

Although the common cast irons are brittle and have lower strength than steels yet they are cheap and can be cast more readily. The cast irons also have other useful properties. Further, by proper alloying, good foundry control, and through appropriate heat treatment, the properties of cast iron may be varied over a wide range. Significant developments in foundry control have led to the production of huge tonnage of cast iron with consistent properties ^[10].

The cast irons generally contain more than 2% C and a variety of other alloying elements. They are classified by a rather simple, somewhat archaic system. They are classified by the appearance of their fracture surface, their microstructure, or their properties. Historically, there were two different cast irons: the cast iron that has a grey fracture appearance and the cast iron that has a white fracture appearance. Thus, the names grey iron and white iron evolved. Those irons that have a mixed grey and white appearance are called mottled iron. These names still apply today. Other cast irons appeared over the years and have names associated with a mechanical property, such as malleable iron and ductile iron ^[9]. More recently, compacted graphite iron and Austempered ductile iron have been introduced, being this last one the concerned of this master thesis and therefore covered in a deep way in the next chapter. This section describes the different cast irons with some of their relevant characteristics:

2.3.1. Grey Iron

It is by far the most common of all cast irons, and it is produced by slow cooling. This iron has a grey fracture appearance because it contains a high volume fraction of graphite flakes. Grey iron is sometimes identified as *FG*, which refers to the flake graphite that is present. Microstructure of a typical grey iron is shown in Figure.2.6.

The grey irons have high silicon content, because silicon (a graphitizer) promotes the formation of graphite during solidification. Grey iron has almost no ductility because of the presence of the graphite flakes. However, it is inexpensive and can be cast into complex shapes. The microstructure of grey iron results from a rather slow cooling rate in the casting process. Gray iron is a common engineering alloy because of its relatively low cost and good machinability, which results from the graphite lubricating the cut and breaking up the chips. It also has good galling and wear resistance because the graphite flakes self-lubricate. The graphite flakes provide grey iron as well with an excellent damping capacity because their ability to absorb the energy ^[12].

For this reason, grey irons are used for flywheels and other parts where their superior vibration absorbance is remarkable. It is also very used for housings where the stiffness of the component is more important than its tensile strength, such as internal combustion engine cylinder blocks, pump housings, valve bodies, electrical boxes, and decorative castings. Grey cast iron's high thermal conductivity and specific heat capacity are often exploited to make cast iron cookware and disc brake rotors ^[12].

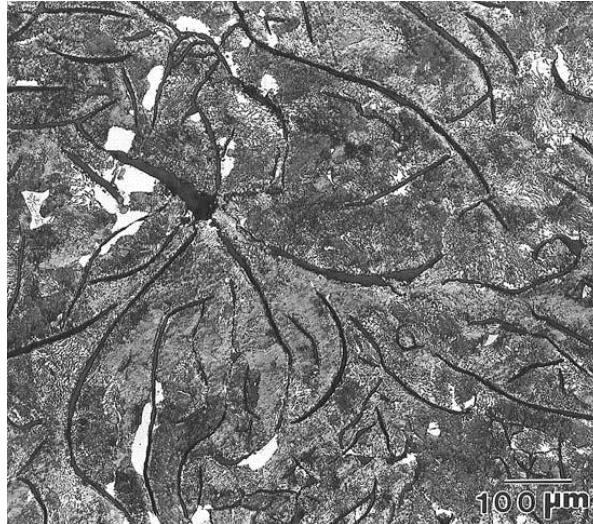


Figure 2.6- Micrograph of a grey cast iron showing a microstructure of pearlite (grey etching constituent), ferrite (light etching constituent), and graphite flakes (dark constituent). Etched in 4% picral. 100x ^[9].

2.3.2. White Iron

If a grey iron is solidified rapidly, it results in white iron. Graphite flakes are not present in white iron. White cast irons are usually made by limiting the silicon content to minimize its graphitizing effect so that no graphite is present and all of the carbon exists as cementite (Fe_3C). The name white refers to the bright appearance of the fracture surfaces when a piece of the iron is broken in two. White irons are too hard to be machined and must be ground to shape. The microstructure of a typical white iron is shown in Figure 2.7 below.

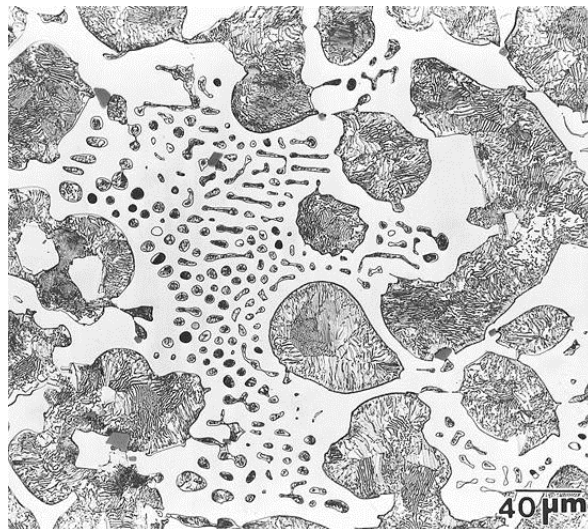


Figure 2.7 - Micrograph of a white cast iron showing a microstructure of pearlite (grey etching constituent), cementite (light etching constituent), and ledeburite (rounded clusters regions). Etched 4% picral. 250x ^[9].

Since white irons are extremely hard and abrasion resistant, they are commonly used for parts like brake shoes and crushers. To enhance their abrasion resistance, they are usually alloyed with nickel, chromium, and/or molybdenum.

2.3.3. Mottled Iron

This type of cast iron is not intentionally produced. It results from a transition between grey and white iron in a casting and is not necessarily a desirable material. The microstructure of a mottled iron is shown in Figure 2.8.

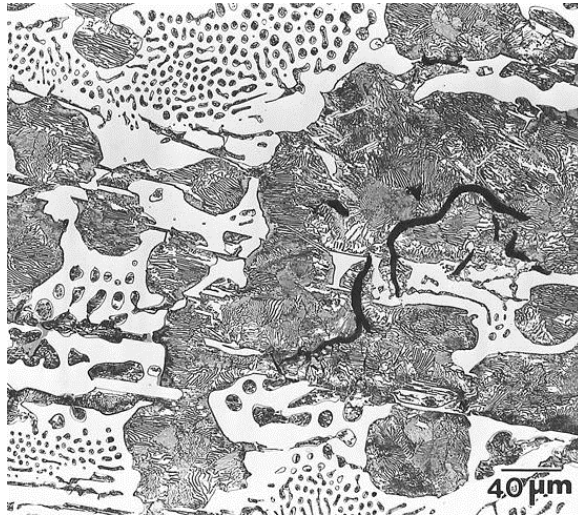


Figure 2.8 - Micrograph of a mottled cast iron showing pearlite microstructure (dark grey etching constituent), cementite (light etching constituent), ledeburite (clusters of small, rounded pearlite particles), and graphite flakes (dark constituent). Etched in 4% picral. 250x ^[9].

2.3.4. Malleable Iron

Malleable iron is produced by heat treating white iron to break down or decompose the iron carbide into a temper carbon (a form of graphite). Malleable iron is sometimes referred to as *TG* iron because of the temper graphite present. Usually, white iron is heated to 800 to 970 °C for long periods of time, on the order of 20 h. During this time, irregularly shaped nodules of graphite form. Because of the absence of the hard and brittle carbide constituent, the iron becomes malleable. Unlike most cast irons, malleable cast irons can be machined. A wide range of mechanical properties can be obtained in malleable iron by controlling the matrix structure around the graphite. Pearlitic and Martensitic matrices are obtained both by rapid cooling through the critical temperature and with alloy additions. Malleable irons containing some combined carbons in the matrix are often referred to as pearlitic malleable, although the microstructure may be Martensitic or spheroidized pearlite. Among their applications, malleable cast irons are used to make railroad and agricultural equipment. The microstructure of a typical malleable iron is shown in Figure 2.9.

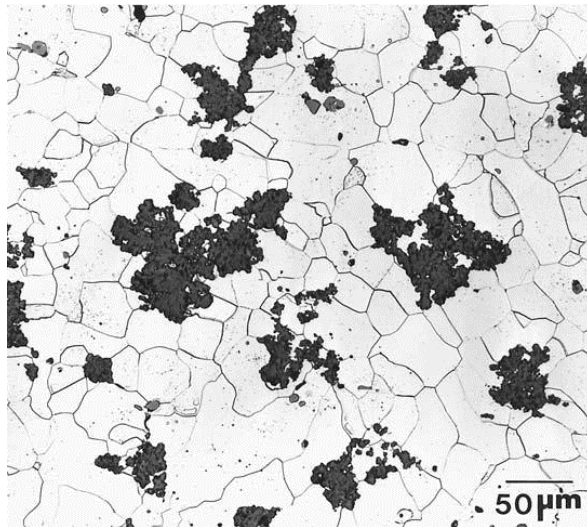


Figure 2.9 - Micrograph of malleable cast iron showing a microstructure consisting of ferrite (light etching constituent) and temper carbon (dark grey irregular-shaped constituent). Etched 2% nital 200x ^[9].

2.3.5. Ductile Iron

Ductile iron, also known as nodular iron and spheroidal graphite cast iron, is a cast iron where the graphite is in the form of spheres or nodules. The nodules are not as irregularly shaped as in malleable iron and are formed during solidification, not by heat treatment. The code SG is sometimes used to refer to the spheroidal graphite that is present in ductile iron. Common standards listing for ductile iron are DIN EN 1563 in Europe, ASTM A536 in the U.S, SAE J434-04, and ISO 1083. Microstructure of a typical ferritic ductile iron is shown in Figure 2.10.

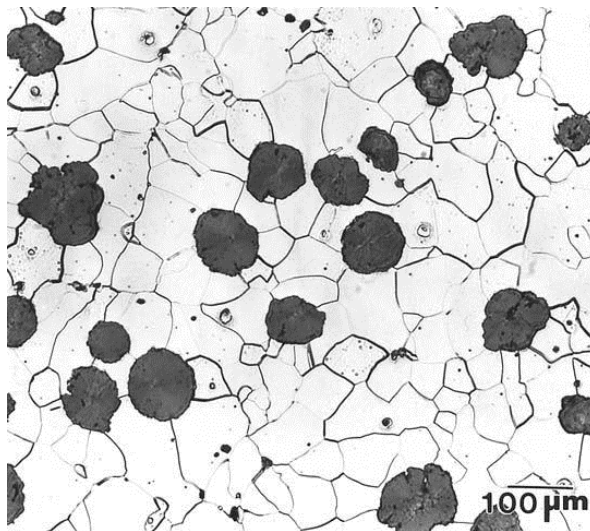


Figure 2.10 - Micrograph of a ferritic ductile (nodular) cast iron showing a microstructure consisting of ferrite (light etching constituent) and graphite nodules (dark grey constituent). Etched in 2% nital. 100x ^[9].

To produce ductile iron, a fairly high-purity cast iron is inoculated with 0.03 to 0.06% Mg or 0.005 to 0.20% Ce. These elements provide nuclei on which the graphite spheroids grow. While most varieties of cast iron are brittle, ductile irons are much more ductile and fatigue resistance due to its nodular graphite inclusions, being their wear resistance also quite good in them. Properties of ductile iron are largely dependent on the relative amounts of ferrite and pearlite within the matrix, decreasing the strength of the iron as the volume of ferrite increases. The chemical composition limits of ductile iron are given below (*wt %*) in Table 2.1.

Table 2.1 – Chemical composition limits for Ductile Irons ^[9]

Element	Content (%)
Carbon	3.0-4.0
Silicon	1.8-2.8
Manganese	0.1-1.0
Phosphorus	0.01-0.1
Sulfur	0.01-0.03

The advantages of Ductile iron which have led to its success are numerous, but they can be resumed in versatility, and higher performance with low cost. The cast irons already described, may have individual specific properties which might make them the choice for some applications, but none of them have the versatility offered by Ductile iron and that provides the designer with the best combination of overall properties.

Additionally to the important cost advantages offered by all castings, Ductile iron in comparison with steel and Malleable Iron offers also further cost savings. Like most commercial cast metals, steel and Malleable Iron decrease in volume during solidification requiring in consequence attached feeders or risers of liquid metal to offset the shrinkage and prevent the formation of defects. The formation of graphite during solidification causes an internal expansion of Ductile iron as it solidifies and as a result, it may be cast free of significant shrinkage defects either with feeders that are much smaller than those used for Malleable Iron and steel or, in the case of large castings produced in rigid molds, without the use of feeders. The reduction or elimination of feeders can only be obtained in correctly design castings. This reduced requirement for feed metal increases the productivity of Ductile iron and reduces its material and energy requirements, resulting in substantial cost savings. Furthermore, the use of the most common grades of Ductile iron *as-cast* eliminates heat treatment costs, offering an additional advantage ^[6].

Much of the world production of ductile iron is in the form of ductile iron pipe, used for water and sewer lines. Additionally, ductile irons are especially useful in many automotive components, where strength needs surpass that of aluminum but do not necessarily require the use of steel. Other major industrial applications include off-highway diesel trucks, Class 8 trucks, agricultural tractors, and oil well pumps.

2.3.6. Compacted Graphite Iron

Compacted Graphite Cast Iron (CGI), also known as Vermicular Graphite Iron, or *GGV* from the German: *Gusseisen mit Vermiculargraphit*, has a graphite shape somewhere between the flake graphite found in grey cast iron and the nodular graphite found in ductile iron. Therefore, the properties of compacted graphite cast irons are in-between those of grey and ductile iron. The amount of nodular graphite presents in *CGI* is the first measure for assessment. Therefore when nodularity increases, the strength and stiffness also increase but only at the expense of castability, machinability and thermal conductivity ^[11]. The microstructure of a typical compacted graphite iron is shown in Figure.2.11.

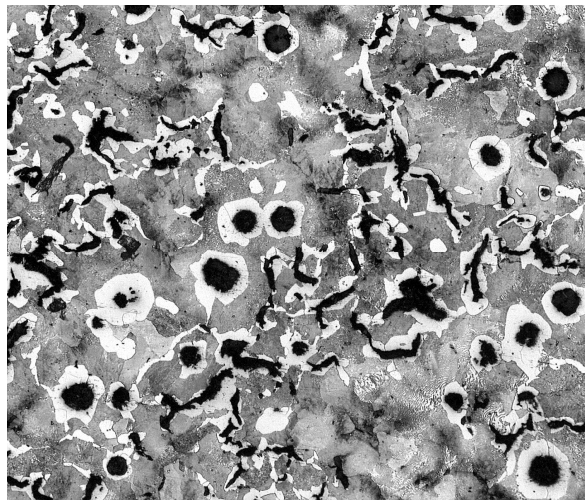


Figure 2.11 - Micrograph of Compacted Graphite Iron showing a microstructure consisting of vermicular graphite (dark flakes with rounded ends) and graphite nodules (dark islands), pearlite (grey constituent) and ferrite (light constituent). Etched in 3% nital. 100x.
Courtesy of Frank Vincentz, Own work.

Compacted graphite appears as short thick flakes, with an irregular surface and rounded edges. The iron is also referred to as *CG iron* because of the presence of compacted graphite. The worm-like shape of the graphite provides physical properties that reflect the most beneficial properties of grey and ductile irons, being this controlled by the addition of alloying elements such as magnesium, titanium, calcium, cerium, and/or aluminum.

The first commercial application for compacted graphite iron was for the brake discs in high-speed trains. Nevertheless one of the largest applications for compacted graphite cast iron is in the manufacture of ingot molds, where the mold life can be extended by 20 to 70% over the life of molds made from normal grey cast iron.

Chapter 3

3. AUSTEMPERED DUCTILE IRON (ADI)

3.1. Introduction

Austempered ductile iron is basically a subclass of ductile iron. It has same spherical or nodular graphite as normal ductile iron, but the matrix is a combination of bainite (acicular ferrite and carbides) and stabilized Austenite ^[9]. The microstructure of a typical Austempered ductile iron is shown in Figure 3.1.

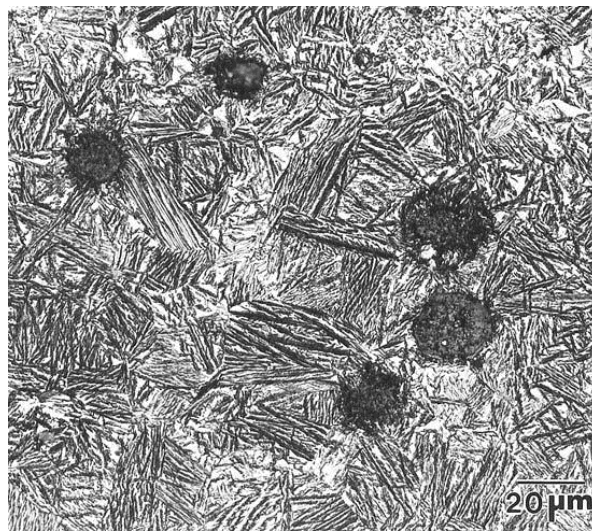


Figure 3.1 – Micrograph of an Austempered ductile cast iron showing a microstructure consisting of bainite (acicular constituent) and graphite nodules (dark grey constituent). Etched in 2% nital. 500x ^[9]

This particular microstructure is obtained by a special heat treatment called Austempering. The heat treatment involves Austenitizing, followed by a quench and an isothermal hold at a specific temperature (usually obtained by quenching into a molten salt bath). The result of this heat treatment is an excellent improvement in strength, toughness, and fatigue characteristics. ADI become stronger per unit weight than aluminum, as wear resistant as steel and has the potential for up to 50% savings ^[12].

3.2. Standards of ADI

With the development of ADI, the standards for ADI have also been published. The United States ASTM standard ^[17] was created in 1990 becoming the first ADI standard. Japan standard JIS G5503 was released five years later in 1995 and the European standard ^[16] EN 1564 followed two years later in 1997. Other relevant Standards regarding ADI are SAE J2477 ^[18] and ISO 17804 ^[19]. In the last years, the research and application of ADI has been developed rapidly in China and therefore, the Chinese standard GB/T 24733 deserves to be mention. Table 3.1 compares those standards in tensile strength (MPa), yield strength (MPa) and elongation (%) ^[20].

These standards describe the quality of iron which is adequate for Austempering, as well as the suitable uses of the different grades in multiple ways. The SAE standard as an example includes photomicrographs of the ADI grades, while the ISO standard defines varying property minimums with section size and typical monotonic, dynamic and intrinsic properties.

Table 3.1 – Comparison ADI standards (Tensile strength - Yield strength - Elongation) ^[15]

ASTM A897/A897M Issued 1990 Revised 2006	EN 1564 Issued 1997 Revised 2012	ISO 17804 Issued 2005	SAE J2477 Issued 2003 Revised 2004	China Standard GB/T24733 Issued 2009
750-500-11	800-500-10	800-500-10	750-500-11	800-500-10
900-650-09	900-600-08	900-600-08	900-650-09	900-600-08
1050-750-07	1050-700-06	1050-700-06	1050-750-07	1050-700-06
1200-850-04	1200-850-03	1200-850-03	1200-850-04	1200-850-03
1400-1100-02	1400-1100-01	1400-1100-01	1400-1100-02	1400-1100-01
1600-1300-01	-	-	1600-1300-01	-

Regarding the European Standard, concretely the DIN EN 1564, five different grades of ADI are specified by a classification based on mechanical properties measured on machined test pieces prepared from cast samples as shown in Table 3.2. United States based ASTM standard is also described more in detail in Table 3.3. The different grades of ADI represent the range in microstructure fineness that can be developed by varying the temperature during the Austempering process.

Table 3.2 – The European Standard Grades of ADI as designated by DIN EN1564:2012 at a relevant wall thickness of $t \leq 30$ mm ^[19]

Common Name	DIN EN 1564	Tensile strength R_m min (MPa)	Yield strength $R_{p0.2}$ min (MPa)	Elongation A min (%)	Typical Hardness (HBW)
ADI 800	EN-GJS-800-10	800	500	10	250-310
ADI 900	EN-GJS-900-8	900	600	8	280-340
ADI 1050	EN-GJS-1050-6	1050	700	6	320-380
ADI 1200	EN-GJS-1200-3	1200	850	3	340-420
ADI 1400	EN-GJS-1400-1	1400	1100	1	380-480

*Note 1: Selected ADI grade for the desired rail wheel application.

*Note 2: All properties are minimum requirements except hardness which is typical.

*Note 3: The relevant wall thickness does not affect the minimum Yield strength provided the heat treatment parameters and alloying are adjusted as a function of the relevant wall thickness.

Table 3.3 – The American Standard Grades of ADI as designated by ASTM A897M-06 ^[17]

Grade	ASTM A897	Tensile strength R_m min (MPa)	Yield strength $R_{p0.2}$ min (MPa)	Elongation A min (%)	Typical Hardness (HBW)
	750-500-11	750	500	11	241-302
1	900-650-09	900	650	9	269-341
2	1050-750-07	1050	750	7	302-375
3	1200-850-04	1200	850	4	341-444
4	1400-1100-02	1400	1100	2	388-477
5	1600-1300-01	1600	1300	1	402-512

*Note 1: Equivalent ADI grade in the ASTM Standard for the desired rail wheel application.

The micrographs of two different grades of ADI such 900 (*grade 1*) and 1600 (*grade 5*) are provided in Figure 3.2 and Figure 3.3 to show this mentioned range in microstructure fineness that can be obtained depending on the Austempering temperature.

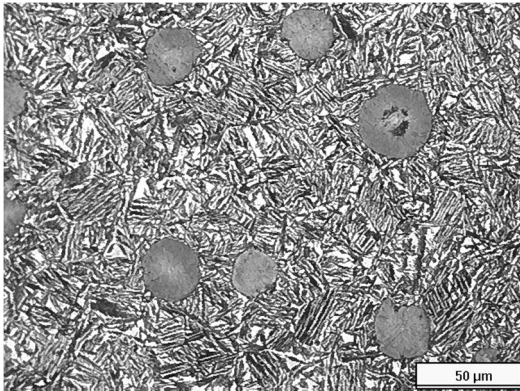


Figure 3.2 – ADI 900 with 371°C quench ^[13]

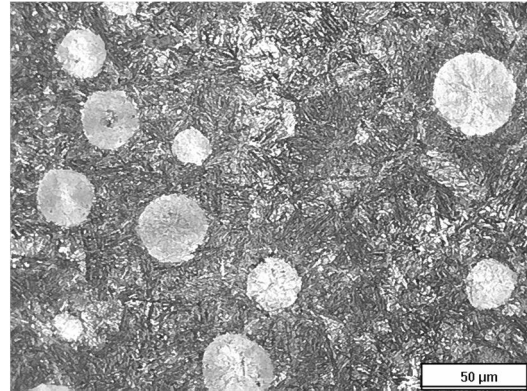


Figure 3.3 – ADI 1600 with 260°C quench ^[13]

It must be noted that ADI grades 750 and 800 are produced in a different way than the rest of grades. They have a mixed structure of proeutectoid ferrite and Ausferrite that makes heat treatment rules and hardenability relationships a little different for them. This particular mixed microstructure is achieved by heating the part to a temperature range that is between the upper critical part and the lower critical temperatures, where Austenite and ferrite are in equilibrium. Then, after the quenching and the Austempering process, the proeutectoid ferrite remains unaffected while the Austenite transforms to Ausferrite as shown in Figure 3.4.

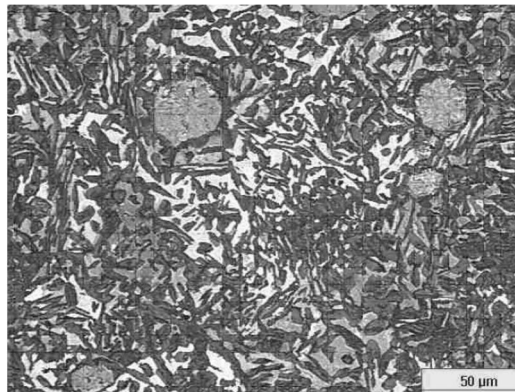


Figure 3.4 – ADI 750 showing the mixed proeutectoid ferrite (light) and Ausferrite microstructure ^[15]

This intercritically Austenitized ductile iron (IADI) was developed in 1970's in Germany ^[12] with the aim of improving the machinability of regular ADI. It became quite popular in many designs in Europe since most of the ADI parts here are completely machined after heat treatment in contrast with the North American approach of doing it before. Therefore, an ADI component requiring from an important machining and with tight tolerances can really benefit from this grade reducing significantly the post heat treatment machining cost.

3.3. Performance Properties of ADI

Manufacturers have traditionally satisfied themselves by providing mechanical engineers with those three properties easily obtainable in one test: Tensile Strength, Yield Strength, and Elongation. Those properties have been over the time well known and important to engineers since the official material standards are built on them. However, it could be considered that nowadays, properties like Tensile Strength and Elongation have become a little meaningless.

Although it is true that many interdependent property relationships related to tensile strength continue to exist, the problem is that for most design applications, if the part has already yielded (plastically deformed or elongated), then it is not useful anymore. The fact that Finite Element Analysis models do not consider either tensile strength or elongation between all their coefficients and exponents is because those models are for the design of parts that are not plastically deformed. Instead, those models include other values such as the Young Modulus for the stiffness and the Poisson's Ratio for the directional deflection. Yield Strength therefore remains useful since it is able to predict the beginning of undesired plastic deformations. Elongation is only useful in the way that provides the designer with a relative feeling about the ductility of the material.

Due to its excellent performance, ADI castings in their different grades are rapidly displacing steel forgings, welded fabrications, carburized steel, and aluminum in many applications. Important reasons for that are summed up as follows:

- *Strength comparable to steel:* Because of its equivalent strength, nearly 80% of all cast and forged steels can be replaced with some grade of ductile iron or ADI.

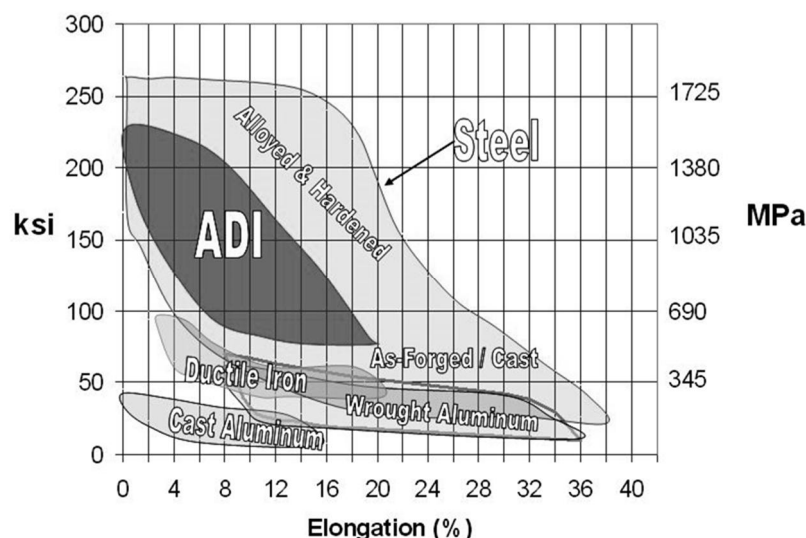


Figure 3.5 – Relationship between Yield Strength and Elongation for ADI and other common engineering materials ^[13].

From examination of Figure 3.5 then, it is clear that ADI represents a real alternative to steel for mechanical design in those applications with levels of stress above 500 MPa. Standards with minimum requirements defined in tensile strength, yield strength, elongation and hardness exist in order to make ADI design more comfortable as it was shown in point 3.2 of this chapter.

- *Lower density than steel:* The relative weight per unit of strength of ADI allows economy in design without loss of performance. For a given shape, an ADI component will be 10% lighter than steel.
- *'Lighter' than aluminum:* ADI is three times stronger than the best cast or forged aluminum and weighs only 2.5 times as much. When trying to make components lighter, the first parameter to look for is often the material density. However, the problem of low density materials is that they tend to have a very low stiffness (Young's Modulus). In the case of ADI, its density is 2.5 times that of aluminum alloys, being also twice stiffer as shown in Figure 3.6.

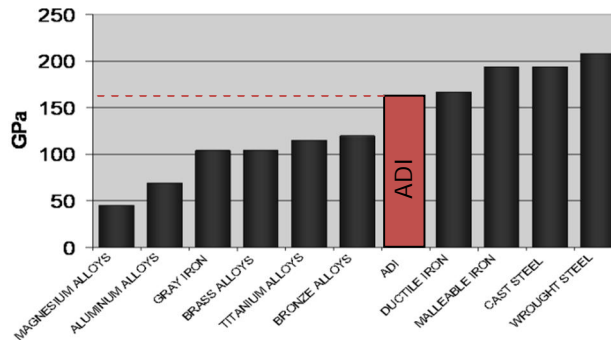


Figure 3.6 – Young's Modulus (Stiffness) for several materials. Adapted ^[14].

- *Excellent fatigue strength:* ADI's dynamic properties exceed those of forged, cast and micro alloyed steels. On the contrary to aluminum, ADI's endurance limit remains nearly constant after tens of millions of cycles. A deeper study on fatigue strength is considered in point 5.2 of Chapter 5.
- *Improved noise damping:* The presence of graphite in the ADI matrix improves noise damping, for quieter, smoother running components. The topic of damping and noise reduction is deeper covered in point 6.1 of Chapter 6.
- *Superior wear and abrasion resistance:* ADI's abrasion resistance exceeds that of conventionally processed steels and irons at a lower 'bulk' hardness level. In contrast to carburized steel, which loses wear resistance as the carburized layer is removed, ADI improves in service. ADI wear resistance is superior to steel at any given hardness level, becoming excellent on high abrasion applications. The topic of wear resistance is covered more in detail in point 5.1 of Chapter 5.

Chapter 4

4. THE PRODUCTION OF ADI

4.1. Introduction

The Austempering heat treatment process was first developed ^[20] and applied to steels in the 1930's. This consists of heating a material into the Austenite phase field and then quenching it to a lower temperature (the Austempering temperature) and holding at this temperature to allow the Austenite to transform isothermally to an acicular ferrite phase containing carbides known as Bainite.

Early trials to Austempered ductile iron were undertaken ^[21] in the 1950's, soon after the development of ductile iron. Although further development continued during the 1960's by various companies, it was not until the middle 1970's when a significant commercial production started around the world ^[22].

4.2. Previous Considerations

The production of ADI must start with the production of high quality ductile iron of an appropriate composition in the foundry. Austempering process creates a product that is stronger than conventional grades of ductile iron, but nevertheless it is not a remedy to solve the problem of a poor quality iron. Rather, the effects of the small defects on the mechanical properties of ductile iron become enlarged as a result of Austempering. Therefore, the toughness of an ADI component can be really compromised by the presence of non-metallic inclusions, carbides, shrink and dross even if their levels were acceptable for conventional ductile iron ^[23].

In this way, there is not a perfect and optimum recipe for ductile iron to be Austempered. Instead, for the purpose of Austempering, high quality ductile iron can be defined through certain parameters:

4.2.1. Nodule Count and Nodularity

- *Minimum nodule count of 100 per mm² (with a uniform distribution).*

Nodule count is extremely important when alloy additions are made. Low nodule counts lead to larger spacing between the graphite nodules and larger regions of segregation. In the worst case scenario, these regions can become so heavy segregated that they do not fully transform during Austempering, resulting in the formation of low carbon Austenite or even Martensite.

- *Nodularity of 90%.*

The nodularity is defined as the percentage of graphite particles that are spheroidal or nodular in shape. While the classification of the graphite form is accomplished on the basis of the standards in comparison to reference pictures, the computer aided image analysis with specific software parameters might be applied for this material as well.

Ultrasonic velocity and sound resonance frequency are influenced by graphite structure. Their measurement, after calibration, can give information about the nodularity. However, this measurement cannot replace the metallographic examination. The level of nodularity depends not only on the manufacturing process but also on the cooling modulus of the melt. Furthermore, the graphite form in the surface rim is affected by the contact with the mould:

The nodule roundness marks only one aspect of the material. Further parameters influencing the material qualities are, among others, the number of graphite particles and their distribution, the matrix or the micro shrinkage. It is therefore not possible to define precisely the graphite structure for the various grades and thicknesses. However, a level of nodularity of 90% or more generally ensures (more than enough for $R_{p0,2}$) the minimum tensile properties appearing in the standards ^[16].

4.2.2. Casting Quality

Castings to be Austempered should be free of non-metallic inclusions, carbides, shrink and porosity in order to achieve the property minimums in the standards.

- Carbides + Nonmetallic inclusions → maximum 0.5%
- Porosity and/or Microshrinkage → maximum 1%

4.2.3. Carbon Equivalent

The Carbon Equivalent ($CE = \%C + 1/3 \%Si$) should be controlled to produce sound castings. General Guidelines regarding this are as follows:

Table 4.1 – Carbon Equivalent Guidelines for the Production of ADI ^[23].

Section Size	CE Range
0-13 mm	4.4-4.6
13-51 mm	4.3-4.6
Over 51mm	4.3-4.5

4.2.4. Chemical Composition

Chemical composition (or hardenability) of the iron, is extremely important in order to be successful in ADI. Hardenability refers to the ability to form Martensite or the ability to cool from the Austenitizing temperature to the Austempering temperature without forming any undesirable micro constituents such as pearlite. Because heavy sections cool more slowly, they require more hardenability or more alloy additions ^[13].

The chemical composition ranges for a component should initially be established between the foundry and the heat treater. The amount of alloy (if needed) will be a function of the alloy in the foundry's base metal, the part configuration (section size and shape) and the Austempering equipment that is used.

The alloying elements that are typically added for hardenability purposes are basically Copper (Cu), Nickel (Ni), and Molybdenum (Mo). Manganese (Mn) additions are usually not recommended because of the tendency of Mn to segregate to the regions in between the graphite nodules.

4.3. The Austempering Process

The process carried out for achieving the desired Ausferric microstructure in ductile irons is called Austempering. The complete heat treatment with the different stages is depicted in Figure 4.1 and briefly explained below. Some variations in the cycle are possible when specific properties are necessary just by adding intermediate processes.

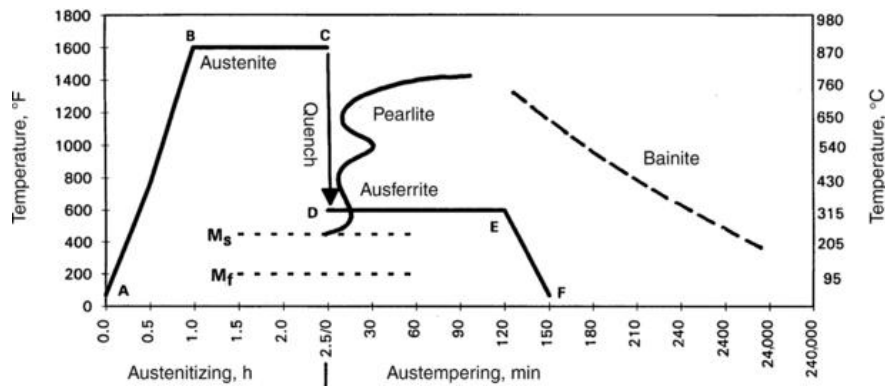


Figure 4.1–Typical Austempering cycle according to time and temperature ^[23]

1. Heating to a temperature to produce Austenite (A to B);
2. Hold at Austenitizing temperature to dissolve carbon in Austenite (B to C);
3. Quenching (cooling) rapidly to avoid the formation of pearlite or other micro constituents to a temperature above the Martensite start (M_s). (C to D)
4. Holding at the selected temperature for a time sufficient to transform the Austenite to the desired product; Bainite for steel and Ausferrite for ductile iron (D to E);
5. Cooling to room temperature (E to F).

4.3.1. Austenitizing Temperature and Time

The choice of Austenitizing temperature is dependent on the chemical composition of the ductile iron. Austenitizing temperature ranges often between 850 and 950° C and can last from 15 minutes to 2 hours approximately. Figure 3 shows a schematic of an equilibrium diagram for a graphitic ductile iron.

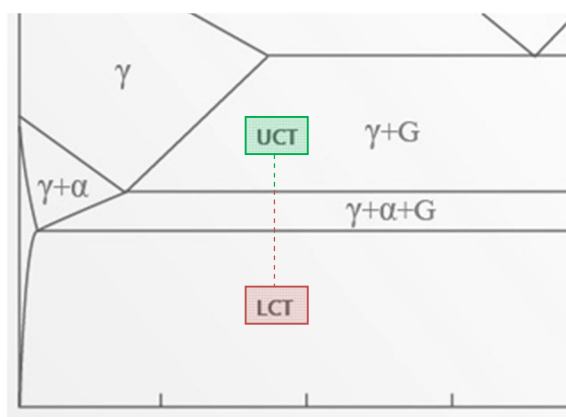


Figure 4.3 - Schematic of an equilibrium phase diagram of graphitic ductile iron. The symbols present represent Austenite (γ), ferrite (α), and graphite (G). The Upper Critical Temperature (UCT) and Low Critical Temperature (LCT) are indicated. Adapted ^[23].

The Austenitizing temperature should be chosen so that the component is in the *Austenite + graphite* ($\gamma + G$) phase field. Elements like Silicon raise the Upper Critical Temperature (UCT) while Manganese will lower it. If the Austenitizing temperature is below the UCT or in the subcritical range ($\gamma + \alpha + G$), then proeutectoid ferrite will be present in the final microstructure, resulting in a lower strength and hardness material. Once the ferrite forms, the only way to eliminate it is to reheat above the UCT.

The time at the Austenitizing temperature is equally as important as the choice of temperature. The ductile iron components should be held for a time sufficient to create an Austenite matrix that is saturated with carbon. This time is additionally affected by the alloy content of the ductile iron with heavily alloyed material taking longer to Austenitize.

4.3.2. Cooling to the Austempering Temperature (Quenching)

Cooling from the austenitizing temperature to the austempering temperature (from C to D in Figure 4.1) must be done fast enough to avoid the formation of pearlite. The main reason is that when pearlite is formed, the strength, elongation and toughness are all reduced. Figure 4.2 shows a photomicrograph of a Grade 2 ADI (1050-750-07) that contains pearlite due to improper cooling.

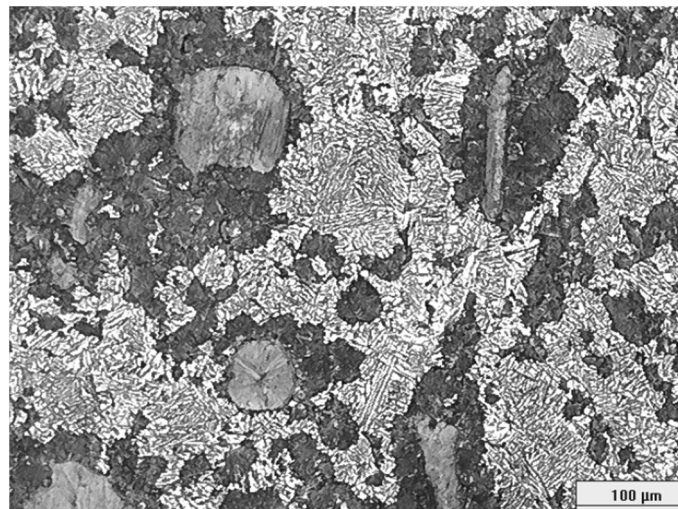


Figure 4.2 – Pearlite (dark constituent) in Ausferrite on an ADI grade 2 micrograph (1050-750-07) ^[23].

The formation of pearlite can be caused by several things, most notably a lack of quench severity or a low hardenability for the effective section size. It is possible to increase the quench severity of molten salt quench bathes by making water additions. The use of oil for quenching equipment is just used in the production of ADI Grade 5 (1600-1300-01), because of the quench temperatures needed to produce such grades.

The alloy content in ADI is necessary for hardenability purposes or the Austemperability of the ductile iron. In general, section sizes greater than 19 mm require an alloy addition. The alloying elements that are typically added for hardenability purposes include: *Copper* (Cu), *Nickel* (Ni) and *Molybdenum* (Mo). Additions of *Manganese* (Mn) are not recommended because of the tendency of this element is to segregate to the regions in between the graphite nodules. Manganese delays the Austempering reaction, which can result in the formation of Martensite due to the presence of low carbon Austenite ^[23].

Copper additions are often initially recommended because of price considerations. However, more is not necessarily better when Cu additions are considered. Levels in excess of 0.80 can create diffusion barriers around the graphite nodules and inhibit carbon diffusion during Austenitizing.

Nickel additions are made when the level of Cu has been maximized. Ni additions of up to 2 % are typically made. Beyond that, the price becomes an important consideration.

Lastly, *Molybdenum* is a potent hardenability agent. Unfortunately, it segregates highly to the intercellular/interdendritic locations between the graphite nodules. Molybdenum is strong carbide former. The formation of Mo carbides is undesirable, especially if a component is to be machined after heat treatment.

4.3.3. Choice of Austempering temperature and Time

The choice of Austempering temperature and time is dependent on the final properties desired. The typical temperature ranges are 235 - 400°C. The lower grades (1 and 2) require temperature choices at the upper end of the range while the higher grades are produced at lower quench temperatures. Time at temperature is dependent on the choice of temperature as well as the alloy content. For example, Grade 1 ADI will transform faster than Grade 5 as the quench temperature is approximately 93°C higher.

The components are held for a sufficient time at temperature for Ausferrite to form. Ausferrite consists of ferrite in a high carbon, stabilized Austenite. If held for long time periods, the high carbon Austenite will eventually undergo a transformation to Bainite, the two phase ferrite and carbide ($\alpha + \text{Fe}_3\text{C}$). In order for this transformation to occur, longer periods of time are typically needed – much longer than would be economically feasible for the production of ADI.

Once the Ausferrite has been produced, the components are cooled to room temperature. The cooling rate will not affect the final microstructure as the carbon content of the Austenite is high enough to lower the Martensite start temperature to a temperature significantly below room temperature.

Chapter 5

5. DYNAMIC PROPERTIES OF ADI

5.1. Wear Resistance

5.1.1. Introduction to Wear

Wear is related to interactions between surfaces and more specifically the removal and deformation of material on a surface as a result of mechanical action of the opposite surface^[24]. The need for relative motion between two surfaces and initial mechanical contact between asperities is an important distinction between mechanical wear compared to other processes with similar outcomes^[25].

The study of the processes of wear is part of the discipline of Tribology. The complex nature of wear has delayed its investigations and resulted in isolated studies towards specific wear mechanisms or processes^[26]. Some of them include:

- *Adhesive wear*: It can be found between surfaces during frictional contact and generally refers to unwanted displacement and attachment of wear debris and material compounds from one surface to another. Two separate mechanisms operate between the surfaces. Galling is a type of severe adhesive wear.
- *Abrasive wear*: Abrasive wear occurs when a hard rough surface slides across a softer surface^[24]. ASTM International (American Society for Testing and Materials) defines it as the loss of material due to hard particles or hard protuberances that are forced against and move along a solid surface.^[28]
- *Surface fatigue*: Surface fatigue is a process by which the surface of a material is weakened by cyclic loading, which is one type of general material fatigue. Fatigue wear is produced when the wear particles are detached by cyclic crack growth of micro cracks on the surface. These micro cracks are either superficial cracks or subsurface cracks.
- *Fretting wear*: refers to wear and sometimes corrosion damage at the asperities of contact surfaces. This damage is induced under load and in the presence of repeated relative surface motion, as induced for example by vibration.
- *Erosive wear*: Erosive wear can be described as an extremely short sliding motion and is executed within a short time interval. Erosive wear is caused by the impact of particles of solid or liquid against the surface of an object.^[27] The impacting particles gradually remove material from the surface through repeated deformations and cutting actions.^[29]

5.1.2. Background

Previous investigations have shown that ADI has a better wear resistance than cast irons [30, 31] as well as grey cast irons [29]. Such a superior wear behavior of ADI has been found to be affected by the presence of graphite nodules as well as for the ability of the retained Austenite to transform to Martensite when load is applied [33–36]. Moreover, it has been found that ADI exhibits a lower coefficient of friction and wear than those of nitride steel during dry rolling-sliding wear testing [34]. This fact is attributed to the smearing or “spread” of graphite on the contact surface, serving in that way as a solid lubricant between the two surfaces.

Following with the concept of ADI as a lubricant material in wear applications, the National Railway from Finland (VR) made an attempt in the application of ADI as alternative material for railway wheels [5]. In their experiments, they used ADI with 980N/mm^2 of minimum tensile strength and 5 % elongation for passenger train car wheels, demonstrating with it a remarkable 30 % reduction in life-cycle cost approximately. However, despite of their pioneer experiments, no practical advance in ADI wheels came out from them afterwards. Main reason for that was the origination of failures in the wheel tread as a consequence of a deficient manufacturing.

In view of this, Dr. Katrin Mädler investigated for the Deutsche Bahn AG the use of ADI as a potential material for railway wheels as well [4]. Rolling-wear tests were conducted with different loads on ADI wheels for being later compared with other tests already published for conventional wheel/rail steel pairings under the same conditions. It was clear that an ADI/steel pairing for wheel and rail had the most beneficial wear characteristics. Mass loss at higher contact forces was reduced remarkably with the ADI wheel. Mädler’s proved that both ADI wheel and the steel track wore considerably less as shown in Figure 5.1. It was concluded then that the lubricating action of the graphite was missing between normal steel pairing contacts.

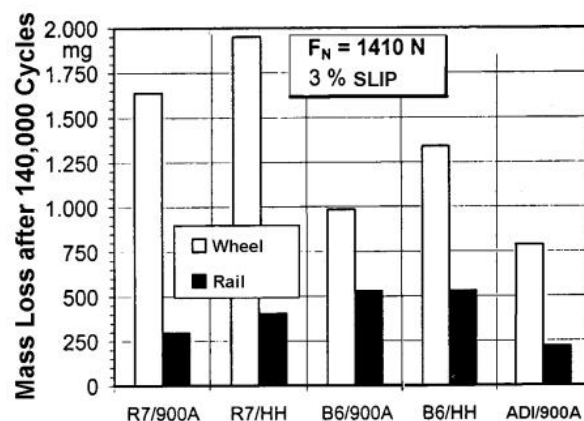


Figure 5.1 - Mass loss after 140.000 cycles for various wheel/rail material combinations. Figure shows how ADI wheel and steel track wore less than conventional steel/steel pairings in a test conducted with 1410N normal force and 3% slip [4].

A Cu, Ni and Mo alloyed ductile iron, whose Mn content was limited to 0.3% was chosen for the first test wheels. The track plates were Austenitized in an inert gas atmosphere at 910°C, quenched briefly in a salt bath operating at 220°C, then immediately transferred to a second salt bath for Austempering at 370°C.

5.1.3. Wear Behavior of ADI

The influence of different Austempering temperatures during the Austempering process can be noticed on microstructural parameters and wear behavior of ADI. During the Austempering, a variety of microstructures are obtained depending on selected heat treatment parameters such as Austenitizing time-temperature and the Austempering time-temperature.

Wear resistance is a significant mechanical property regarding all kind of designs. Good wear resistance is usually accomplished in any material by ensuring a high hardness. Low Austempering temperatures (~235-250°C) produce hard ADI grades (~480-550 HBW), which are used when good wear resistance is the main requirement [34]. On the other hand, as the Austempering temperature increases, the hardness decreases resulting in more wear.

Although the softer ADI grades have a low hardness (typically ~280-320 HBW), they contain large amounts of Austenite that when subjected to strains in service, it rapidly works harden and transform into Martensite. This effect that is a disadvantage when machining, it can be very beneficial for certain ADI components. That is because as the surface is worn away, it is continuously being replaced by a freshly formed hardened layer. Depth of such a new surface is quite superficial as shown in figure 5.2.

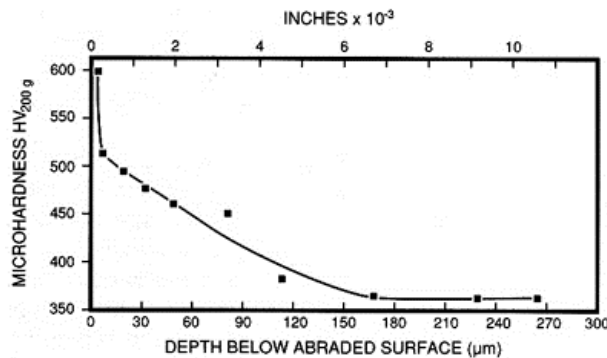


Figure 5.2 – Depth of the transformed layer in ADI after the exposure to high normal force is illustrated by an increase in micro Vickers hardness near the surface [38].

The superior wear performance when strain transformation to Martensite occurs is better depicted in the results of the so called pin abrasion testing, where a high stress abrasion environment is provided. In this way, Figure 5.3 compares the performance of ADI with other different competitive materials through this kind of test.

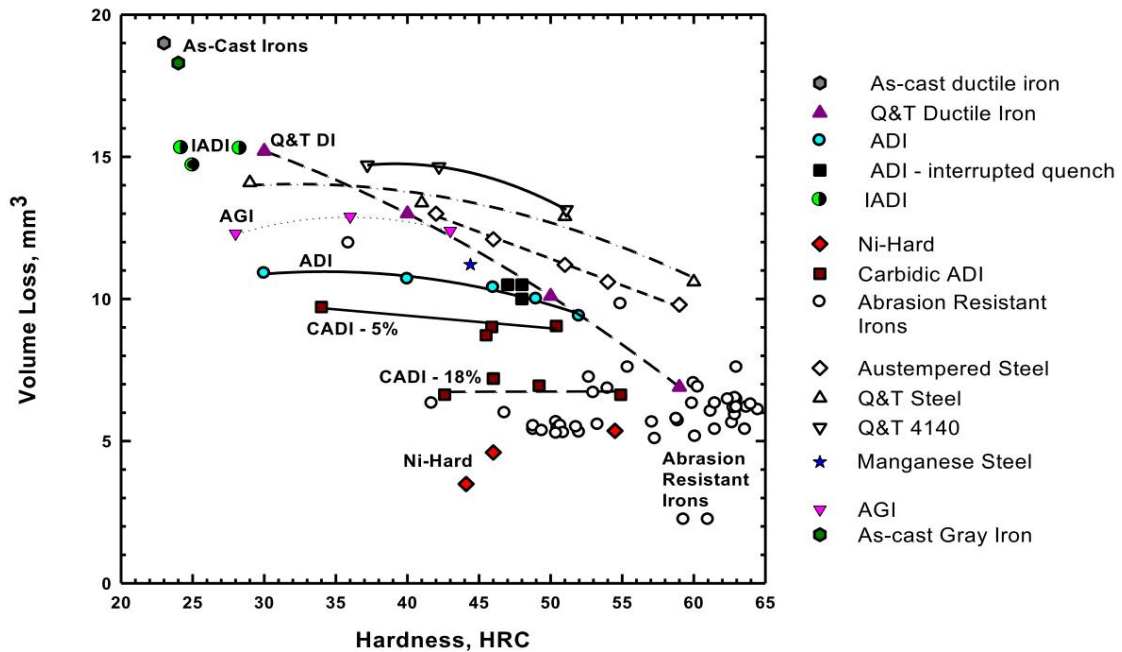


Figure 5.3 - Comparison of the pin abrasion test results for different ADI microstructures compared to competitive materials as a function of matrix hardness. Tested completed in accordance with ASTM G132-96 (2007) ^[39].

When interpreting Figure 5.3, the overall slope of the curve for each of the materials is important. When a curve is relatively flat, that means that the overall wear resistance becomes almost independent from bulk hardness. A steep slope on the other hand corresponds to a dependence of wear performance on bulk hardness or also to materials that do not undergo a strain transformation at the contact surface.

5.1.4. Improving ADI Wear

Wear performance of ADI can be improved for those applications that require from it. The controlled addition of carbides to ADI produces as a result Carbide ADI, which is more commonly known as CADI. This variant of ADI is represented in Figure 5.3 for two different percentages of carbides, becoming abrasion resistant more competitive as the percentage of carbide volume increases ^[39].

Different surface engineering techniques are usually applied to improve the surface properties by changing the microstructure or the composition of it. This can be achieved by different thermal, chemical, thermo chemical or mechanical treatments. According to this, it has been reported that after laser hardening, the surface hardness and abrasive wear resistance of nodular cast irons could be considerably improved due to a predominantly Martensitic structure produced in the hardened zone ^[32]. In the case of ADI specimens, with and without laser hardening, they showed a higher contact fatigue resistance than that of induction hardened steel ^[33].

Mechanical surface treatments like shot peening, are commonly used to improve the fatigue strength of components under fatigue loading. For the purpose of determining the effect of shot peening on the tribological behavior of Cu–Ni alloyed Austempered ductile iron, sliding wear tests were carried out^[33]. Results concluded that besides shot peening of ADI results in an increase in surface roughness and hardness, together with Austenite to Martensite transformation, no improvements concerning the sliding wear resistance were achieved.

5.1.5. Galling in ADI

Galling is a form of wear caused by adhesion between sliding surfaces. When a material galls, some of it is pulled with the contacting surface, especially if there is a large amount of force compressing the surfaces together. Galling is caused by a combination of friction and adhesion between the surfaces, followed by slipping and tearing of crystal structure beneath the surface. Galling is most commonly found in metal surfaces that are in sliding contact with each other, being especially common where there is inadequate lubrication between the surfaces. However, certain metals will generally be more prone to galling, due to the atomic structure of their crystals. For example, aluminum is a metal which will gall very easily, whereas annealed (softened) steel is slightly more resistant to galling. Steel that is fully hardened is very resistant to galling. Some initial research on galling has shown some interesting data. A step-load galling test was conducted to compare carburized and hardened, Carbo-Austempered steels together with grades of ADI 900 and 1600 as shown in Figure 5.4.

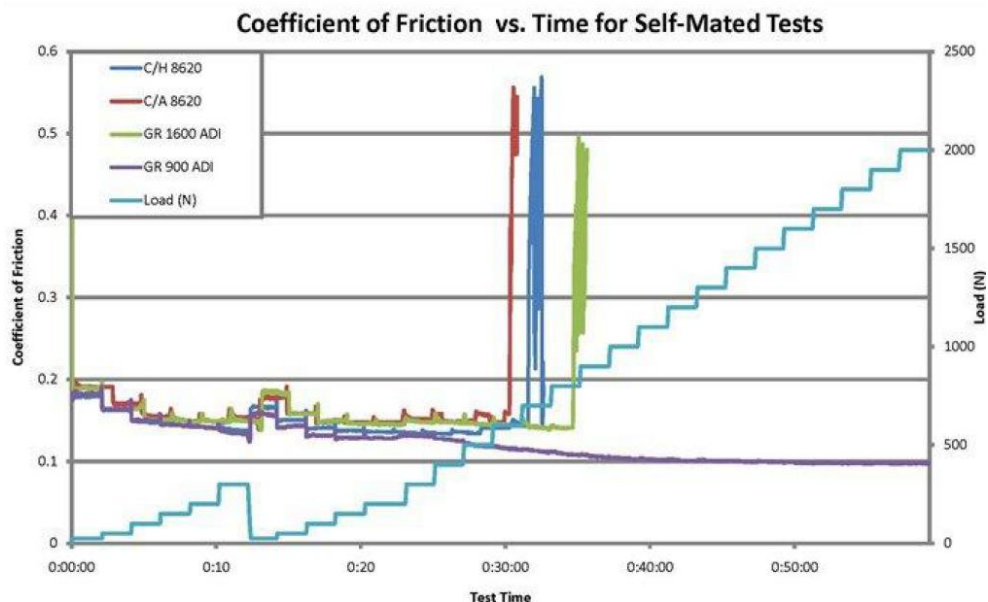


Figure 5.4 – Comparison of Carburized & Hardened and Carbo-Austempered steels to ADI 900 and ADI 1600 in a step load galling test^[15].

Conclusion from the evaluation of Figure 5.4 is that all of the materials tested with the exception of ADI 900, experienced the classic spike in coefficient of friction that denotes the onset of galling. It is hypothesized that the high Austenite content in this particular Grade of ADI facilitates this behavior.

5.2. Fatigue Strength

5.2.1. Introduction to Fatigue

Many different mechanical failure modes exist in all fields of engineering. These failures can occur in simple, complex, inexpensive, or expensive components or structures. Failure due to fatigue is multidisciplinary and is the most common cause of mechanical failure. Even though the number of mechanical failures compared to successes is minimal, the cost in lives, injuries, and dollars is too large. Proper fatigue design includes synthesis, analysis and testing are to the real product and its usage, the greater confidence in the engineering results. Applicable fatigue behavior and fatigue design principles have been formulated many years ago with Wöhler's early work. These principles have been developed, used, and tested by engineers and scientists in all disciplines and in many countries ^[40].

A standard definition ^[41] of fatigue is that is the process of progressive localized and permanent structural change occurring in a material subjected to conditions:

- that produce fluctuating stresses and strains at some point or points, and
- that may culminate in cracks or complete fracture after a sufficient number of fluctuations.

Another common definition ^[43] introduces the concepts that:

- fatigue fractures occur at fluctuating stresses with a maximum value less than the ultimate tensile strength of the material;
- fatigue failure generally occurs at loads which applied statically would produce little perceptible effect
- fatigue fractures begin as minute cracks that grow under the action of fluctuating stress.

The term “fatigue” refers to gradual degradation and eventual failure that occur under loads which vary with time, and which are, most of the time, lower than the yield strength of the specimen, component or structure concerned ^[42]. These loads are cycling in nature, but the cycles are not necessarily all of the same size or clearly discernible. A fatigue load in which individual cycles can be distinguished is usually called a cyclic load ^[42]. When a specimen is subjected to a cyclic load, a fatigue crack nucleus can be initiated on a microscopically small scale (mode I), followed by crack growth to a macroscopic size (mode II), and finally specimen failure in the last cycle of the fatigue life (mode III) ^[44].

Understanding of the fatigue mechanism is essential for considering various technical conditions which affect fatigue life and fatigue crack growth, such as the material surface quality, residual stress, and environmental influence. This knowledge is essential for the analysis of fatigue properties of an engineering structure. Fatigue prediction methods can only be evaluated if fatigue is understood as a crack initiation process followed by a crack growth period ^[44].

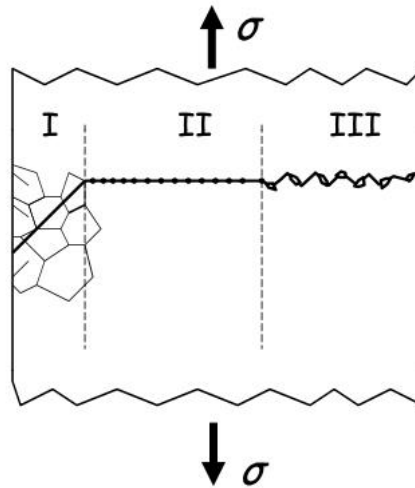


Figure 5.5– The fatigue process: crack initiation (I), crack propagation (II), unstable crack or failure (III). Adapted from M.A. Meyers & K.K. Chawla, *Mechanical Behavior of Materials*, 1st edition. Prentice-Hall, 1999, p. 607.

Constant Amplitude Fatigue Loading is that fatigue loading in which all the load cycles are identical as shown in Figure 5.6. A cycle can be defined as the smallest unit of the stress history repeating itself exactly and being often but not always sinusoidal.

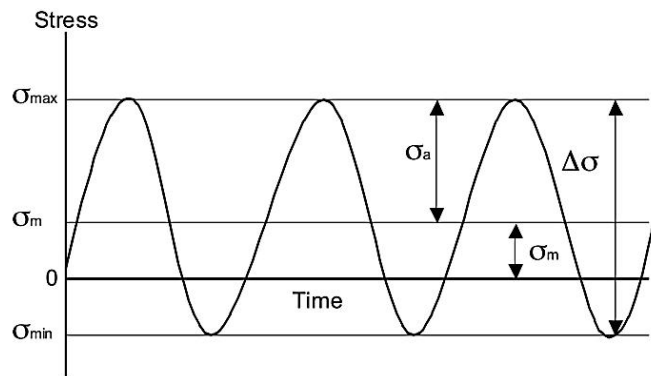


Figure 5.6 - Constant amplitude fatigue loading with identical loading cycles and relevant parameters.

Where	σ_a	is the stress amplitude.	Stress Range $\rightarrow \Delta\sigma = \sigma_{max} - \sigma_{min}$
	σ_m	is the mean stress.	Mean Stress $\rightarrow \sigma_m = \frac{\sigma_{max} + \sigma_{min}}{2}$
	σ_{max}	is the maximum cycle stress.	Stress Amplitude $\rightarrow \sigma_a = \frac{\sigma_{max} - \sigma_{min}}{2}$
	σ_{min}	is the minimum cycle stress.	Stress Ratio $\rightarrow R = \frac{\sigma_{min}}{\sigma_{max}}$
	$\sigma_{max} = \sigma_m + \sigma_a$		Amplitude Ratio $\rightarrow A = \frac{\sigma_a}{\sigma_m} = \frac{1-R}{1+R}$
	$\sigma_{min} = \sigma_m - \sigma_a$		

Fatigue results, are usually presented as S/N curves (Wöhler curves). These are plots of alternating stress versus number of cycles to failure, with an appropriate curve fitted through the individual data points (sometimes, stress range is used) ^[42].

Failure is usually defined as the separation of a specimen into two parts, but other definitions are sometimes used such as the loss of a specified amount of stiffness or the appearance of a crack of a specified size. The number of cycles to failure is sometimes called the life or the endurance. It is usually plotted on a logarithmic scale, but alternating stress may be plotted on either a linear or a logarithmic scale ^[42]. As used to be conventional (Frost et al. 1974) these S/N curves are for endurances of less than 10^8 cycles. The region where failure takes place in less than about 10^4 cycles is called low cycle fatigue, and the region for longer endurances high cycle fatigue. In some cases the tests were stopped before 10^8 cycles, when the specimens were still unbroken, and suggested that the line through the points in the S/N curves became horizontal. When it occurs, the stress corresponding to the horizontal line is called the fatigue limit ^[42].

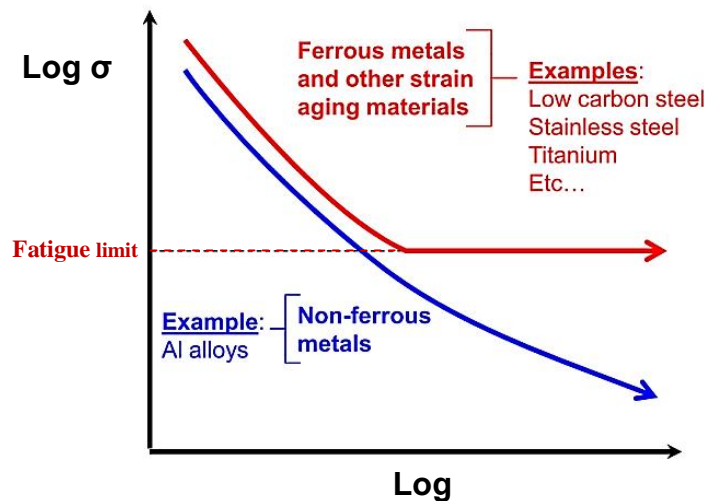


Figure 5.7 – Typical S/N curve for different materials.

The major share of the fatigue life of the component may be taken up in the propagation of crack. By applying fracture mechanics principles it is possible to predict the number of cycles spent in growing a crack to some specified length or to final failure.

The aircraft industry has led the effort to understand and predict fatigue crack growth. They have developed the safe-life or fail-safe design approach. In this method, a component is designed in a way that if a crack forms, it will not grow to a critical size between specified inspection intervals. Thus, by knowing the material growth rate characteristics and with regular inspections, a cracked component may be kept in service for an extended useful life. This concept is shown schematically in Figure 5.8.

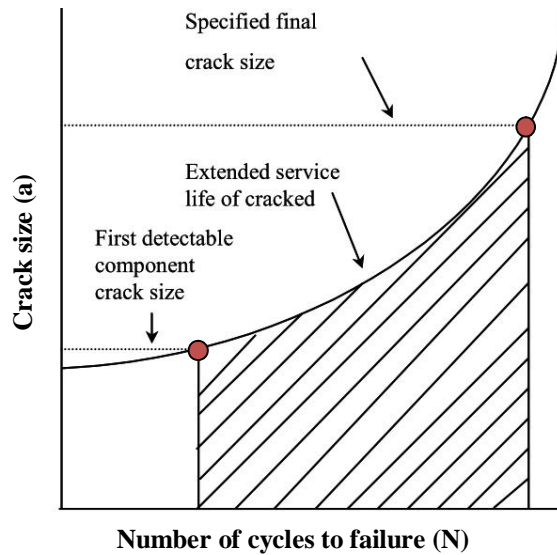


Figure 5.8 - Extended service life of a cracked component

Constant Amplitude Crack Growth

To obtain a fatigue crack growth curve, it is necessary to establish reliable fatigue crack growth rate data. Typically, a cracked test specimen is subjected to a constant amplitude cyclic load with a remote stress range given by: $\Delta\sigma = \sigma_{max} - \sigma_{min}$

Typical constant amplitude crack propagation data are shown in Figure 5.9. The crack length, a, is plotted versus the corresponding number of cycles, N, at which the crack was measured. As shown in the figure, a majority of the life of the component is spent while the crack length is relatively small.

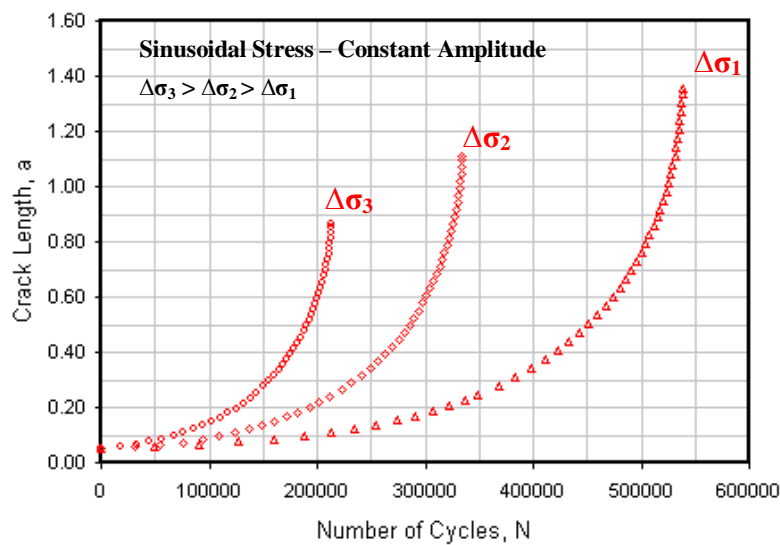


Figure 5.9 - Constant amplitude crack growth data.

Crack growth rate is defined as crack extension per cycle, da/dN . The crack growth rate is obtained by taking the slope of the crack growth curve at the crack length, a , as shown in Figure 5.10. Various crack growth rate curves can be generated by varying the magnitude of the cyclic loading and/or the size of the initial crack.

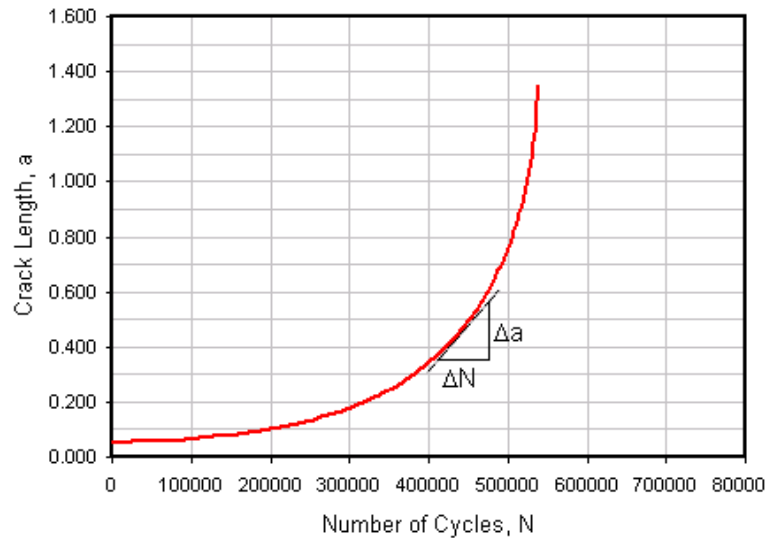


Figure 5.10 - Fatigue crack growth rate, da/dN . Courtesy of *ETBX fea-optimization*.

As shown, most of the life of the component is spent while the crack length is relatively small. In addition, the crack growth rate increases with increased applied stress.

Consider a crack that is propagating in the presence of a constant amplitude cyclic stress intensity factor ΔK . A cyclic plastic zone forms at the crack tip, and the growing crack leaves behind a plastic wake. If the plastic zone is sufficiently small that it is embedded within an elastic singularity zone, the stress intensity factor may still give a good indication of the stress environment at the crack tip. If two different cracks have the same stress environment (i.e., the same stress intensity factor), they behave in the same manner and show equal rates of growth. Under such conditions the rate of fatigue crack growth per cycle, da/dN , is governed by the stress intensity factor range:

$$\Delta K = (K_{max} - K_{min}) = \beta \cdot \Delta\sigma \cdot \sqrt{\pi a}$$

Where: $\Delta\sigma$ is the remote stress applied to the component: $\Delta\sigma = \sigma_{max} - \sigma_{min}$

β is a factor depending on geometry and loading conditions.

a is the crack length.

A stress intensity factor has the dimensions of $(stress) \times (\sqrt{length})$, being the most widely used units $MPa\sqrt{m}$. These units appear in many different standards and are therefore to be preferred.

The use of $MPa\sqrt{m}$ however, is not particularly convenient since crack sizes are normally measured in mm, and $N/mm^{3/2}$ units are often used for easier calculations.
 $1 MPa\sqrt{m} = \sqrt{1000 N/mm^{3/2}} \approx 31.62 N/mm^{3/2}$.

A plot of $\log da/dN$ versus $\log \Delta K$, a sigmoidal curve, is shown in Figure 5.11. This curve may be divided into three regions. At low stress intensities, Region I, cracking behavior is associated with threshold, ΔK_{th} , effects. In the mid-region, Region II, the curve is essentially linear. Many structures operate in this region. Finally, in the Region III, at high ΔK values, crack growth rates are extremely high and little fatigue life is involved.

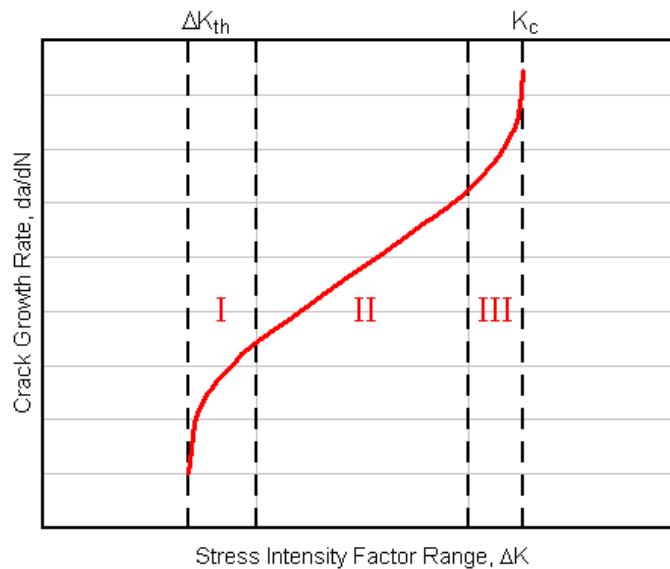


Figure 5.11 - Three regions of crack growth rate curve.
 Courtesy of ETBX fea-optimization.

Region I

At low ΔK values, crack propagation is extremely slow. Conceivably there is a threshold stress intensity value ΔK_{th} below which there is no fatigue crack growth or the growth is too small to measure. The fatigue threshold decreases with an increasing stress ratio R , where R is given by:

$$\text{Stress Ratio} \rightarrow R = \frac{\sigma_{min}}{\sigma_{max}}$$

The fatigue threshold also depends on the frequency of loading and environmental conditions. Due to the sensitivity of the fatigue threshold to the environment and load history, the best method to determine the threshold value is through testing under conditions that simulate actual service conditions. Designing a component such that the ΔK for the service conditions would be below the fatigue threshold is desirable.

Although this would ensure a low probability of fatigue failure, this is often impractical for design conditions due to either the low level of operating stress or the small crack size required. The threshold value may be useful when a component is subjected to low stress levels and a very large number of cycles. An example would be power trains that operate at very high speeds.

Region II

In the mid-region of stress intensities, the log da/dN versus log ΔK curve is essentially linear. Most structures operate in this region. Most of the current applications of linear elastic fracture mechanics (LEFM) concepts used to describe fatigue crack growth behavior are associated with Region II.

Region II is generally the largest region of the fatigue crack growth rate curve and many curve fits for this region have been suggested. The Paris and Erdogan formulation, which is commonly referred to as the Paris Equation or Paris' Law, was proposed in 1963 and is the most widely accepted. The Paris Equation is:

$$\frac{da}{dN} = C(\Delta K)^m$$

Where:

$\frac{da}{dN}$	is the rate of crack growth per cycle.
N	is the number of cycles.
C^*	is a material constant.
ΔK	is the stress intensity range $K_{\max} - K_{\min}$.
K_c	is the fracture toughness.
m^*	is an exponent representing the slope of the curve when plotting $\log(da/dN)$ against $\log(\Delta K)$ data.

*The material constants C and m can be found in literature or by performing tests (ASTM E647 sets guidelines for these tests). Values of the exponent m can range from 2.0 to 7.0 with most values being between 3.0 and 4.0.

Region III

At high stress intensities, crack growth rates are extremely high and little fatigue life is involved. Region III is characterized by rapid, unstable crack growth. The crack growth rate accelerates as the maximum stress intensity factor approaches the fracture toughness of the material. In many practical engineering situations this region may be ignored because it does not affect the total crack propagation life. The point of transition from Region II and Region III behavior is dependent on the yield strength of the material, stress intensity factor, and stress ratio.

5.2.2. High Cycle Fatigue (HCF) versus Low Cycle Fatigue (LCF)

For over hundred years, the stress-life or S-N method was the first approach used in an attempt to quantify and design by fatigue. Although the S-N approach can be used in design applications where the applied stress is primarily within the elastic range of material response, the strain-life approach is required for low cycle fatigue life predictions between 10 and 100,000 cycles ^[45].

The low cycle or strain-life approach also offers the advantage that both fatigue stress and strain are tested, analyzed, and modeled. Although high cycle fatigue only handles stress, low cycle or strain-life fatigue testing offers the opportunity for stress and strain to be calculated from each other. It is nearly impossible to measure stress with load cells in complex and moving structures, whereas strain can be readily measured with optical or strain gauge methods.

Another important difference between high and low cycle fatigue is that high cycle fatigue is strength and crack-initiation controlled where stronger materials exhibit greater fatigue lives in the high cycle range. High cycle fatigue testing commonly produces an endurance or fatigue limit (strength) at long lives (10 million cycles). The fatigue limit for p% survival is defined as the limiting value of fatigue strength for p% survival as N becomes very large (like 10 million cycles), where p may be any number, such as 95, 90, and so on ^[41]. Low cycle fatigue on the other hand considers the regime where ductility and crack propagation dominate life such that more ductile materials exhibit greater fatigue lives in the low cycle range.

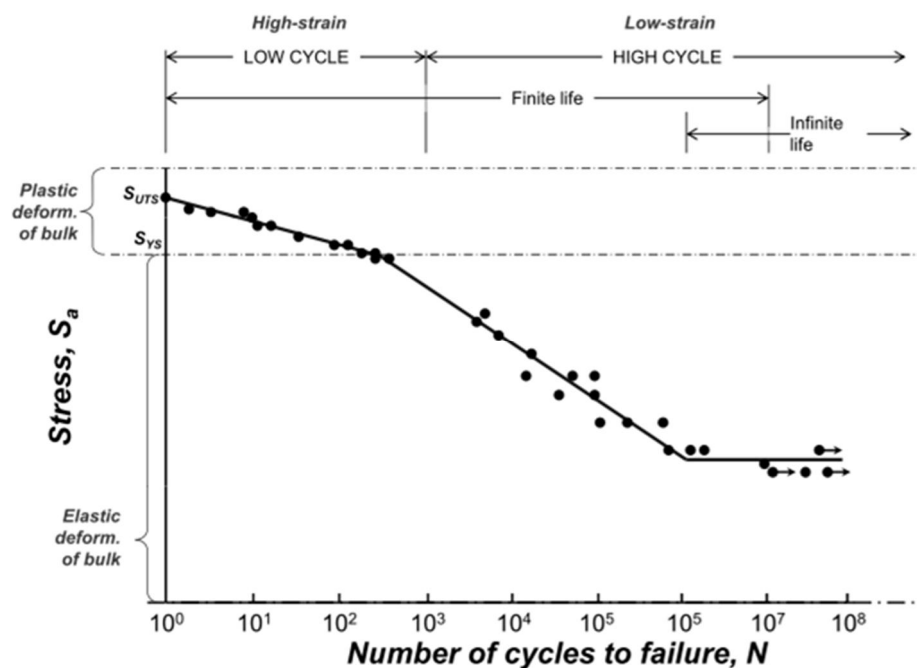


Figure 5.12 – Categories of fatigue. Adapted from J.E. Shigley, C.R. Mischke, and R.G. Budynas, *Mechanical Engineering Design, 7th Edition*, McGraw-Hill, Boston (2004), p. 314

For several reasons, bending fatigue strength has been a property that was measured historically. Now, modern designers require low cycle or strain-life fatigue properties of cast iron to populate their computer-aided design databases so that cast iron can be compared to compendia ^[46] of strain-life properties of steels and other competing materials. Strain-life fatigue properties cannot be determined in bending and must be determined axially so that the cyclic stress and strain can be related. Another important distinction is that modern fatigue databases do not contain fatigue limits, which are essentially the stresses below which materials are expected to survive fatigue. Rather, finite element modeling programs must be able to predict lives and locations of fatigue fractures in the vicinity of holes, thickness changes, and other stress concentrators.

5.2.3. High Cycle Fatigue of ADI

5.2.3.1. Introduction

The presence of large amounts of retained Austenite should lead to better wear fatigue resistance in ADI, due to the high strain-hardening nature of the Austenite. The fatigue limit of ADI is in the range of 200-500 MPa, depending always on the chemical composition, heat treatment, loading type and number of cycles defined for fatigue limit.

The fatigue limit of ADI is not proportional to the tensile strength or hardness, but is related to the toughness and retained Austenite content ^[47, 48]. Retained Austenite content is connected with the carbon content of the Austenite; the higher the carbon content the higher the retained Austenite content. Large amounts of retained Austenite are related at the same time with the creation of more barriers for fatigue crack growth and are believed they extend component fatigue life.

In contrast to all the other ferrous and non-ferrous materials, the bending fatigue strength of ADI is at maximum in the lower strength grades of the material. Additionally, most materials show an increase in fatigue strength if they undergo processes like shot peened, fillet rolled or ground. This occurs because the dislocations in the metal matrix generated by one of the already mentioned processes increase the compressive stresses at the surface. As a result, a 5-20% increase in allowable bending fatigue load is achieved. In addition to the creation of matrix dislocations during surface working, the carbon-stabilized Austenite in the Ausferrite structure undergoes a metallurgical transformation to Martensite in a ferrite “nest” ^[49]. This results in a local volumetric expansion that dramatically increases surface compressive stress and allowable fatigue load, making ADI competitive with carburized steel.

5.2.3.1. Rotary Bending Tests

In the study of Lin et al. ^[50], rotary bending tests with stress ratio $R = -1$ were conducted on four grades of Austempered Ductile iron (A, B, C and D), each one of them different in chemical composition and nodule parameters as shown in Table 5.1.

The ADI heat treatment cycle for this purpose consisted of an Austenitization in a salt bath at 900 °C for a time of 1.5-2 h and two different Austempering conditions in order to obtain different mechanical properties related to changed microstructure. The first Austempering, that generated the optimum strength (with a optimum combination of ultimate tensile strength, yield strength and hardness), took place at 300 °C. At this transformation temperature it was found that the ferrite laths were finer and closer between them. The second Austempering that generated the optimum strength (with a maximum value of impact energy), took place at 360 °C. It was at this temperature that the ferrite laths became coarser and shorter.

Table 5.1 – Chemical composition (%wt) and nodule data of the ductile irons used in Lin's fatigue study. Adapted ^[50].

		ELEMENTS	DUCTILE IRONS			
			A	B	C	D
CHEMICAL COMPOSITION	Carbon (C)	3.6	3.6	3.6	3.6	
	Silicon (Si)	2.3	2.5	2.6	2.6	
	Copper (Cu)	0.5	0.5	0.4	0.5	
	Nickel (Ni)	0.5	0.4	0.4	0.4	
	Manganese (Mn)	0.1	0.2	0.2	0.3	
	Phosphorus (P)	0.04	0.02	0.02	0.05	
	Magnesium (Mg)	0.04	0.04	0.05	0.04	
	Sulfur (S)	0.01	0.01	0.01	0.01	
	Molybdenum (Mo)	-	-	-	0.2	
NODULE DATA	Nodule count (n°/mm ²)	~ 100	~ 110	~ 150	~ 200	
	Nodule Radius (μm)	25	20	17	12	
	Nodularity (%)	~ 80	~ 90	~ 90	~ 90	

The different effects of the Austempering temperatures, nodularity, nodule count and amount of retained Austenite were discussed in Lin's study ^[50], coming up in consequence with some interesting results as shown below.

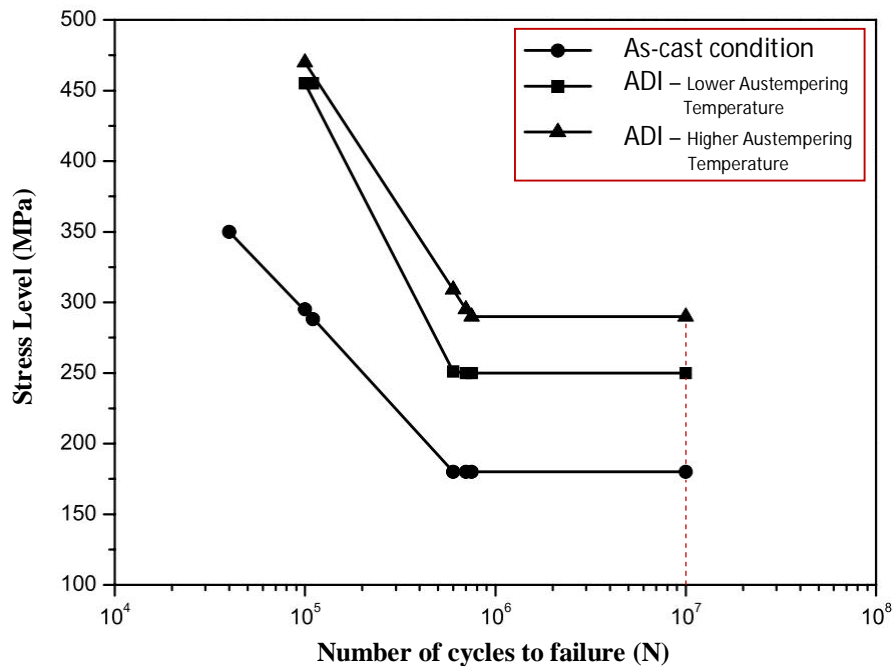


Figure 5.13 – example of S/N curves for high cycle fatigue (HCF) obtained for as-cast iron and ADI treated at two different temperatures in order to get optimum strength and toughness. Adapted ^[51].

Important to mention is that although the fatigue limit is not proportional to its tensile strength, it is related to its toughness and retained Austenite content ^[50]. In general, ADI was achieved with Austempering treatment that gave optimum toughness and larger amounts of retained Austenite, which has a better HCF performance. In addition, the fatigue ratio of ADI increased with a decrease in tensile strength but with an increase in toughness and retained Austenite content ^[50].

The high cycle fatigue strength (HCF) of ADI is increased when increasing nodularity. Results showed that a higher nodularity ($\geq 90\%$) tended to have a better HCF performance including higher fatigue limits and longer lives at stress levels above the fatigue limit. A lower nodularity on the other hand, means more non-spheroidal graphite nodules which lead to higher stress concentration factors and higher stress concentration at the graphite/matrix interface as compared to spheroidal shape. Additionally, the difference in HCF strength due to varying nodularity was enhanced when the Austempered temperature was reduced. This provided to the more severe notch effect of graphite nodules in a matrix with a higher strength and hardness formed at lower Austempering temperatures ^[50].

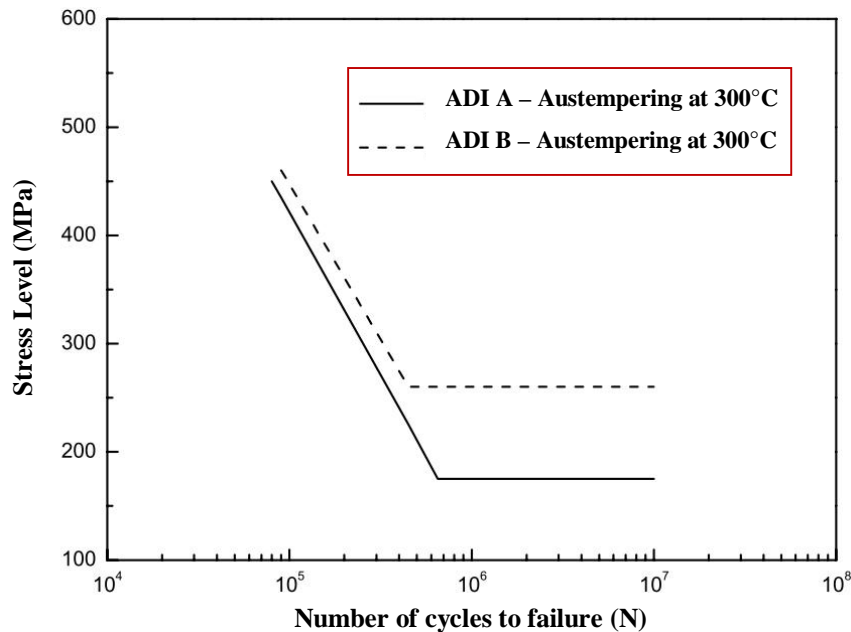


Figure 5.14 - comparison of S/N curves between irons A and B at Austempered temperature of 300 °C. Adapted ^[51].

In order to show the effect of nodularity on HCF, in Figure 5.14 the comparison between irons A and B is shown. These grades of ADI have difference in nodularity (~ 80% and ~ 90% respectively), but otherwise similar chemistries and close nodule counts. It can be observed that iron B (with higher nodularity) tended to have a better HCF performance including higher fatigue limit and a longer life at stress levels above the fatigue limit. The difference between the two HCF behaviors is not remarkable at low cycles, but it increases when the stress levels are close to the fatigue limit, where it shifts to lower value for iron with less nodularity.

The HCF resistance of ADI was improved when the nodule count increased, in particular at Austempered temperatures for optimum toughness. Therefore, ADI with a greater nodule count or a smaller nodule size exhibits a better HCF behavior. The more pronounced beneficial effect of a large nodule count on the HCF properties of ADI for the matrix structure with optimum toughness may be explained by the difference in the amounts of retained Austenite. Greater amounts of retained Austenite can create more barriers for fatigue crack growth and extend life ^[50].

The better HCF strength is suggested not to be attributed exclusively to the advantage of greater nodule count because this improvement was lost in LCF behavior ^[50, 52]. It has therefore probably to do with the volume fraction, size and distribution of retained Austenite in the matrix. It can be attributed also to the larger amounts of retained Austenite and to a greater fraction of retained Austenite in low concentration of carbon ^[50].

This low carbon Austenite is more likely to transform to Martensite under plastic deformation (the so-called *Stress Induced Martensitic Transformation*) than carbon-enriched stable Austenite, obtaining as a result a greater fatigue crack growth resistance. The amounts of retained Austenite increased with increasing the Austempering temperature so a larger fraction of retained Austenite would undergo martensitic transformation under plastic deformation. Stress induced Martensitic transformation of Austenite occurred locally in the plastic zone ahead of the crack so as to relax the stress concentration at the crack tip. The accompanying volume change also encouraged plastically induced crack closure to occur, reducing the fatigue crack growth rate and increasing fracture toughness^[50].

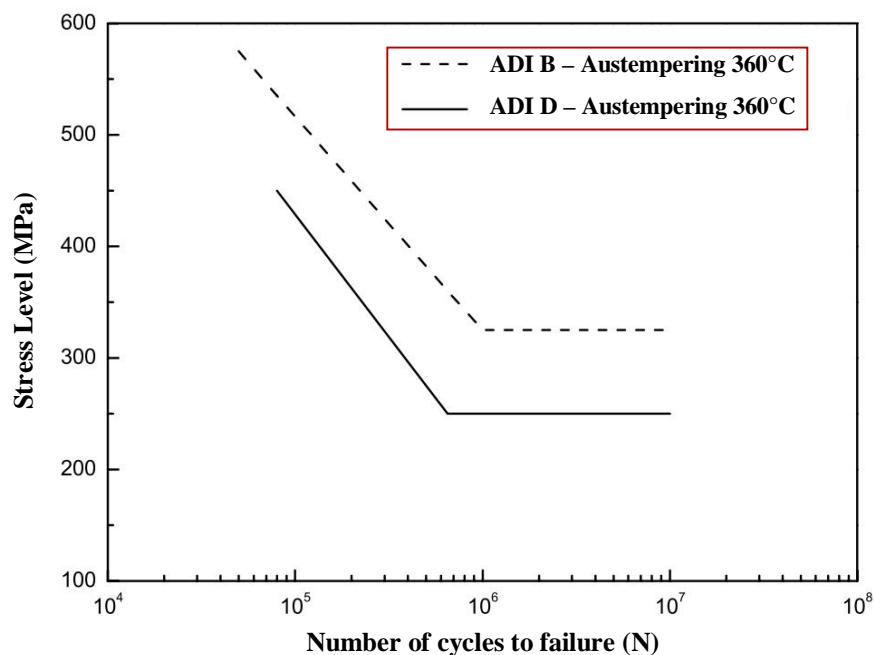


Figure 5.15: comparison of S/N curves between ductile irons B and D at Austempered temperature of 360 °C. Adapted^[51].

Figure 5.15 represents the different behavior between ductile iron B and D. The chemical composition of iron D is close to that of iron B except for the exceptional addition of 0.2% of Mo and a slightly higher amount of Mn. Regarding nodule count, iron D has 200 nodules/mm⁻² versus the 110 nodules/mm⁻² of iron B, being the amount of retained Austenite also higher in iron D. The better HCF strength of iron B over D is not only attributed to the advantage of a greater nodule count as described above, because such improvement was lost in LCF behavior^[52]. So with this in mind, it can be concluded that the effect of volume fraction, size and distribution of retained Austenite in matrix, strongly affect the HCF performance of ADI.

Large graphite nodules, inclusions, micro shrinkage pores, and irregularly shaped graphite clusters at or near the surfaces of the HCF specimens are the typical crack initiation. Failure usually begin with extensive nodule decohesion from the matrix followed by localized plastic deformation in the matrix resulting in microcracks extending from many graphite nodules. Decohesion is due to mismatch in mechanical properties between graphite and matrix structure and take place at the graphite/matrix interface at low level of strain. At the higher values of strain, localized plastic deformation and microcracking occur to relieve the stress concentrations caused by the graphite nodule voids ^[50].

ADI's fatigue crack path largely depends on the location of the next nodule ahead of the crack tip. It usually goes through the areas with highly distributed graphite nodules, which provide the least-energy path to link graphite nodules. For the crack path between two neighboring nodules, fatigue crack was observed to grow along the Austenite/ferrite interfaces or cut through the ferrite laths ^[50].

Results of another study about the high-cycle fatigue of ADI ^[53] show that the fatigue limit in ADI is controlled by a crack arrest. Ausferrite packet boundaries act as barriers for microstructurally-small cracks due to a requirement for the first stage growth in the Ausferrite matrix. The strength of the barrier depends on the relative orientations of the microstructure at the boundary.

5.2.4. Fatigue crack growth in ADI

Fractographic analysis of fatigue fracture surfaces at threshold show striations typical of a ductile fracture mechanism. In the proportional growth regime striations and cleavage planes are shown, revealing a quasi-cleavage failure mode. The effect of matrix microstructure is minor, and can be attributed to the different crack closure contribution of each microstructure ^[54].

The main propagation mechanism is given by small cracks emanating from nodules and growing towards the principal crack. In other words, propagation of the main crack is partly due to the initiation and growth backwards of small cracks started at surface irregularities of the graphite nodules ^[54]. Initiation of these cracks is apparently activated by the stress raise produced when the tip of the main crack is at a sufficiently short distance from the nodule. These small cracks eventually coalesce with the main crack front, which continues to grow in the normal way until a new nodule is reached ^[54]. It is important to take into account that several nodules can be involved in the growth process at the different portions of the crack front, so that the average growth rate is affected by the size, shape and distribution of graphite nodules ^[54].

In the same study ^[54], Threshold and propagation fatigue regimes are analyzed for two commercial low alloy ductile cast irons, both Austenitized at 900 °C for 2 h and then Austempered at different temperatures and times.

Two different casts were used: Cast 1 (0.28% Mn, 0.90% Cu, 0.53% Ni) was used for fatigue threshold measurements (batches named A-D), and Cast 2 (0.20% Mn, 1.33% Cu, 1.03% Ni) was used for fatigue propagation tests (batches named F-I). Samples were machined from ‘Y’ blocks of thickness 1 inch (cast 1), 1/2 inch. (cast 2a) and 3 inch. (cast 2b) respectively. Crack growth rates and threshold stress intensity ranges ΔK_{th} were determined according to ASTM E-647. The results achieved are listed in tables 5.1 and 5.2 ^[54].

Table 5.1 – Threshold stress intensity ranges for different heat treatment. Adapted ^[54].

Batch	Austempering temperature [°C]	Austempering time [min]	ΔK_{th} [MPa \sqrt{m}]
A	260	120	4.77
B	290	120	5.18
C	320	90	5.61
D	360	90	6.35

Table 5.2 – Values of C and m for different heat treatment, Adapted ^[54].

Batch	Austempering temperature [°C]	Austempering time [min]	C	m
F (2a)	260	120	8.18×10^{-12}	2.92
G (2b)	260	120	2.39×10^{-11}	2.66
H (2a)	360	90	1.16×10^{-11}	2.91
I (2b)	360	90	6.79×10^{-12}	2.95

5.3. Fracture Toughness

5.3.1. Introduction to Fracture Toughness

Fracture toughness is a property which describes the ability of a material containing a crack to resist fracture, and is one of the most important properties of any material for many design applications. The linear-elastic fracture toughness of a material is determined from the stress intensity factor (K) at which a thin crack in the material begins to grow. It is denoted K_{Ic} and has the units of $Pa\sqrt{m}$. Plastic-elastic fracture toughness is denoted by J_{Ic} , with the unit of J/cm^2 , and is a measurement of the energy required to grow a thin crack. The subscript Ic denotes mode I crack opening under a normal tensile stress perpendicular to the crack, since the material can be made deep enough to stand shear (mode II) or tear (mode III).

Fracture toughness (K_{Ic}) is a test that measures the energy required to propagate an existing crack, a quantitative way of expressing a material's resistance to brittle fracture when a crack is present. If a material has much fracture toughness it will probably undergo ductile fracture. Brittle fracture is very characteristic of materials with less fracture toughness ^[55].



Figure 5.16 – Brittle Fracture of Steel broken at $-190^{\circ}C$. *Courtesy of Internet Microscope for Schools.*



Figure 5.17 – Ductile Fracture of Steel broken at $-20^{\circ}C$. *Courtesy of Internet Microscope for Schools.*

5.3.2. ADI Toughness

ADI is a reasonably tough material for its strength. The measures of toughness include impact strength (notched and un-notched) and fracture toughness. Existing standards have been developed with the time on impact tests like Charpy and Izod for their relative easiness. On the other hand, the data coming from them does not help in Finite Element Analysis design.

Charpy impact testing has been widely used to compare quality in steels over the time with sufficient success. However, for the particular case of testing ductile iron or ADI, it has been certain controversy about the efficacy of Charpy impact test.

Some publications have proved v-notched Charpy properties for steels to be way better than those of ADI. However, when comparing various steels with ADI in fracture toughness, then results are quite the same for a given hardness.

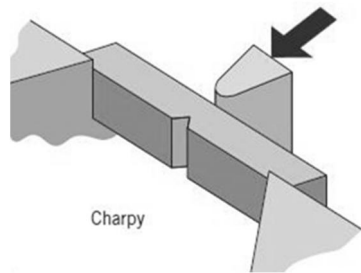


Figure 5.18 – Charpy impact test ^[56].

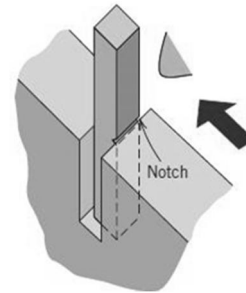


Figure 5.19 – Izod impact test ^[56].

In monotonic testing, ADI does not show necking (extreme plastic deformation local to the fracture site) when it is pulled to failure in a test bar as steel or aluminum do. Instead, the whole length of the test bar reduces its cross section. While the reduction in area for a steel sample may be multiples of the measured elongation, the elongation and reduction in area for an ADI sample are typically the same.

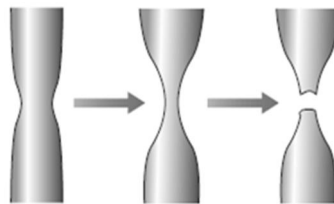


Figure 5.20 – Necking leading to fracture in a typical tensile test with steel or aluminum.

In dynamic testing this effect plays out as lateral expansion of the fractured Charpy sample. A steel sample will exhibit significant lateral expansion at the fracture surface while an ADI sample will not ^[15]. This phenomenon has been examined ^[57] in a mechanical study of notched and un-notched fatigue performance. From this study it can be inferred that with the few available data ADI could perhaps show a lower notch sensitivity than steels of same yield strength and the same or even better than steels and/or Aluminum having a yield strength of one half.

It is possible to conclude then, that the relative toughness of ADI to other competitive materials is still not totally solved. As long as a Charpy test is used as a method for selecting materials, then ADI will keep certain disadvantage over the others. Nevertheless in functional impact testing, as with fracture toughness testing, ADI has proved to be equal to or even better than both wrought and cast steels with equivalent yield proof strength.

Chapter 6

6. OTHER PROPERTIES OF ADI

6.1. Damping and Noise Reduction

6.1.1. Introduction

The damping capacity is the measure of a material's ability to dissipate elastic strain energy during mechanical vibration or wave propagation. When properly used in a structural application, this property allows undesirable noise and vibration to be passively attenuated and removed to the surroundings as heat ^[58].

Components made of materials with a high damping capacity can reduce noise such as chatter, ringing and squealing, and also minimize the level of the applied stresses. An accumulation of vibrational energy without adequate dissipation results in an increasing vibration amplitude that triggers an excessive wear between other problems.

The exceptionally high damping capacity of grey cast iron is one of the most valuable qualities of this material which is also commonly known as *damped iron* for its ability to damp noise. On the other hand, aluminum is a seriously “noisy” material as shown in Table 6.1 where the relative damping capacity of various materials is compared.

Table 6.1– Relative Damping Capacity for various materials. Adapted ^[13].

Material/Process	Relative Damping Capacity*
Grey Iron (high carbon equivalent)	100 - 500
Grey Iron (low carbon equivalent)	20-100
Austempered Ductile iron (ADI)	9-30
Ductile iron (SGI)	5-20
Malleable Iron	8-15
Steel	4
White Iron	2-4
Aluminum (typical)	0.4

*Natural log of the ratio of successive amplitude

For the cast irons, damping capacity decreases when increasing their strength. This happens because the larger amount of graphite present in the lower strength irons is responsible for the energy absorption. Larger cast section thicknesses increase damping capacity while inoculation on the other hand usually decreases it. Finally the heat treating can also have an appreciable effect on damping capacity.

6.1.2. Damping Capacity of ADI

In the case of Austempered ductile irons with their Ausferritic matrix, better damping capacity than regular ferritic/pearlitic ductile irons is achieved. The increase in damping seems to be proportional to the size and distribution of the ferrite plates in ADI's Ausferrite matrix. A higher strength grade of ADI (with a larger volume of finer ferrite platelets) has a higher damping coefficient than a lower strength grade of ADI (with fewer, coarser ferrite platelets) ^[13].

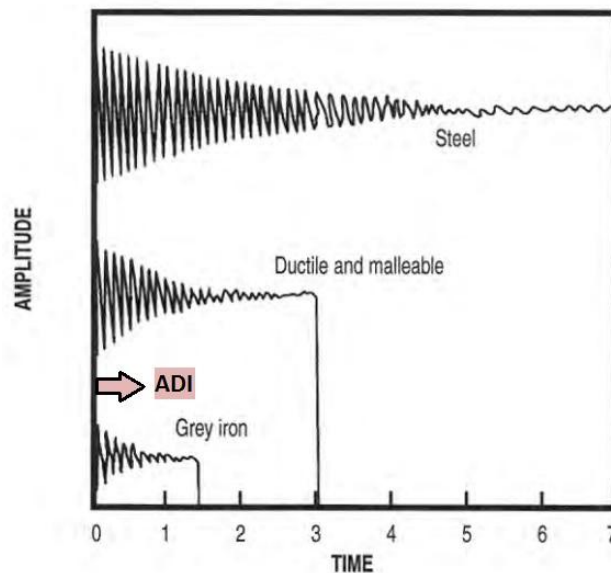


Figure 6.1 – Relative damping behaviors of steel, ductile & malleable iron and grey iron compared to ADI. Adapted ^[59].

ADI has also a superior damping capacity when compared to steel as shown previously in Table 6.1. This is related to the presence of graphite nodules within the matrix, which also improve the lubricity of the material. In some cases this fact has resulted in measured reductions in the frictional losses ^[62]. In order to achieve best damping properties the following are to be considered ^[63]:

1. Carbon equivalent (C.E) should be in the range of 4.6 to 5.1
2. Austempering temperature should be in the range of 300 – 350 °C.
3. Bainitic microstructure is preferred

6.1.3. Noise evaluation in ADI

In order to evaluate acoustic properties of ADI, damping and noise tests have been conducted on gears. Noise tests were done by striking the gear blanks of same material in a semi-anechoic room and recording the noise level reached using a sound analyser. This was done to simulate the gears coming in contact when they are in operation in a vehicle running condition as show in Table 6.2 below ^[64].

Table 6.2 – Noise level recorded ^[64]

Material	Noise (decibels)
Steel	95-96
ADI	90-91

From the above values, one can conclude that the noise levels achieved in case of ADI are significantly low (of the order of 2-3 units) when compared to steel. Another illustrative example shows a study completed on hypoid gear sets, which compares noise output for a steel gear set to an ADI one. It was found that a larger noise reduction could be reached with the ADI gear set as shown in Figure 6.2 below.

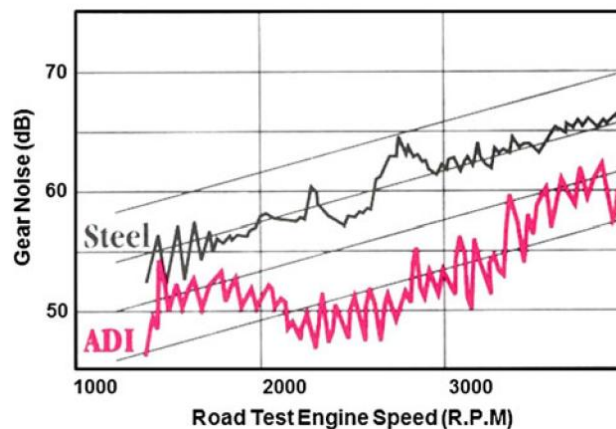
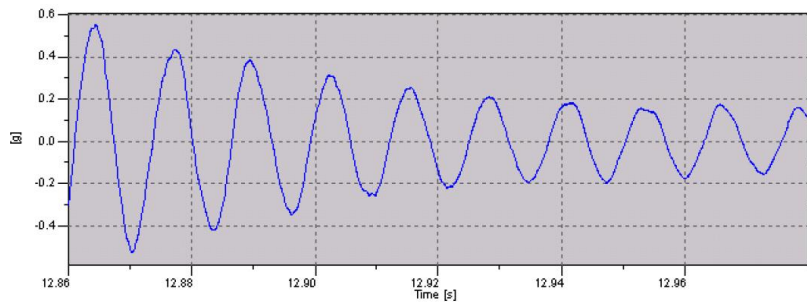
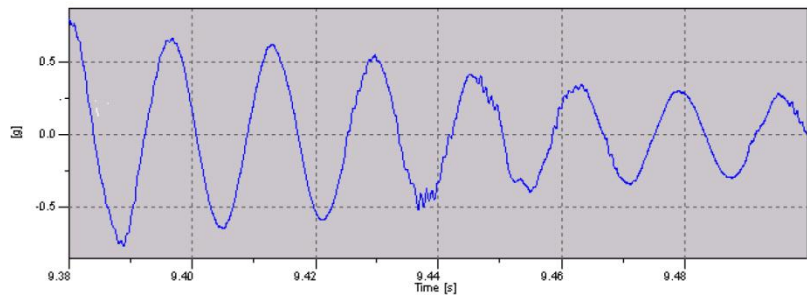
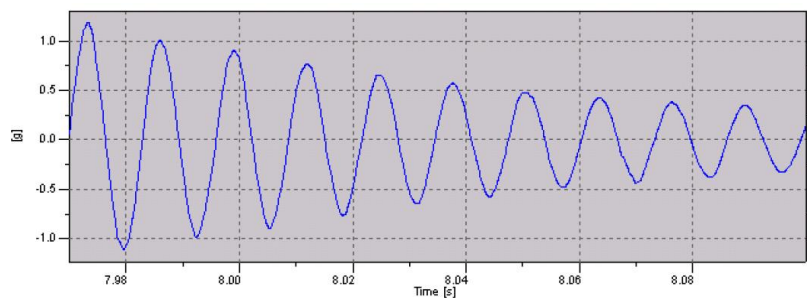
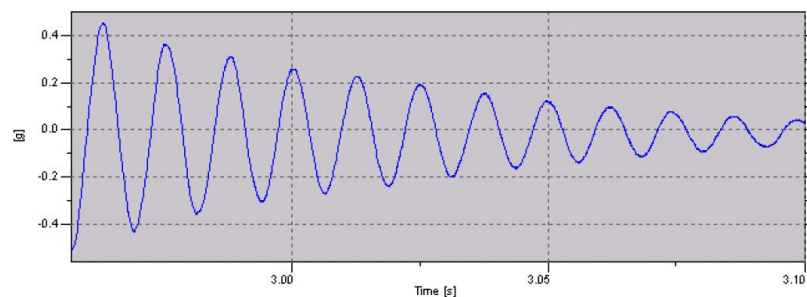


Figure 6.2 – Comparison of noise in hypoid gears during vehicle road tests, from the ASME Gear Research Institute Report A4001 ^[61].

6.1.4 Damping evaluation in ADI

Damping tests on the other hand have been developed using a cantilevered beam arrangement. A cantilever beam of the material was fixed at one end. This beam is then hammered to excite it into the bending mode. At the free end of the beam an accelerometer is fixed. This senses the signals from the beam undergoing vibration and the signals are recorded to a data acquisition system, obtaining a plot of amplitude versus time. Damping property is of primary importance because this measure shows the rate at which the noise signal subsides as soon as it is produced. The material possessing the highest damping capacity can then reduce noise to the maximum.

Figure 6.3 - Plot of amplitude Vs time for Steel ^[64].Figure 6.4 - Plot of amplitude Vs time for SGI, Austempered at 640°C ^[64].Figure 6.5 - Plot of amplitude Vs time for ADI, Austempered at 300°C ^[64].Figure 6.6 - Plot of amplitude Vs time for ADI, Austempered at 340°C ^[64].

The time taken for the signals from steel beam to dampen is high, whereas in case of SGI, the time taken for the signals to dampen is less as shown in Figures 6.3 and 6.4. Even lower time to dampen the signals is achieved in the case of ADI. Now when comparing ADI for damping properties at two different Austempering temperatures, the one which is Austempered at 340 °C gives better damping properties than the one at 300 °C as shown in Figures 6.5 and 6.6. It can be concluded then that the damping properties of ADI are far superior to the other materials.

6.2. Density

Nowadays, weight reductions in all kind of parts and components are a must in order to reduce energy requirements on moving system or even just thinking in reducing shipping costs. Figure 6.7 compares densities for different materials/process combinations where it is patent the superior characteristics of aluminum regarding low density and good manufacturability.

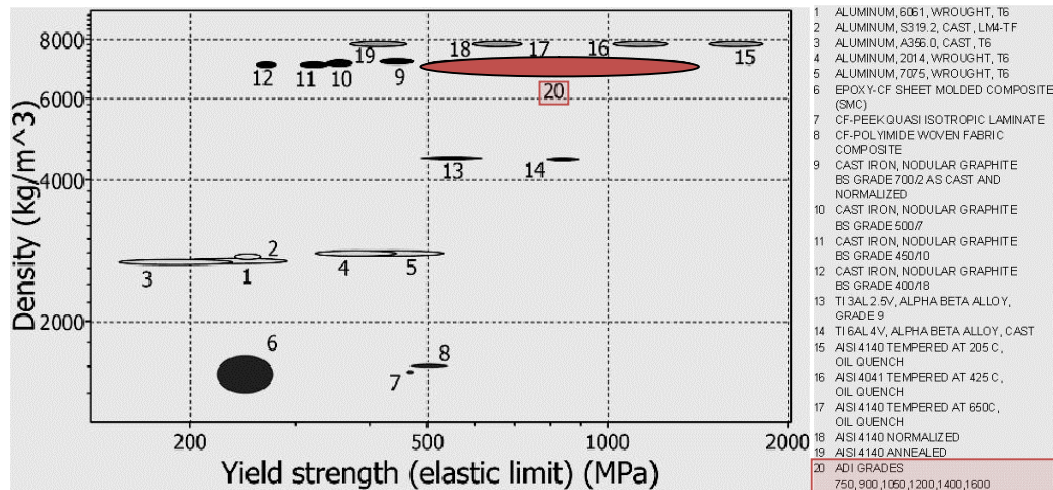


Figure 6.7 – Comparison of typical densities for various material/process combinations. Adapted [10].

However, a low density by itself is not a sufficient characteristic to compare materials because certain minimum strength is required for most component designs. A comparison of the weight per unit of yield strength for several materials is shown in Figure 6.8, where ADI excels over the rest with its relatively low specific weight.

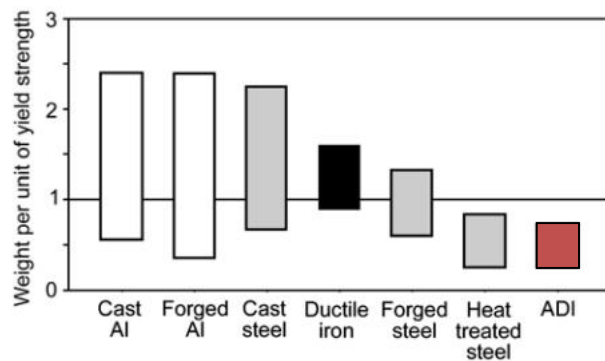


Figure 6.8 – Comparison of the weight per unit of yield strength for different materials/process combinations. Courtesy of Applied Process Inc.

In general, the lowest density materials tend to have the lowest yield strength and the lowest stiffness (Young’s Modulus). Just few special materials like titanium and some carbon composite materials are the exception, but the fact of having considerable high price together with brittleness or poor manufacturability usually excludes them from most designs.

6.3. Corrosion Resistance

6.3.1. Introduction

Corrosion resistance is a material feature that must be taken into account in most designs; even finite life designs. Table 6.9 shows the galvanic series for selected metal alloys. The light metal alloys (magnesium and aluminum) are subject to rapid corrosion and must either be attached with (and to) welds or fasteners of like galvanic behavior or insulated from them. For example, magnesium alloy wheels on cars must be coated and attached with insulating (non-conductive) washers to prevent them from coupling to ground through iron and/or steel components and rapidly corroding in service.

Table 6.3 - The (Relative) Galvanic Series for selected metal alloys. Adapted ^[13].

ANODIC / LEAST NOBLE / CORRODED
Magnesium Alloys
Zinc Alloys
Aluminum Alloys
Mild Steel and Wrought Iron
Alloyed Carbon Steels
Cast Iron (including Ductile iron)
Austempered Ductile iron (ADI)
Ferritic and Martensitic Stainless Steels
Ni-Resist (majority Austenitic Cast iron)
Titanium
Lead
Tin
Brass
Copper
Bronze
Austenitic Stainless Steel (fully Austenitic)
Silver
Graphite
Zirconium
Gold
Platinum
CATHODIC / MOST NOBLE / PROTECTED

6.3.2. Corrosion in ADI

The silicon-iron-graphite oxide that develops on cast iron advances very slowly, once established. ADI is incrementally more corrosion resistant than steels and other cast irons due to the presence of graphite and Austenite in the metal matrix. For example, a Grade 1050-7 ADI has 9% graphite and approximately 30% Austenite in its structure making the material more cathodic than ferritic/pearlitic ductile irons or steels.

Ferrous alloys hardened to high tensile strengths can be subject to the so called Environmentally Assisted Embrittlement (EAE) under the right conditions. In this way ADI is also subject to this failure that is covered more in detail in the next point 6.4.

6.4. Environmental Assisted Embrittlement (EAE)

6.4.1. Introduction

A general definition for embrittlement would be “The reduction in the normal ductility of a metal caused by a physical or chemical change”^[65].

An unusual environmental assisted embrittlement (EAE) effect has been reported to affect ADI when it is tested in tension with its surface in contact with water and other fluids during slow monotonic tensile load applications^[66-71]. This effect has been verified by several laboratories, but the embrittlement mechanism has not been fully explained yet.

6.4.2. Background

Shibutani et al^[66] and Komatsu et al^[67] reported that ADI suffers an uncommon environmental assisted embrittlement (EAE) effect when it is tested in tension with the sample's surface in contact with water. Later, Martínez et al.^[68], obtained similar results in an independent laboratory, using different base ductile iron and several ADI grades. These investigations showed that ADI suffers significant reductions in UTS and elongation that can reach up to 30% and 70% respectively, when tested in tension, as shown in Figure 6.9.

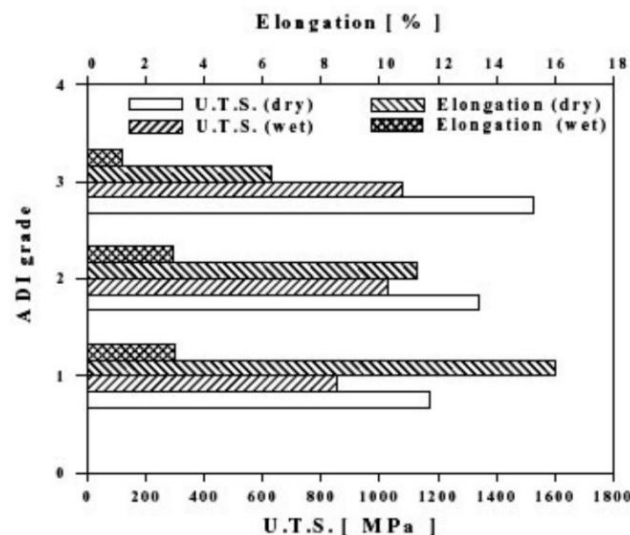


Figure 6.9 - Change in Ultimate Tensile Strength (UTS) and Elongation as a result of tensile testing of ADI grades 1, 2 and 3 (900, 1050 and 1200 respectively) in contact with water^[73].

Although water has shown to be the reason for the greatest degree of embrittlement, Martínez et al. [68] found that EAE of ADI is also caused by contact with other liquids, such as isopropyl alcohol and mineral lubricant oil (SAE 30) as shown in Figure 6.10. It was reported as well that the effect of water is independent from its pH, and remains unchanged when water based solutions of pH ranging from 5.5 to 11.9 are used.

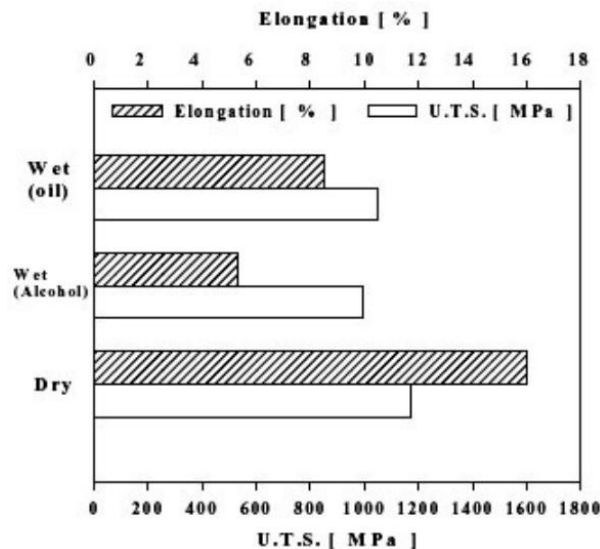


Figure 6.10 - Change of Ultimate Tensile Strength (UTS) and Elongation caused by the contact with lubricant oil and isopropyl alcohol [73].

6.4.3. Environmental Assisted Embrittlement process

It is known the EAE takes place almost instantaneously when in contact with liquids and it reverses immediately when the surface of the sample is dried again [64]. It shows therefore no dependency with the time of exposition to liquid, and the impact properties are not affected by this liquid exposition.

Another important characteristic of EAE is that it is unnoticed at high loading rates. As a result, failure in service requires a relatively slow overloading when the part is in contact with the liquids, which usually does not occur so frequent.

The EAE not only affects ADI, but also ductile irons (DI) of other microstructures, such as those having Martensitic and pearlitic matrices. All investigations showed that the higher the strength of the DI, the greater the embrittlement effect. Only ferritic matrix ductile iron has been found to be immune to the contact with water [66, 67]. It is known that a given ductile iron alloy can be heat treated to show Ausferritic, Martensitic, pearlitic or ferritic matrix. Only the first three matrices will suffer EAE. Therefore, the embrittlement mechanism has to be primarily related to the microstructure, and not to the chemical composition of the alloy.

Martínez et al. ^[68] have discussed the role of the different microconstituents of the matrix on the EAE effect. They pointed out that EAE has so far been identified on DI of matrices composed of ferrite and Austenite (ADI), ferrite and cementite (pearlite) and tempered Martensite (fine dispersion of carbides in a ferritic matrix). Furthermore, in high silicon steels having a composition similar to that of ductile iron matrix, embrittlement is also present in the Bainitic microstructure but only causes a reduction in elongation ^[67].

6.4.4. Protection against EAE

An apparently obvious protection of ADI against the embrittlement caused by liquid environments would be through ADI surface isolation from the environment. Nevertheless, it has been reported that from a good number of protective coatings applied on tensile samples in water contact, only one was able to protect the sample under stress against the embrittlement phenomena ^[73]. Just the antirust and lubricant known as WD40 (Water Displacement, 40th) was effectively protecting against water contact.

Table 6.4 – Mechanical properties of ADI using different protective coating layers. Adapted ^[72].

Coating Layer	σ_R [MPa]	$\sigma_{0,2}$ [MPa]	δ %
ADI Dry	1050	700	14.8
ADI 900	900	650	9.0
ADI (wet) H ₂ O	843	705	1.2
F-Acrylic	1010	696	13.8
WD 40	1040	705	14.6
Polyester-U	807	688	4.0
Polyester	823	707	3.4
E-tin	795	685	3.3
H-Epoxi	873	668	3.0
M-Zincado	833	688	2.8
S-Epoxi	837.5	723.5	1.9
E-Zinc	817	698	1.3

It is possible to conclude then on the basis of all this that despite the excellent properties of ADI, the material is subjected to EAE failure in presence of three conditions: (1) High constant stress near the yield stress and/or plastic deformation; (2) Any liquid presence; and (3) A slow strain rate. Therefore as a rule when designing with ADI, it should not be use in application where the components are locally plastically deformed at a high and prolonged stress level.

6.5. Operating Temperature

6.5.1. Introduction

Since Austenite has a face-centered-cubic (FCC) metallic matrix structure, it has no ductile to brittle transition temperature. Aluminum, that is 100% FCC, is widely used in aviation for airplane's skin and wings since its properties will not be compromised under temperatures around -60°C when flying at high altitude.

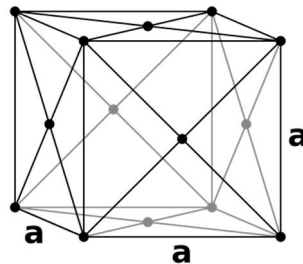


Figure 6.11 - The FCC structure

In the case of ADI, it has FCC Austenite as one of its principal constituents, and the lower strength grades of ADI (those with the highest percentage of Austenite in the microstructure) have the gentlest ductile to brittle profile. Indeed, ADI has good low temperature properties. It is capable of maintaining at least 70% of its room temperature impact strength at -40°C , which compares favorably with most steels ^[74].

6.5.2. Temperatures in Service

Although the Austenite in the Ausferrite structure is thermally stable to very low temperatures, it can happen that the Austenite breaks down into ferrite and carbide when exposed to elevated, long-term service temperatures. Direct consequences of this would be gradual degradation of tensile strength together with the toughness. Previous research ^[75] has demonstrated that the ADI microstructure is long-term stable as long as operating temperatures did not exceed about 60°C less than the Austempering temperature. Table 6:5 shows estimated maximum continuous operating temperatures for the various grades of ADI.

Table 6.5 - Estimated maximum operating temperature for the various grades of ADI ^[13].

Grade of ADI	Maximum Operating Temperature
750-500-11	315°C
900-650-09	315°C
1050-750-07	300°C
1200-850-04	290°C
1400-1100-02	280°C
1600-1300-01	260°C

6.5.3. Coefficient of thermal expansion

The Austenite present in the Ausferric matrix of ADI has also the effect of increasing the coefficient of thermal expansion of the material. Ferritic, Pearlitic and Martensitic irons and steels have a coefficient of thermal expansion around $11(\text{mm}/\text{mm}/^{\circ}\text{C}) \times 10^{-6}$. ADI, depending on the grade, has a coefficient of thermal expansion ranging from about 13.5-14.5 $(\text{mm}/\text{mm}/^{\circ}\text{C}) \times 10^{-6}$. In contrast, aluminum alloys have a coefficient of thermal expansion around 18 $(\text{mm}/\text{mm}/^{\circ}\text{C}) \times 10^{-6}$. Such property needs attention for those cases where tolerance fitting is required at temperature. For example, a forged steel crankshaft rotating in an aluminum block will require special design features to not leak oil at operating temperatures. On the other hand, an ADI crankshaft operating in an iron block would require extra cold space to allow for the crankshaft growth at operating temperatures ^[13].

Chapter 7

7. MANUFACTURABILITY OF ADI AND COSTS

7.1. Introduction

Most components nowadays are designed to reduce the cost in order to make the production cost competitive and more profitable. The task is often to produce a component or a system to the minimum engineering requirement for the application at the lowest price. The cost of the material blank is often surpassed by the price of machining operations, transport, inventory, tooling, and many other factors. For the case of an ADI blank, the cost is common to be around 20-30% lower than a heat treated steel forging. However, the principal savings for that are not in the blank itself. Instead, the money saved comes from machining the part in the soft as-cast condition, proceeding afterwards with the Austempering process. However, although this is the lowest cost path and it is viable for roughly three quarters of the ADI applications, it must be noted that for those uses where the tolerances are on the order of 0.01mm, the part will require to be machined after Austempering.

7.2. Cost Advantages of ADI

The price of ADI material is lower per kilo than steel or aluminum, but this accounts for only a fraction of the potential savings since an ADI component is capable of saving costs at each stage of manufacturing process. ADI components can then be produced for less than a steel forging or even at half the cost in the case of aluminum parts. Several factors are responsible for ADI to be a superior engineering material in manufacturing aspects:

- *Excellent castability:* The casting process allows to cast holes and complex shapes into parts that could not be just forged. Ductile iron has a very high yield rate, which is the proportion of metal poured versus metal shipped.

- *Lower machining cost:* Well adapted to near net shape casting, ADI requires less starting material and less metal to be removed. Before the Austempering process, ductile iron exhibits better machinability than free machining steels. Both ductile iron and ADI produce when machining dense and discontinuous chips that are easily handled, reducing even more the cost per kilo. The machining of ADI is covered in a deeper way in section 7.3.
- *Heat treatment savings:* The Austempering process of ADI is generally cheaper than carburizing or induction hardening, and is able to produce a higher degree of uniformity together with predictable dimensional changes.
- *Low energy consumption:* Casting is the most direct and lowest energy process from raw metal to finished part. The production of a random ADI casting consumes around 50% less energy than a steel casting, and even 80% less energy than in the case of a steel forging.
- *Best value:* When comparing the relative cost per unit of yield strength, ADI is usually the best buy, as depicted in Figure 7.1 below.

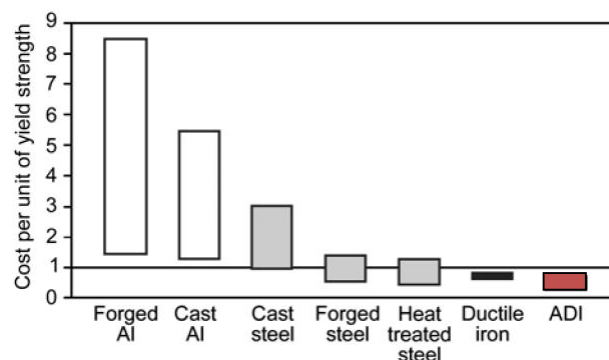


Figure 7.1- Relative cost per unit of yield strength for various material/process combinations. *Courtesy of Applied Process Inc.*

- *Recyclable:* As all ductile irons, ADI grades can be produced from up to 100% recycled materials.

7.3. Machinability

7.3.1. Introduction

The term machinability refers to the ease with which a metal can be machined to an acceptable surface finish ^[76]. Materials with good machinability require little power to cut, can be cut quickly, easily obtain a good finish, and do not wear the tooling much; such materials are said to be free machining. The factors that typically improve a material's performance often degrade its machinability. Therefore, to manufacture components economically, engineers are challenged to find ways to improve machinability without harming performance.

The machinability of a material can be described by four different criteria: chip form, cutting forces, tool wear/tool life, and surface quality. In general, it is right to say that the machining characteristics of conventional cast iron materials depend strongly on the quantity and the form of the graphite inclusions. These graphite inclusions are responsible to reduce the friction between the tool and the workpiece on one hand and breaking up the metallic base structure on the other hand. Apart from the graphite, the metallic base structure of the cast iron materials makes considerable influence on machining properties. For those low-strength materials, it consists mainly of ferrite, while increasing the pearlite content results in higher levels of material strength and tool wear ^[77].

7.3.2. Machining characteristics of ADI

When ADI started years ago taking place in different engineering applications, certain difficulties were experienced in the machining process. The hardest grades of ADI reach hardness near 500 HBW which would represent a challenge for any high volume machining operation. Although the softer grades of ADI have a typical hardness around 300-350 HBW, their matrix structure contains up to 40% retained Austenite. When subjected to strains in service, this phase rapidly work hardens and can transform to Martensite, reducing in this way the machinability compared with a steel of equivalent hardness ^[37].

Nowadays, the use of components made of ADI has reached certain popularity in several fields. In this sense, a wide range of requirements regarding accuracy and surface finish must be taken into account. The integration of machining operations into the ADI production line is summed up in Figure 7.2. It can be appreciated how a certain number of ADI components do not need to be machined; examples in this group include agricultural tools in contact with the ground, and earth moving tools. Nevertheless, most automotive components will need from machining operations. Most of those components made with the softer grades of ADI can be easily machined after heat treatment when using appropriate machining tools. On the other hand, as the hardness of the ADI increases, machining operations become increasingly more complicated.

Is therefore in those cases more appropriate to machine before heat treatment by making an allowance for the dimensional growth assuming that this is predictable and that distortion is not significant.

In case the dimensional growth is not sufficiently consistent, the only option would be to do most of the machining before Austempering and then finish machining any critical dimensions after Austempering. Main disadvantage from this option would be the logistical difficulties in case the casting, machining and heat treatment are done by different companies located far from each other. This route has been extensively used for ADI gears requiring accuracy on quietly operation, as well as for a long life.

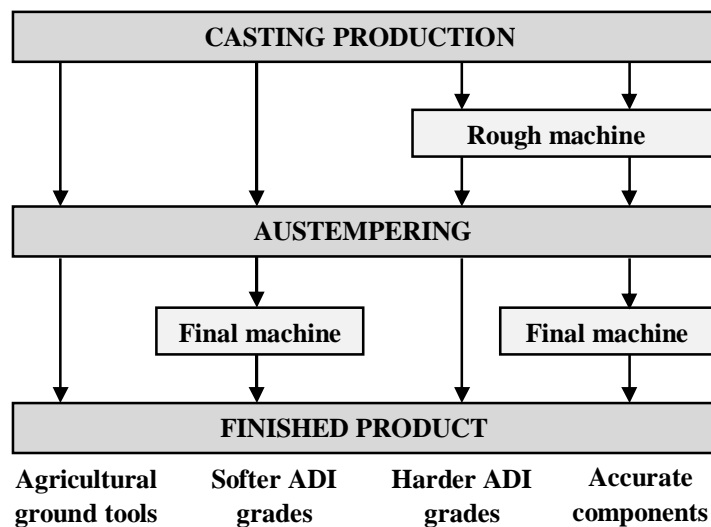


Figure 7.2 – Options for integrating casting, machining and heat treatment of ADI components.

7.3.3. Machining in North America and Europe

It can be observed that the North American approach^[78] with ADI has commonly been to use a higher Manganese base iron than in Europe to reduce the foundry costs. Direct consequence of that is an ADI way harder to machine. For that reason, more than the half of the ADI components produced in North America are finish machined before the Austempering process. In Europe, in contrast, more than 60% of all commercial ADI components are machined after the Austempering process is complete.

7.3.4. High volume machining

It is considered^[79] that the limited use of ADI for high volume applications is partly due to machining difficulties. In consequence, there have been two different approaches to solve this:

-Establishment of the best machining tools and conditions:

An important amount of research has been done in this area to optimize machining through the selection of optimum cutting tools and optimum parameters.

-Development of machinable grades of ADI:

By optimizing the composition and heat treatment it is possible to maximize the machinability. In this way, the influence of Austenitizing and Austempering temperatures on the machinability of ADI has been reported ^[80, 81] in some publications.

It was in the 1980's, when Muhlberger ^[82] developed in Germany a machinable grade of ADI by carefully selecting the composition (low Mn) and heat treatment variables. This new creation was better known as intercritically Austenitized ductile iron (IADI), and through grades of 750 or 800 MPa offered reasonable strength, good toughness and machining similar to pearlitic ductile iron. IADI became popular especially in Europe, where most of ADI parts are machined completely after heat treatment.

After that, two other grades of machinable ADI (MADI) have been developed in the US ^[83, 84] with the specific purpose of increasing the use of ADI for automotive applications such as chassis components and crankshafts. Although there are some differences between both, common feature for them is that the matrix structure contains a considerable amount of ferrite.

Finally, and in a continuing effort to overcome the deficiencies of conventional ADI, extensive efforts have been made to develop the dual-phase (ferritic-Ausferritic) grades of ADI with enhanced machinability properties in order to compete with forged steel for power train applications ^[85-89]. The properties of this dual phase matrix ADI have been the subject of extensive studies over the last years.

PART II

EXPERIMENTAL APPROACH

Chapter 8

8. INTRODUCTION TO WHEELSETS

8.1. Introduction

The wheelset, by its functions and position under the train is the prime safety-critical component. Reliability of railway running gear is based on three fundamental factors: design, manufacture and maintenance ^[87]. Until now this has been achieved with some success by each of the long-established rail networks in accordance with their own policy and experience. Standardizing rules (CEN, UIC, etc) and local regulations have often been put in place to convey these experiences.

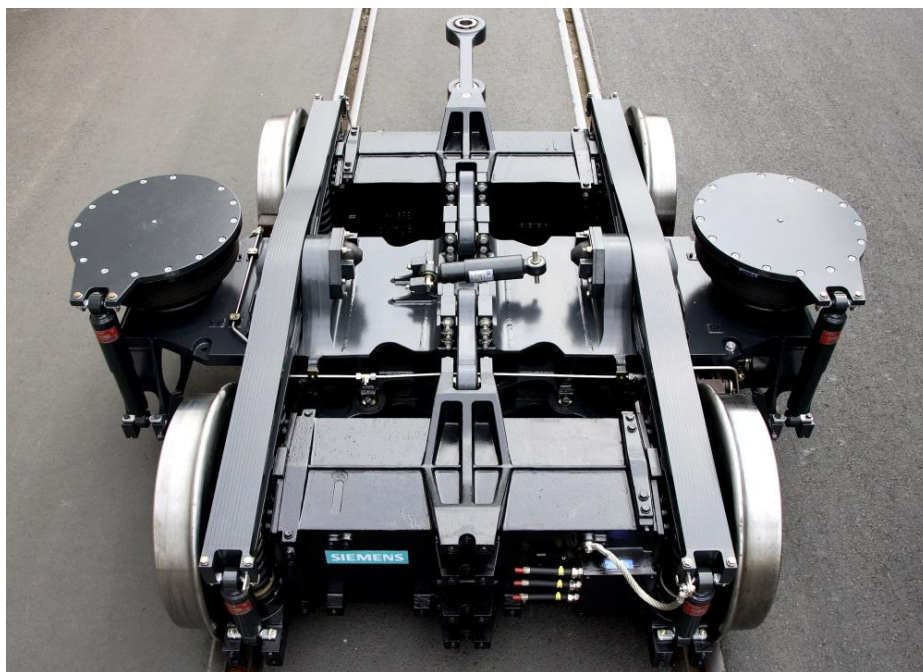


Figure 8.1 - Syntegra bogie for metro and suburban. *Siemens Railway Systems*.

8.2. Developments in the Railway Context

The global analysis of current Research and Development work in Europe and in the world, carried out on running gear, shows that development in this field, as with other railway components, is governed by three factors ^[90]:

a) *Operation*

- The nature and characteristics of the infrastructure: rail/sleeper/ties/ballast/...
- The nature and characteristics of the defects of the wheel running surfaces;
- The nature of future operation: higher axle-loads, higher running speeds, increase in intervals between maintenance operations;

b) *Technology*

- The nature and characteristics of new materials.
- The nature and characteristics of new vehicles.
- The diameter of smaller wheels

c) *Regulation*

- Reduction in railway noise at the wheel/rail level including expert knowledge of the roughness of surfaces in contact and of the wheel/brake-block;
- Formalization of the evaluation of the conformity of products to need;
- A contribution of design and content for establishing a European maintenance programme.

8.3. Design

When talking about running gear design, the directive is based on three fundamental parameters: *calculation*, *stresses* and *fatigue criteria*.

Up to now, the directive of design has been achieved using rules worked out in the 1970s and 80s by the historical railways. The European standardization, underway since the 90s, is to set out a common rule derived from those different experiences. European Standards (ENs) should replace the present documents, reforming them or elaborating upon them, as follows:

- for wheels: UIC Leaflet 510-5, standard EN 13979
- for powered axles: UIC Leaflet 515-3, standard EN 13104
- for non-powered axles: UIC Leaflet 515-3, standard EN 13103
- for wheelsets: UIC Leaflet 510-1
- for journal bearings: UIC Leaflet 515-5, DIN EN 12080 & EN 12082
- for axlebox grease: UIC Leaflet 814, DIN EN 12081 & EN 12082
- for axleboxes: UIC Leaflet 515-5, DIN EN 13749
- for bogie frames: UIC Leaflets 510-3, 515-4, 615-4, EN 13749

The conventional loads referred to in these standards are defined on the basis of the axle load (load per wheelset) on the track. They are fairly independent of the dynamic behavior of the rolling stock, i.e. high-speed rolling stock, wagon, locomotive, electric multiple unit or other, and even more independent of the condition of the infrastructure.

8.3.1. Current calculation of wheels

Axisymmetric wheel centers are calculated by the finite element method in order to determine the principal stresses under conventional loads following the procedure describe in EN 13979 and UIC 510-5.

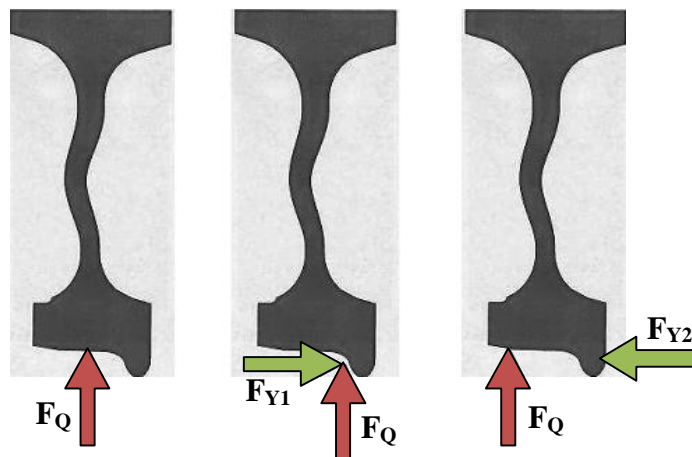


Figure 8.2 – The three conventional loading cases

It must be noted that the maximum principal stress corresponds to the maximum radial stress. The surface roughness of the wheel center ($R_a \leq 3.2 \mu\text{m}$ or $R_a \leq 12.5 \mu\text{m}$) is taken into account in the permissible stresses.

The principle of conventional loading defined in RP11 of ERI Committee B136 and in UIC Leaflet 515-3 is characterized by the vertical and transverse forces on straight track, curves and reverse curves.

The stresses are analyzed according to B12/RP17 or UIC 510-5 in what can be broken down into five steps:

- 1) Search for principal stresses at all points of the wheel/center under each of the load cases (straight, curved, reverse-curved track);
- 2) Determine for each node the maximum stress (σ_{max}) and its direction (δ);
- 3) Determine for each node the minimum stress (σ_{min}) in the direction (δ);

- 4) Determine for each node the mean stress and the stress range;

$$\sigma_{middle} = \frac{\sigma_{max} + \sigma_{min}}{2} \quad \text{and} \quad \Delta\sigma = \sigma_{max} - \sigma_{min}$$

- 5) Verify that for the entire wheel the stress range thus calculated remains less than the permissible stress range, which is 360 MPa or 290 MPa depending on the roughness of the wheel centers.

All these calculations must integrate the geometrical parameters of interchangeability tied to the functional requirements (nominal diameter at the bearing, width of wheel rim, profile...etc.), to the assembly requirements (bore diameter, length of the wheel boss) and to the maintenance requirements (wheel wear limit diameter, position of oil injection hole), which leaves little latitude for creativeness except as concerns the wheel center.

In parallel with this mechanical calculation of wheel fatigue, a thermo-mechanical assessment is made in accordance with RP17 of ERRI Committee B169 for braked wheels in order to comply with the permitted deflection thresholds, for cold and hot wheels, and with the permissible residual stresses.

To date, the experimental procedure remains essential in the railway wheel product acceptance process.

8.3.2. Loads

As mentioned previously, the conventional loads considered in the specifications are defined on the basis of the axle load on the rail. Research done in the ERRI/B169 committee for the UIC has helped to develop the ERRI/B169 RP12 method for determining a set of loads or *load case* that depends on the track quality and geometry and the vehicle's duty.

New works should allow developing different load cases expressed as probabilities of appearance based on on-line tests of the most-relevant traffics for Europe, namely: *freight*, *locomotive*, *tilting stock*, *high-speed stock*, or *suburban stock*. Moreover, weighting these load case components should allow assessing damage to other rolling stock without testing and there by speed development working ^[90].

8.3.3. Fatigue criteria

Today, the rotating-bending fatigue criteria for axles put in place in Europe concern two materials. An evolution will consist to express them as cracks appearance probability or survival probability. The reverse-bending fatigue criteria for wheels put forward so far by ERRI Committee B169 concern only the material ER7 from the standpoint of mono-axial fatigue of the wheel centers – the Wöhler curves and Haigh or Goodman diagrams at 10^7 cycles.

Works have been done to propose multi-axial fatigue criteria for wheel designing (RP19) and the different threshold to consider for ER7 steel ^[91]. Fatigue limits have been determined for other wheel materials, more resistant to Hertzian stresses or thermo mechanical loads (ER6 and ER8). However, in order to find out how the material will react to long-life fatigue (polycyclic fatigue), and to take into account the loads applied to the test piece which are most often multi-axial (due at least to residual stresses), it is necessary to use fatigue criteria that take into account the multi-axiality of stresses. Most often, loads are multi-axial, non-proportional and of variable amplitude.

That is why fatigue criteria integrating these parameters were ultimately developed ^[90]. Traditionally, the multi-axial fatigue criteria have been classified as: *empirical approach*, *global approach*, and *critical plane approach*.

8.4. Manufacture

Once the running gear is designed following the concepts outlined above, command of manufacturing relies on three principal parameters as diagrammed opposite. The European standardization underway today covers this topic almost completely. Railway experience is incorporated into the standards EN 13261 on axles, EN 13260 on wheelsets and EN 13262 on wheels.

The material must not only have minimum characteristics of resistance to tensile loads, to fatigue, to toughness for the wheels, but also not present any internal or external flaws where cracks can initiate and then propagate. In particular, inclusions in wheel rims can be the source of cracks parallel to the wheel tread ^[92].

The quality of the machining must be controlled to guarantee the previously determined minimum level of fatigue strength. In the case of the axle shaft, protection must be carefully applied to prevent their corrosion and/or dents that considerably weaken their fatigue characteristics ^[93].

8.4.1. Wheel materials

As a proper response to the known mechanisms of damage, the materials employed in wheels and rails all around Europe are basically steels whose predominantly pearlitic structures guarantee a high resistance to wear. At the same time a pearlitic microstructure formed by transformation close to the equilibrium point, ensures higher resistance to transformation in operation than Bainitic or Martensitic structures ^[94].

Although UIC Leaflet 812-3 for solid wheels lists seven types of steel, which differ significantly in carbon content, heat treatment state and strength, the EN 13262 contains only four types of them as shown on Table 8.1 below.

Table 8.1 – Wheel steel requirements according to UIC 812-3 and EN 13262. Adapted ^[94].

Steel category		Carbon content (%)	Yield Strength (N/mm ²)	Tensile Strength (N/mm ²)	Elongation (%)	Notch impact energy (J)	
UIC 812-3	EN 13262	UIC/EN	EN 13262	UIC/EN	UIC/EN	UIC 812-3 U-notch (RT)	EN 13262 V-notch (-20°C)
R1 N	-	≤ 0.48	-	600 / 720	≤ 18	≤ 15	-
R2 N	-	≤ 0.58	-	700 / 840	≤ 14	≤ 10	-
R3 N	-	≤ 0.70	-	800 / 940	≤ 10	≤ 10	-
R6 T, E	ER6	≤ 0.48	≤ 500	780 / 900	≤ 15	≤ 15	≤ 12
R7 T, E	ER7	≤ 0.52	≤ 520	820 / 940	≤ 14	≤ 15	≤ 10
R8 T, E	ER8	≤ 0.56	≤ 540	860 / 980	≤ 13	≤ 15	≤ 10
R9 T, E	ER9	≤ 0.6	≤ 580	900 / 1050	≤ 12	≤ 10	≤ 8

N...normalized, T...rim heat treated, E...whole wheel heat treated

From all them, it could be said that ER7 steel represents the most commonly reliable technology in Europe. It is used for all freight wagon wheels and on most passenger coaches. Where wheels made of ER7 are intended for use in vehicles with tread brakes, the fracture toughness requirements (K_{IC}) must be fulfilled as well as the usual characteristic mechanical values. Experience have shown that where carbon content exceeds 0.5%, the K_{IC} values of 80MPa \sqrt{m} called for in UIC 812-3 and EN 13262 can only be attained where comparatively small grain, high purity and high homogeneity are present in the structure throughout the circumference of the wheel ^[94].

This places heavy demands on manufacturing quality, and for this reason these wheels are commonly supplied with lower carbon contents (<0.5%C) which therefore put them in the lower strength tolerance range. This means that besides pearlite, large amount of pre-eutectoid ferrite are present in the tread. Although this leads to greater toughness, the wear resistance is correspondingly reduced.

In summary, materials employed for solid wheels in Europe are largely restricted to unalloyed steels with maximum carbon content of 0.56% and – after appropriate fine pearlitization treatment of the tread – tensile strengths of 820 – 950 MPa ^[94].

8.5. Maintenance

Directive of the maintenance of running gear relies on three main parameters: *non-destructive tests*, *experience feedback* and *fracture mechanics*.

There is actually little standardization in the field of maintenance, or practically none. Some prescriptions have been put in place, mainly for freight rolling stock, in the context of the UIC. For running gear, it is worth mentioning:

- regarding wheelsets for freight: UIC Leaflets 510-2 and 579-2
- regarding wheelsets in general: DIN EN 15313

Control of the non-destructive testing techniques is assured by different standards, in particular standard EN ISO 9712 for the certification of operators. Maintenance therefore relies almost exclusively on the standards or codes of practice of the historical railways.

Chapter 9

9. THE MEAN STRESS EFFECT

9.1. Introduction

A major problem in fatigue design is the knowledge of the effect of static mean stresses σ_m on the endurable stress amplitude σ_a . Accessible data have led to the general observation that the endurable stress amplitude $S \equiv \sigma_a$ drops with increasing static mean stress. Figure 9.1 gives a schematic overview of the amplitude reduction influenced by static compression or tension preloads. Although this effect has been known for hundred years, occasional failures due to this cause are still encountered based on only qualitative assumptions of this kind.

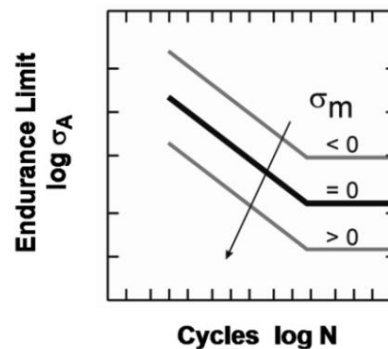


Figure 9.1 – Mean stress effect in the S-N diagram (schematic) ^[95]

The stress ratio R is defined as the quotient of minimum and maximum stress within a full sinusoidal loading cycle $\sigma(t) = \sigma_m + \sigma_a \cdot \sin(\sigma t)$, as depicted in Figure 9.2.

$$\text{Stress Ratio} \rightarrow R = \frac{\sigma_{min}}{\sigma_{max}} = \frac{\sigma_m - \sigma_a}{\sigma_m + \sigma_a} \quad (1)$$

Where:

σ_m mean static stress.

σ_a stress amplitude.

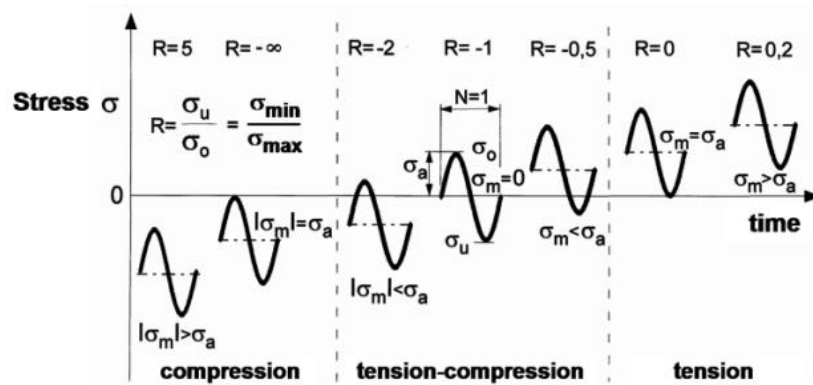


Figure 9.2 – Definition of the stress ratio R and stress amplitude at various mean stresses ^[95].

9.2. General description of Mean Stress Effect

Mean stress effects in fatigue are usually presented as plots of the stress amplitude σ_a versus the corresponding mean stress σ_m according to Haigh, with the life to failure N as a parameter, particular the limiting value of stress cycle N_G in the fatigue tests in case of the endurance limit with the average failure probability $P = 50\%$. With the exception of aluminum alloys, the fatigue endurance limit or the knee in the fatigue curve usually occurs between 10^6 and 10^7 cycles at a given stress. In axial testing, for instance, an absolutely limiting engineering stress would be the tensile strength R_m of the material. For the sake of better comparison and if possible generalization, Haigh diagrams can be presented in a dimensionless version by normalizing the stress amplitude to the fully reversed amplitude at $\sigma_m = 0$ and formulating a stress ratio also for the mean stress on the abscissa, e.g. in axial tests by dividing the mean stress by the tensile strength. A schematic example is given in Figure 9.3 for endurance limits σ_a .

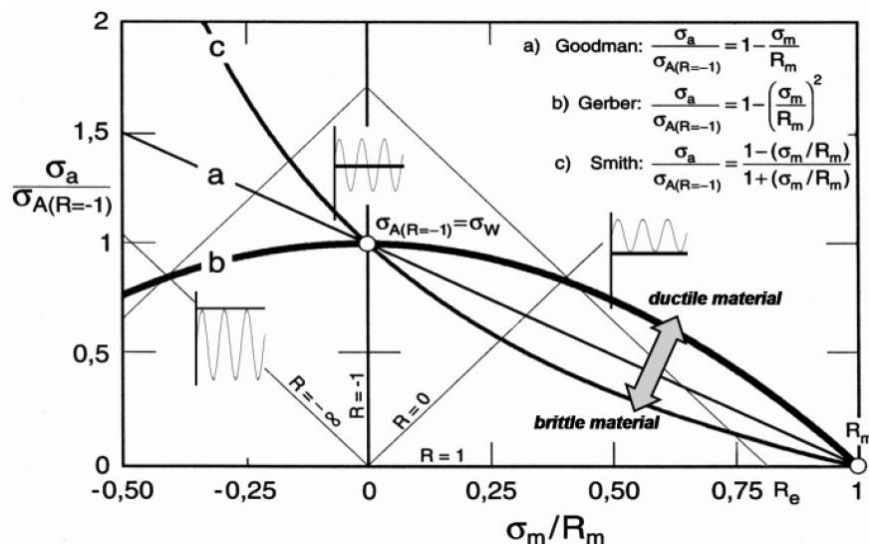


Figure 9.3 – Mean stress effect for endurance limits in non-dimensional form of the amplitude versus mean stress plot according to Haigh and general description models ^[95].

For generalization purposes several types of equations have been proposed. Goodman suggested to estimate the endurable amplitude by a straight line through $\sigma_A/\sigma_{A(R=-1)} = 1$ and $\sigma_m/R_m=1$ which gives reasonable results for partly brittle materials, yet, underestimates the behavior of ductile materials. Gerber introduced a parabola through $\sigma_A/\sigma_{A(R=-1)} = 1$ and $\sigma_m/R_m=1$ which was in fair agreement with experimental observations of ductile materials with positive mean stresses. Additional Smith proposed a progressive description for extremely brittle materials. In general, however, the fatigue performance of materials is not sufficiently described in the form of these simple theoretical models. They are not intended for precise use, but rather to give a picture of the relations involved. In further approaches the endurable amplitude is discontinuously described by straight line segment between certain defined stress ratios R [96] but there are much more flexible relations by higher order polynomials proposed [97, 98] considering material specific mean stress sensitivity, e.g.:

$$\frac{\sigma_A}{\sigma_w} = 1 - p \left(\frac{\sigma_m}{R_m} \right) - (1 - p) \left(\frac{\sigma_m}{R_m} \right)^2 \quad (2)$$

with respect to the sensitivity parameter p [97]. For $p = 1$ in eq. (2) the linear relation by Goodman (line a in figure 9.3) and for $p = 0$ the Gerber parabola relation (linie b in figure 9.3) are resulting. The sensitivity parameter p can be calculated from ultimate tensile strength R_m , reversed axial and pulsating axial endurance limits $\sigma_{A(R=-1)} \equiv \sigma_w$ and $2 \cdot \sigma_{A(R=0)} \equiv \sigma_{Sch}$ respectively, based on constant-load amplitude tests at $R = -1$ and $R = 0$:

$$p = \frac{4 - 2 \frac{\sigma_{A(R=0)}}{\sigma_{A(R=-1)}} - \left(\frac{\sigma_{A(R=0)}}{\sigma_{A(R=-1)}} \right)^2}{\frac{\sigma_{A(R=0)}}{R_m} \left(2 - \frac{\sigma_{A(R=0)}}{R_m} \right)} \quad (3)$$

Unfortunately, however, only very few results of good reliability are reported in the literature. For a given material, there are often no pulsating fatigue strength results at hand. Therefore a statistically backed estimate of the pulsating fatigue strength dependence on the alternating strength amplitude by a two parameter power law was proposed [99, 100].

$$\sigma_{A(R=0)} = K_A \cdot [\sigma_{A(R=-1)}]^q \quad (4)$$

With material group specific parameters K_A and q , which can be gained by regression analysis on basis of a sufficient number of available data pairs. Especially K_A in eq. (4) is affected by the material ductility and indicates the declining, straight line or progressive character of mean stress influence. The accuracy of the proposed eq. (4) was tested by comparing the calculated with the predicted pulsating stress amplitude for about 1700 pairs of data [100].

9.3. Mean Stress Sensitivity Factor

In 1968 Morrow ^[101], differing from Goodman and Gerber, underlined that the mean stress could go beyond the ultimate strength of the material reaching the fatigue strength coefficient that represents the highest stress amplitude that may produce failure in a single cycle, which is the true failure stress of the material. The Resulting Morrow line is shown in Figure 9.4.

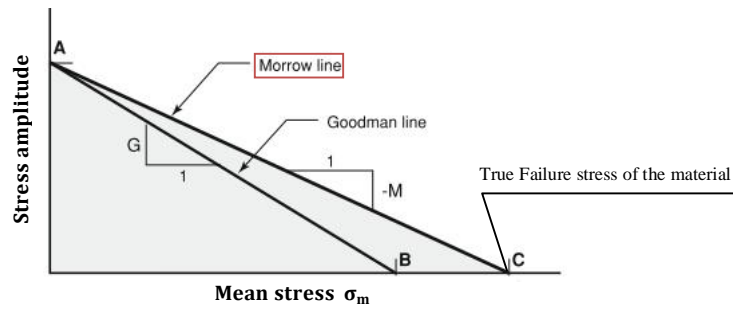


Figure 9.4 - Goodman and Morrow models to take into consideration the mean stress effect. Adapted ^[102].

The Morrow M factor appears to be a function of material and mean stress ^[103, 104] and for that reason is also known as mean stress sensitivity factor. For low values of the mean stress ($-1 \leq R < 0$) the Morrow's factor is indicated by letter M and its value, referring to Figure 9.5, is given by:

$$M = \tan \alpha = \frac{\sigma_a}{\sigma_m} = \frac{1 - R}{1 + R}$$

$$M = \tan \alpha = \frac{\sigma_{a,(R=-1)} - \sigma_{a,(R=0)}}{\sigma_{a,(R=0)}} = \frac{\sigma_{a,(R=-1)}}{\sigma_{a,(R=0)}} - 1$$

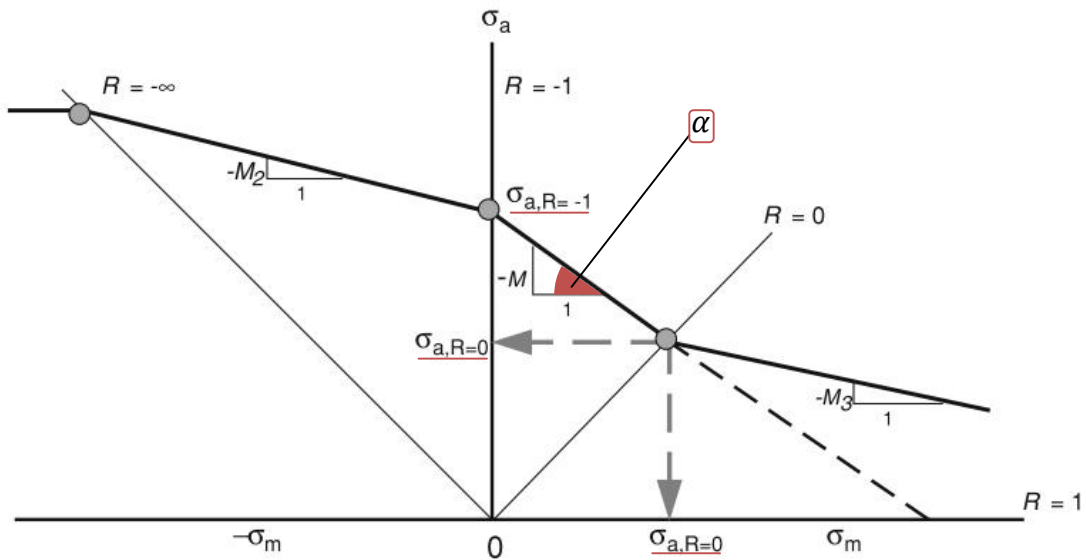


Figure 9.5 - Haigh diagram showing the mean stress sensitivity factor M and its dependence on the mean stress. Adapted ^[102].

Large values of M indicate a high σ_m sensitivity. In the negative mean stress quadrant ($-\infty \leq R < -1$) it is indicated by M_2 while for high mean stress values ($0 \leq R < 1$) it is referred to as M_3 . Usually, M_3 is lower than M by a factor of 3 ($M_3 \approx 1/3 M$).

Mean Stress Sensitivity in FKM

The *FKM Guideline* ^[105] presents a formula for the calculation of this mean stress sensitivity for normal stress (M_σ) in non-welded components in case of normal or elevated temperature:

$$M_\sigma = a_M \cdot 10^{-3} \cdot R_m / \text{MPa} + b_M$$

Where a_M and b_M are constants depending on the material as shown in table:

Table 9.1 – Constants a_M and b_M for different materials ^[105]

Maerial Group	Steel	GS	GJS	GJM	GJL
a_M	0.35	0.35	0.35	0.35	0
b_M	-0.1	0.05	0.08	0.13	0.5

Therefore {

- For Ductile Iron (GJS) $\rightarrow M_\sigma = a_M \cdot 10^{-3} \cdot R_m(\text{MPa}) + b_M$
 $M_\sigma = 0.35 \cdot 10^{-3} \cdot 900 + 0.08$
 $M_\sigma = 0.395$
- For Steel ER7 $\rightarrow M_\sigma = a_M \cdot 10^{-3} \cdot R_m(\text{MPa}) + b_M$
 $M_\sigma = 0.35 \cdot 10^{-3} \cdot 880 + (-0.1)$
 $M_\sigma = 0.208$

Chapter 10

10. NON DESTRUCTIVE TESTING OF WHEELS (NDT)

10.1. Introduction

Wheel-sets of rail vehicles are safety relevant components. A failure on them may cause serious accidents with personal injury as major consequence between many others. For this reason, the wheel-sets of all kind of passenger and freight trains are subject to a permanent control.

Due to the long history of railroad companies around the world, varying means of examination according to the specifications for the different railroad components have been carried out based on the general industrial progress of the country ^[106–108]. For more than 50 years the application of customized ultrasonic techniques for the examination of railroad components has increased, in comparison to conventional ultrasonic techniques used until the end of 20th century. More than ever, with safety always in mind, it is required that advanced examination techniques take part within the wheelsets. For practical application new ultrasonic and eddy current techniques ^[108–110] have been developed and optimized in cooperation with Die Bahn AG.

10.2. Non-destructive testing of ADI castings

Successful production of Austempered ductile iron components in a reliable way requires a lot of care. Operations in the foundry, heat treatment and later machining must be carried out in a consistent proper way. Main concern is usually regarding the difficulty of ensuring that every ADI component meets the minimum specified properties. These properties are tightly linked to composition and the heat treatment parameters of the process. For this reason, non destructive techniques enable a proper assessment of the quality while keeping the component undamaged.

The general conditions for the production and distribution of Austempered Ductile iron come from DIN EN 1564 ^[126, 127]. The monitoring of the ADI production process by non-destructive testing targets three groups of errors ^[128]:

- *Casting defects*: poor nodularity, inclusions, pores and micro cavities.
- *Heat treatment defects*: Insufficient carbon content in the Austenite by a non-optimal Austenitizing time and/or temperature, pearlite formation because of slow quenching or transformation of Austenite into Martensite.
- *Other errors*: lack of coordination of alloying and microstructure.

The complex task behind a non-destructive examination can be better understood through Figure 10.1, where the only fixed variables are the customer requirements.

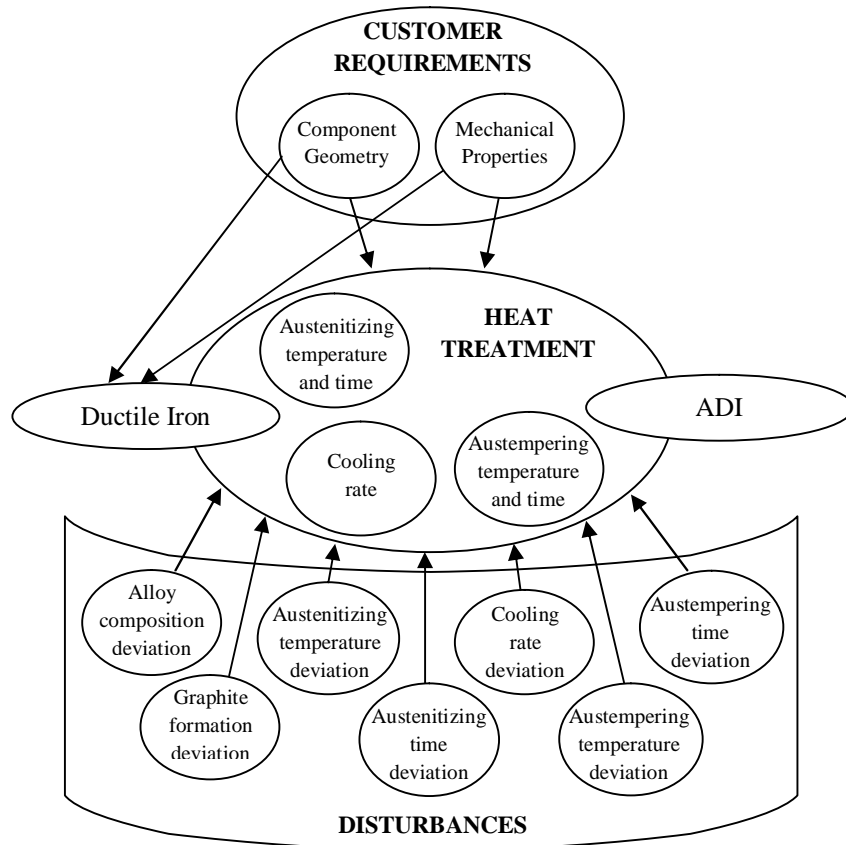


Figure 10.1 Complexity of the task behind a non-destructive examination. Adapted ^[129].

10.3. Inspection of Rolling Surface and Tread

10.3.1. In-motion inspection of the rolling surface of the wheel

In modern rail traffic the rolling surface of wheels is exposed to high dynamic loads due to an increase of speed as well as a higher rate of service time. The development of cracks is monitored by periodic non-destructive testing. Apart from visual testing, objectively operating automated testing methods are necessary to be used directly at the vehicle without special manipulations.

The Fraunhofer Institute for Nondestructive Testing (IZFP) in Germany has developed in close co-operation with the German Railway Company (Deutsche Bahn AG) methods and equipment for in-service inspection of wheel-sets in maintenance stations without dismounting the wheel sets.

The system detects critical defects whilst the vehicle passes over ultrasonic transducers embedded in the rail heads. Four couplant-free operating EMAT transducers are applied for the inspection, two each per rail. As soon as the wheel gets into contact with a transducer, a Rayleigh surface wave is transmitted as shown in Figure 10.2. The wheel is circulated several times by the ultrasonic pulse and, consequently, a series of repetition echoes (round-trip signals) is detected by the receiver if the rolling surface is undamaged.

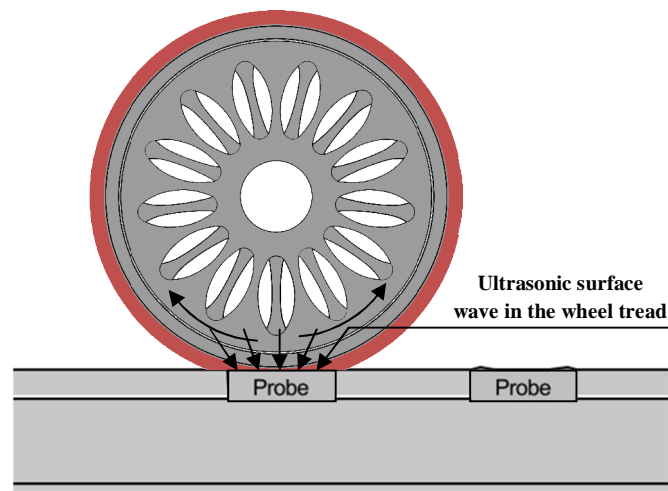


Figure 10.2 - Testing principle

Figure 10.3 shows the construction of the transducer. The transducer coil is passed by an alternating-current pulse inducing eddy-currents in the rolling surface. The coil is positioned near to the transducer contact area. By means of an electromagnet a steady magnetic field is generated which penetrates the rolling surface perpendicularly, superimposing the eddy-currents. Through Lorentz forces a deflection of the metal lattice takes place, thus generating an elastic wave. The ultrasonic testing frequency is equal to the frequency of the applied alternating-current pulse.

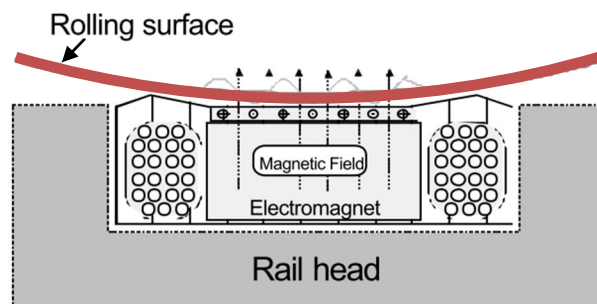


Figure 10.3 - Construction of the EMAT transducer. Adapted ^[113].

If the rolling surface is undamaged, only the round-trip signals (RT) will be received by the EMAT transducer. In case damages exist such as cracks or material shelling or spalling, apart from the round-trip signals (RT), echoes (E) of these defects will be registered as shown in Figure 10.4.

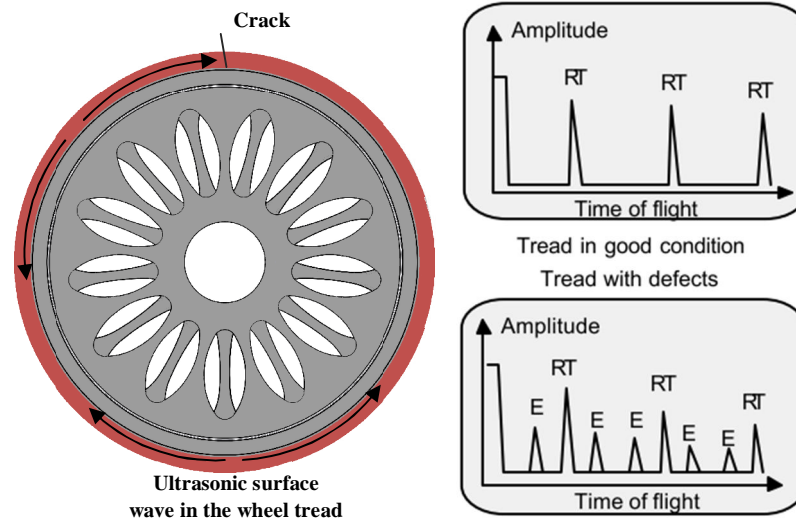


Figure 10.4 -. Schematic A-scan for undamaged and damaged tread of wheel. Adapted ^[113].

The evaluation of the recorded ultrasonic signals is performed by computer programs according to criteria considering amplitude values of the echoes and signal form. For each wheel a status class is determined and transferred to the central computer system at the maintenance facilities. License has been given to the company *Hegenscheidt* in Germany for industrial production and sales of the inspection equipment.

10.3.2. Detection and sizing of crack like defects in the tread

The high loads acting to railroad wheels can result in surface breaking cracks in the tread of the wheel. By routine non-destructive inspection the development of cracks is controlled. A technique for the fast detection and localization of crack-like defects using ultrasonic surface waves propagating in the near surface zone of the wheel, which is in field operation since some years for the In-Service Inspection (ISI) of the wheels of the German High-speed Train ICE was described in the previous section 10.3.1. Once a crack in the tread has been detected its depth is of most interest first due to safety considerations and second due to economic aspects.

With the exact knowledge of the crack depth, e.g. the depth of cut during re-shaping of the tread can be minimized saving manpower and material costs. To localize a crack-like defect and to determine its depth an ultrasonic technique has been developed which is based on the mode conversion of linearly polarized shear waves ^[114, 115]. The transducer is positioned at the inside surface of the rim as shown in Figure 10.5.

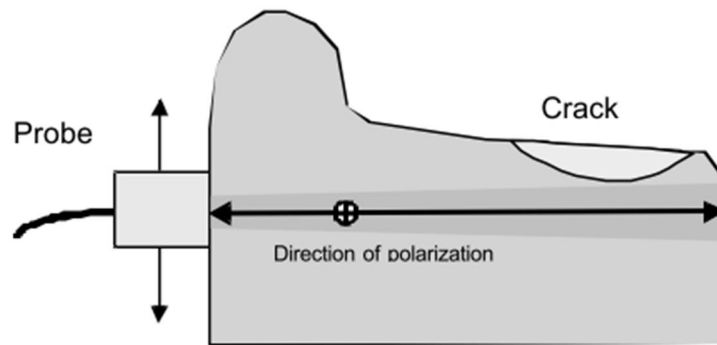


Figure 10.5 - Principle of the testing method ^[113].

The beam direction is normal to the surface; the polarization of the shear wave is in circumferential direction. By the use of couplant free electromagnetic acoustic transducers (EMAT's) a simple way to generate the shear motion inside the wheel is assured. In case there is a crack-like defect with transversal orientation (with respect to the circumferential direction of the wheel) within the sound field of the transducer, a part of the shear wave is mode-converted into a surface wave travelling along the flanks of the crack and reducing the amplitude of the reflected backwall echo (BWE).

This effect has a very steep local gradient and can easily be differentiated from any other effects also reducing the echo-amplitude. Besides the change in amplitude there is also a phase shift of the BWE which is a further reliable indicator for the presence of a crack-like defect.

When the probe is approaching a defect, the amplitude of the BWE first increases slightly and drops down when the probe index is at the position of the crack. The amount of this amplitude drop depends on that part of the sound-field interacting with the defect, which means it depends on the depth of the defect and on the beam spreading of the probe.

The depth of a defect is determined by moving the transducer in radial direction towards the center of the wheel and finding out that position of the transducer at which the BWE has the same level like at defect free positions.

The construction of the EMAT probes, which are used to generate the linearly polarized shear waves, is sketched in Figure 10.6. By two permanent-magnets with opposite magnetic polarity and a soft iron yoke a magnetic field is generated which penetrates the RF-coils of transmitter and receiver perpendicularly. These are flat rectangular coils and generate together with the magnetic field the transversal displacement-field. The effective aperture of the probe is 20 x 20 mm².

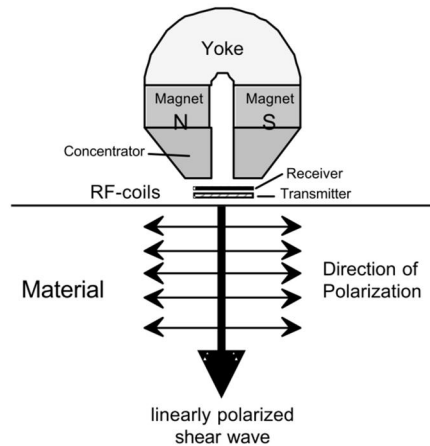


Figure 10.6 - Principle of the EMAT probe ^[113]

First results of manual inspections performed at test specimen with artificial defects (saw cuts), at samples of wheel tyres with real defects as well as at complete wheel-sets showed that the evaluation of the amplitude of the first BWE is not reliable enough for the detection and localization of cracks. The amplitude is also influenced by other parameters, e.g. surface conditions, which can lead to amplitude drops of the BWE similar to those caused by a defect. However the ALC (Amplitude Locus Curve) of the BWE recorded by scanning the probe along the circumference of the wheel shows a characteristic pattern with strong gradients caused by a crack-like defect, i.e. increase of the amplitude before and behind the main amplitude drop.

10.4. Wheel spoke inspection

Unfortunately, due to the complex geometry that a spoke wheel represents, the performance of the current nondestructive inspection techniques is not sufficient for the spokes in terms of detection sensitivity, quantitative evaluation and field applicability. For this reason, alternative nondestructive testing and evaluation techniques based on electrical potential application are suggested and presented.

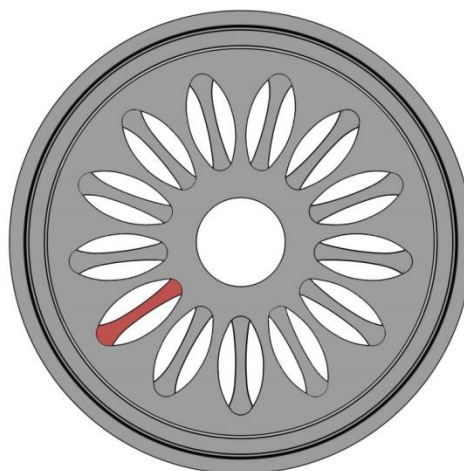


Figure 10.7 – Front side of the wheel with one of the many spokes for inspection highlighted.

Potential drop (PD) methods can detect and size defects with high sensitivity, as well as monitor them under on-line condition. They are divided in two groups, namely Direct Current Potential Drop (DCPD) technique and Alternative Current Potential Drop (ACPD) technique. Generally, the measurements are performed using a pair of measurement terminals and a pair of current terminals which are spot welded to the specimen. In order to scanning the specimen, the sensor contains a pair of terminal pins for current supply and measurement ^[116].

10.4.1. Potential Drop Methods

The Potential Drop (PD) method is based on a change of the electrical resistance with the change of the specimen cross section area. For a constant current flow, the electric potential or voltage difference across the crack plane will increase with increasing crack size due to modification of the electrical field and associated perturbation of the current lines. This method is applicable for any electric conductive material in wide range of testing environments ^[117].

Standard Methods

As said, there are two basic variations of potential drop method, the AC potential drop and DC potential drop. As their respective names suggest, either an alternating or direct current is passed through the specimen under test and the resultant potential developed between two points on the specimen is monitored. If a constant current is used then the initiation or propagation of a defect, sited between the two voltage measurement points, will lead to an increase in the measured voltage. In essence, both techniques, detect a change in the specimen resistance (or the impedance in the case of ACPD) and this can be interpreted as either the initiation or propagation of a defect such as a crack ^[117].

The simplest implementation of the potential drop method requires four electrical connections, appropriately placed as shown below in Figure 10.8 and linked to suitable current generation and measurement apparatus.

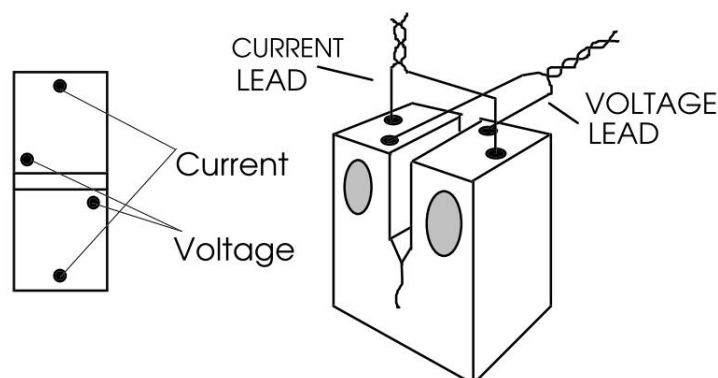


Figure 10.8 – Implementation of the potential drop method ^[122].

Naturally there are further considerations to both the DCPD and ACPD techniques and knowledge of these is required before any meaningful data can be obtained. In this way, the measurement with use of the potential drop is affected by many factors, the most important are: current level, current input/output location, potential drop measuring locations and frequency in case of ACPD. To attain the highest sensitivity the measuring points should be as close to the crack plane as possible.

ACPD offers some advantages over DCPD, not least of which is the greater degree of sensitivity to the presence of a defect. Additionally ACPD requires a constant current supply that is an order of magnitude below that of DCPD, thus permitting a commensurate reduction in the thickness of the supply leads. ACPD equipment tends, however, to be more sophisticated and therefore more costly and the technique is not as conceptually simple to understand as DCPD.

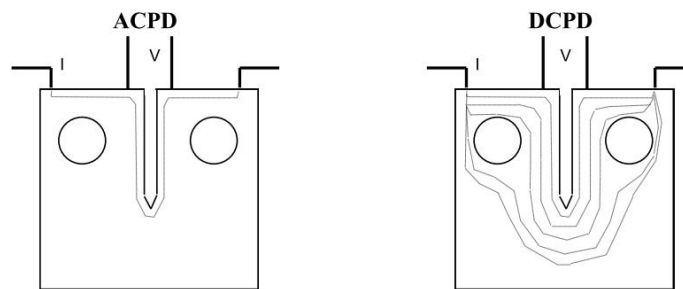


Figure 10.9 - Current flow lines in a typical CT specimen ^[123].

The measurement with use of the potential drop is affected by many factors, the most important are: current level, current input/output location, potential drop measuring locations and frequency in case of ACPD. The crack length measurement by both ACPD as well as DCPD method is using the relation of the crack length to the potential change in the crack extension region. The calibration curve should be determined for each tested material to provide reliable results. Formulas for the crack length calculation can be found ^[118-121].

When using the PD method, it is important not to compromise the integrity of the contacts by the action of the corrosive media. Thus, resistant materials such as nickel, silver or platinum are used as appropriate. Electrical contact can be made either mechanically, for example, by clamping or by using a screwed connection, or alternatively by a bonding method such as spot welding.

A further electrochemical consideration is the fact that traditional DCPD methods can often cause enhanced corrosion both at the point of electrical contact and, more seriously, at the crack site. This is because the DC current causes a potential drop which can drive a corrosive chemical reaction, similar in this respect to electrochemical etching. Unfortunately, this is a prime example of an experimental result being affected by the method employed to observe it.

Such detrimental effects can be countered by using a pulsed direct current technique. Here the excitation current is passed through the specimen for a short period of time and then turned off. This is repeated at regular intervals. Measurements of the DCPD are taken during the *on* period. A schematic of a pulsed DC system is shown below in Figure 10.10 for a particular spoke inspection.

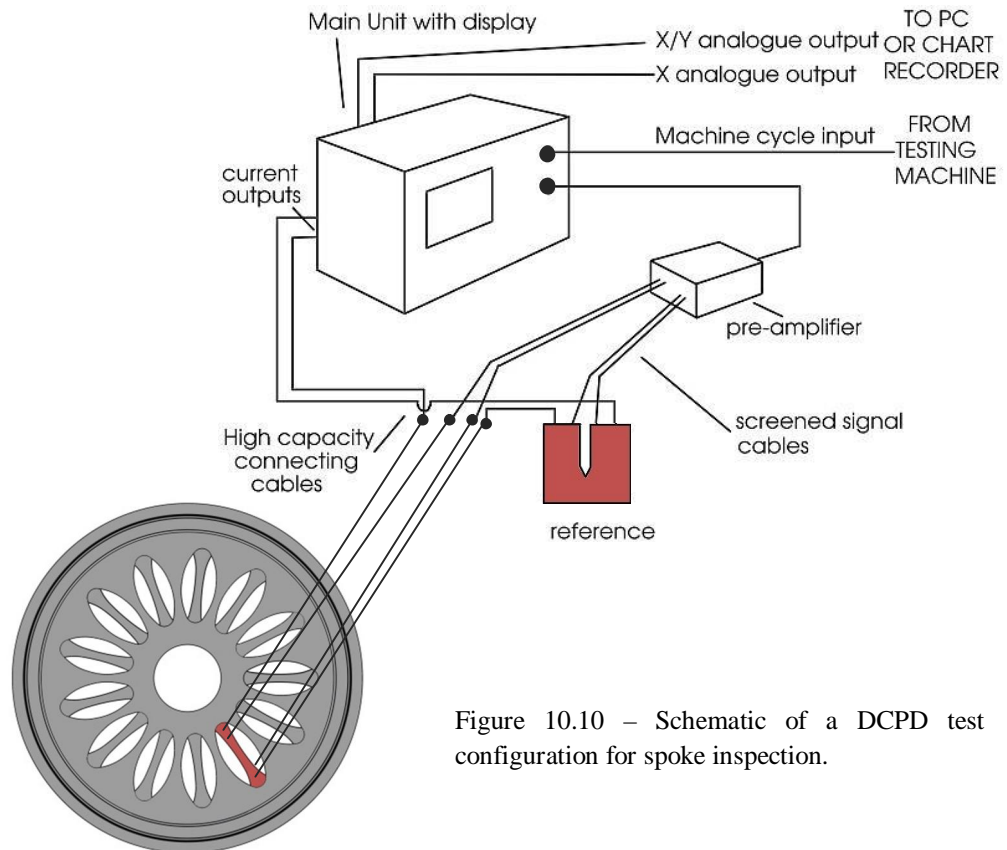


Figure 10.10 – Schematic of a DCPD test configuration for spoke inspection.

The fact that the current is pulsed means that, on average, a reduction in the electrochemical effects is observed. By adjustment of the *on* with respect to the *off* periods, users can largely eliminate these effects.

A better method would be to reverse the DC current at regular intervals. Reversing DCPD was developed for this very purpose. The technique is not common and the equipment tends to be expensive. More importantly, the pulse widths utilized still give rise to electrochemical effects within each *cycle*.

Conceptually, the step from reversing DCPD to ACPD is small and the distinction between the two is, at first, difficult to see. However, a difference does indeed exist. This subtlety is responsible for two further enhancements in the use of PD methods for stress corrosion studies. The reversing frequency of a DC system is very much less than that of an AC instrument. In the latter case, frequencies of 10-100 kHz are usually employed, with research work being conducted at even higher values.

Unlike DCPD, at these frequencies, the excitation current flows non uniformly through the specimen with more current flowing in the surface regions than through the bulk. This phenomenon is known as the skin effect and its occurrence leads to several significant advantages of ACPD over DCPD.

Since most defects originate and propagate from the specimen surface, it is sensible to confine the excitation current to these regions, thereby maximizing sensitivity to the initiation or propagation of the said defects. This is also the reason why the ACPD technique utilizes lower specimen currents - less current is required to obtain a similar defect sensitivity.

Additionally, using alternating currents naturally gives rise to an alternating voltage. Sophisticated electronics can then be employed to lock-in to the frequency of the AC voltage and measure its magnitude. This effectively eliminates other frequencies that usually manifest themselves as noise on the signal of interest.

A reduction in noise further improves the resolution of the potential drop technique. Thanks to its increased sensitivity, ACPD is often used to detect defect initiation in addition to the monitoring of defect propagation. In conclusion, potential drop techniques offer a highly effective method of obtaining information on stress corrosion cracking. Their main advantages lie in their simplicity of operation, ease of integration and sensitivity to the phenomenon under investigation.

As a conclusion, both DC and AC potential drop techniques can be used to monitor initiation and propagation of defects in electrically conducting materials. ACPD offers the highest sensitivity with the minimum detrimental electrochemical interaction, whilst DCPD equipment tends to be cheaper and still maintains a popular following.

Chapter 11

11. FACTOR OF SAFETY AS DESIGN VARIABLE

(Determination of the minimum fatigue strength for accepting track service of the ADI wheels)

11.1 Introduction

The factor of safety is a factor of ignorance. If the applied stress on a part at a critical location is known precisely, if the material's strength (allowable strength) is also known with precision, and the allowable strength is greater than the applied stress, then the part will not fail.

However, in the real world, all of the aspects of the design have some degree of uncertainty, and therefore a factor of safety is needed. A factor of safety is one way to account for the uncontrollable *noises* caused by uncertainties in knowledge about the material properties, the load causing the stress, unit-to-unit variations, and the ability to analyze failure. In practice the factor of safety is used in one of three ways:

1. It can be used to reduce allowable strength, such as the yield or ultimate strength of the material, to a lower level for comparison with the applied stress;
2. It can be used to increase applied stress for compare with allowable strength;
3. It can be used as a comparison for the ratio of the allowable strength to the applied stress as we apply here, but all three are based on the simple formula:

$$FS = \frac{S_{al}}{\sigma_{ap}}$$

Here S_{al} is the allowable strength, σ_{ap} is the applied stress, and FS is the factor of safety. If the material properties are known precisely and there is no variation in them (as well as for the load and geometry), then the part can be designed with a factor of safety of 1, the applied stress can be equal to the allowable strength, and the resulting design will not fail. However, not only are these measures not known with precision, they are not constant from sample to sample or use to use. In a statistical sense all these measures have some variance about their mean values.

For example, typical material properties, such as ultimate strength, even when measured from the same bar of material, show a distribution of values (a variance) around a nominal mean of about 5%. This distribution is due to inconsistencies in the material itself and in the instrumentation used to take the data. If strength figures are taken from handbook values based on different samples and instrumentations, the variance of the values may be 15% or higher. Thus, the allowable strength must be characterized as a nominal or mean value with some statistical variation about it.

Even more difficult to establish are the statistics of the applied stress. The exact magnitude of the applied stress is a factor of the loading on the part (the forces and moments on the part), the geometry of the part at the critical location, and the accuracy of the analytic method used to determine the stress at the critical point due to the load.

The accuracy of the comparison of the applied stress to the allowable strength is a function of the accuracy and applicability of the failure theory used. If the stress is steady and the failure mode yielding, then accurate failure theories exist and can be used with little error. However, if the stress state is multiaxial and fluctuating (with a non-zero mean stress), there are no directly applicable failure theories and the error incurred in using the best available theory must be taken into account.

11.2 The Statistical Reliability-Based Factor of Safety

The classical approach to establishing factors of safety is not very precise and the tendency is to use it very conservatively. This results in large factors of safety and overdesigned components. Consider now the approach based on statistical measures of the material properties, of the stress developed in the component, of the applicability of the failure theory, and of the reliability required. This technique gives the designer a better feel for just how conservative, or non-conservative, he or she is being.

With this technique, all measures are assumed to have normal distributions. This assumption is a reasonable one, though not as accurate as the Weibull distribution for representing material-fatigue properties. What makes the normal distribution an acceptable representation of all the measures is the simple fact that, for most of them, not enough data are available to warrant anything more sophisticated. In addition, the normal distribution is easy to understand and work with. In upcoming sections, each measure is discussed in terms of the two factors needed to characterize a normal distribution—the mean and the standard deviation (or variance).

The factor of safety is defined as the ratio of the allowable strength, S_{al} , to the applied stress, σ_{ap} . The allowable strength is a measure of the material properties; the applied stress is a measure of the stress (as a function of both the applied load and the stress analysis technique used to find the stress), the geometry, and the failure theory used. Since both of these measures are distributions, the factor of safety is better defined as the ratio of their mean values:

$$FS = \frac{\bar{S}_{al}}{\bar{\sigma}_{ap}}$$

Figure 9.1 shows the distribution about the mean for both the applied stress and the allowable strength. There is an area of overlap between these two curves no matter how large the factor of safety is and no matter how far apart the mean values are. This area of overlap is where the allowable strength has a probability of being smaller than the applied stress; the area of overlap is thus the region of potential failure. Keeping in mind that areas under normal distribution curves represent probabilities, we see that this area of overlap then is the Probability of Failure (*PF*). The reliability, the probability of no failure, is simply $1 - PF$. Thus, by considering the statistical nature of these curves, the factor of safety is directly related to the reliability.

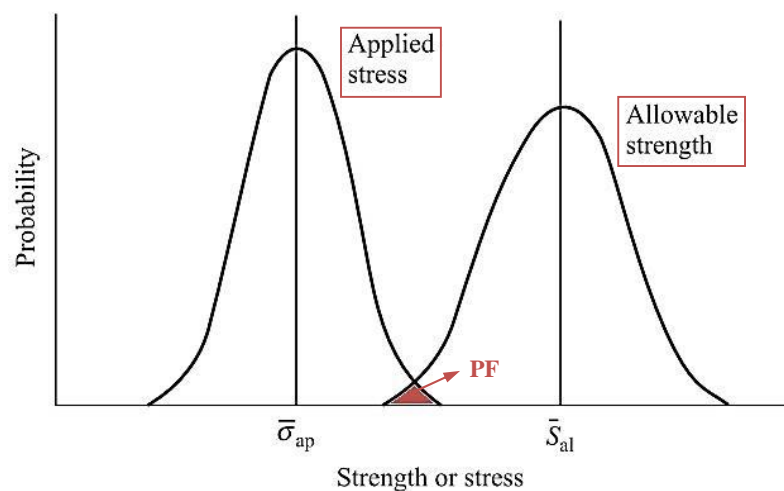


Figure 11.1 - Distribution of applied stress & allowable strength. Adapted ^[124].

To develop this relationship more formally, we define a new variable, the difference between the allowable strength and the applied stress:

$$z = S_{al} - \sigma_{ap}$$

Therefore, we have that:

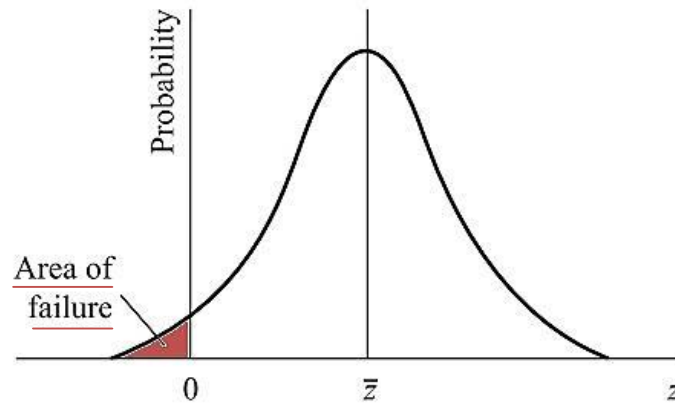
- If $z > 0$, then the part will not fail.
- If $z \leq 0$, then failure will occur.

The distribution of z is also normal (the difference between two normal distributions is also normal), as shown in Figure 11.2. The mean value of z is simply:

$$\bar{z} = \bar{S}_{al} - \bar{\sigma}_{ap}$$

If the allowable strength and the applied stress are considered as independent variables (which is the case), then the standard deviation of z is:

$$\rho_z = \sqrt{\rho_{al}^2 + \rho_{ap}^2}$$

Figure 11.2 - Distribution of z . Adapted ^[124].

Normalizing any value of z by subtracting the mean and dividing by the standard deviation, we can define the variable t_z as:

$$t_z = \frac{(S_{al} - \sigma_{ap}) - (\bar{S}_{al} - \bar{\sigma}_{ap})}{\sqrt{\rho_{al}^2 + \rho_{ap}^2}}$$

The variable t_z has a mean value of 0 and a standard deviation of 1. Since failure will occur when the applied stress is greater than the allowable stress, a critical point to consider is when $z = 0$, $S_{al} = \sigma_{ap}$. So, for $z = 0$ we have:

$$t_{z=0} = \frac{-(\bar{S}_{al} - \bar{\sigma}_{ap})}{\sqrt{\rho_{al}^2 + \rho_{ap}^2}}$$

Thus, any value of t that is calculated to be less than $t_{z=0}$ represents a failure situation. The probability of a failure is then $Pr(t_z < t_{z=0})$, which, assuming the normal distribution, can be found directly from a normal distribution table. If the distributions of the applied stress and the allowable strength are known, $t_{z=0}$ can be found from the preceding equation and the probability of failure can be found from normal distribution tables. Finally, the reliability is 1 minus the probability of failure:

$$R = 1 - Pr(t_z \leq t_{z=0})$$

Using a cumulative standard normal distribution table will be easier by utilizing the symmetry of the distribution, so we can drop the minus sign on the preceding equation and consider values of $t_z > t_{z=0}$ to represent failure.

To reduce the equations to a usable form in which the factor of safety is the independent variable, we rewrite the previous equation, dividing by the mean value of the applied stress and using the definition of the factor of safety:

$$t_{z=0} = \frac{FS - 1}{\sqrt{FS^2 \left(\frac{\rho_{al}}{\bar{S}_{al}}\right)^2 + \left(\frac{\rho_{ap}}{\bar{\sigma}_{ap}}\right)^2}}$$

With $t_{z=0}$ directly dependent on the reliability, there are four variables related by this equation: the reliability, the factor of safety, and the coefficients of variation (standard deviation divided by the mean) for the allowable and applied stresses.

The relation therefore between the reliability and $t_{z=0}$ can be guessed from cumulative standard normal distribution table like table 11.1 below. Then for our desired reliability of 99.7% we look for the percentile 0,9970 and proceed as it follows :

$$t_{z=0} = 2,7 + 0,05 = 2,75$$

Table 11.1 - Standard normal distribution table. Cumulative probabilities for positive z-values.

z	0.00	0.01	0.02	0.03	0.04	0.05	0.06	0.07	0.08	0.09
0.0	0.5000	0.5040	0.5080	0.5120	0.5160	0.5199	0.5239	0.5279	0.5319	0.5359
0.1	0.5398	0.5438	0.5478	0.5517	0.5557	0.5596	0.5636	0.5675	0.5714	0.5753
0.2	0.5793	0.5832	0.5871	0.5910	0.5948	0.5987	0.6026	0.6064	0.6103	0.6141
0.3	0.6179	0.6217	0.6255	0.6293	0.6331	0.6368	0.6406	0.6443	0.6480	0.6517
0.4	0.6554	0.6591	0.6628	0.6664	0.6700	0.6736	0.6772	0.6808	0.6844	0.6879
0.5	0.6915	0.6950	0.6985	0.7019	0.7054	0.7088	0.7123	0.7157	0.7190	0.7224
0.6	0.7257	0.7291	0.7324	0.7357	0.7389	0.7422	0.7454	0.7486	0.7517	0.7549
0.7	0.7580	0.7611	0.7642	0.7673	0.7704	0.7734	0.7764	0.7794	0.7823	0.7852
0.8	0.7881	0.7910	0.7939	0.7967	0.7995	0.8023	0.8051	0.8078	0.8106	0.8133
0.9	0.8159	0.8186	0.8212	0.8238	0.8264	0.8289	0.8315	0.8340	0.8365	0.8389
1.0	0.8413	0.8438	0.8461	0.8485	0.8508	0.8531	0.8554	0.8577	0.8599	0.8621
1.1	0.8643	0.8665	0.8686	0.8708	0.8729	0.8749	0.8770	0.8790	0.8810	0.8830
1.2	0.8849	0.8869	0.8888	0.8907	0.8925	0.8944	0.8962	0.8980	0.8997	0.9015
1.3	0.9032	0.9049	0.9066	0.9082	0.9099	0.9115	0.9131	0.9147	0.9162	0.9177
1.4	0.9192	0.9207	0.9222	0.9236	0.9251	0.9265	0.9279	0.9292	0.9306	0.9319
1.5	0.9332	0.9345	0.9357	0.9370	0.9382	0.9394	0.9406	0.9418	0.9429	0.9441
1.6	0.9452	0.9463	0.9474	0.9484	0.9495	0.9505	0.9515	0.9525	0.9535	0.9545
1.7	0.9554	0.9564	0.9573	0.9582	0.9591	0.9599	0.9608	0.9616	0.9625	0.9633
1.8	0.9641	0.9649	0.9656	0.9664	0.9671	0.9678	0.9686	0.9693	0.9699	0.9706
1.9	0.9713	0.9719	0.9726	0.9732	0.9738	0.9744	0.9750	0.9756	0.9761	0.9767
2.0	0.9772	0.9778	0.9783	0.9788	0.9793	0.9798	0.9803	0.9808	0.9812	0.9817
2.1	0.9821	0.9826	0.9830	0.9834	0.9838	0.9842	0.9846	0.9850	0.9854	0.9857
2.2	0.9861	0.9864	0.9868	0.9871	0.9875	0.9878	0.9881	0.9884	0.9887	0.9890
2.3	0.9893	0.9896	0.9898	0.9901	0.9904	0.9906	0.9909	0.9911	0.9913	0.9916
2.4	0.9918	0.9920	0.9922	0.9925	0.9927	0.9929	0.9931	0.9932	0.9934	0.9936
2.5	0.9938	0.9940	0.9941	0.9943	0.9945	0.9946	0.9948	0.9949	0.9951	0.9952
2.6	0.9953	0.9955	0.9956	0.9957	0.9959	0.9960	0.9961	0.9962	0.9963	0.9964
2.7	0.9965	0.9966	0.9967	0.9968	0.9969	0.9970	0.9971	0.9972	0.9973	0.9974
2.8	0.9974	0.9975	0.9976	0.9977	0.9977	0.9978	0.9979	0.9979	0.9980	0.9981
2.9	0.9981	0.9982	0.9982	0.9983	0.9984	0.9984	0.9985	0.9985	0.9986	0.9986
3.0	0.9987	0.9987	0.9987	0.9988	0.9988	0.9989	0.9989	0.9989	0.9990	0.9990
3.1	0.9990	0.9991	0.9991	0.9991	0.9992	0.9992	0.9992	0.9992	0.9993	0.9993
3.2	0.9993	0.9993	0.9994	0.9994	0.9994	0.9994	0.9994	0.9995	0.9995	0.9995
3.3	0.9995	0.9995	0.9995	0.9996	0.9996	0.9996	0.9996	0.9996	0.9996	0.9997
3.4	0.9997	0.9997	0.9997	0.9997	0.9997	0.9997	0.9997	0.9997	0.9997	0.9998

In the development here, the unknown will be the factor of safety. Thus, the final form of the statistical factor of safety equation is as follows:

$$FS = 1 + t_{z=0} \cdot \frac{\sqrt{\left(\frac{\rho_{al}}{\bar{S}_{al}}\right)^2 + \left(\frac{\rho_{ap}}{\bar{\sigma}_{ap}}\right)^2 - t_{z=0}^2 \cdot \left(\frac{\rho_{ap}}{\bar{\sigma}_{ap}}\right)^2 \cdot \left(\frac{\rho_{al}}{\bar{S}_{al}}\right)^2}}{1 - t_{z=0}^2 \cdot \left(\frac{\rho_{al}}{\bar{S}_{al}}\right)^2}$$

Continuing with the solving, it must be noted that in our particular case the applied stress ($\bar{\sigma}_{ap}$) is going to be a fixed value. This concrete value is set according with the standard DIN EN 13979-1^[125], which establish a value of 145 MPa. Reason behind considering always 145 MPa, is that of guarantee that such a stress level will never be reached, working always on a lower and safer stress level. Direct consequence of this is the absence of allowable strength standard deviation (ρ_{al}), fact which will simplify considerably the previous equation. Now according to this and using again the definition of factor of safety as $\bar{S}_{al}/\bar{\sigma}_{ap}$, we come out with a substantial reduced easier equation:

$$FS = \frac{\bar{S}_{al}}{\bar{\sigma}_{ap}} = 1 + t_{z=0} \cdot \sqrt{\left(\frac{\rho_{ap}}{\bar{\sigma}_{ap}}\right)^2}$$

And continuing with the solving, an equation depending of three terms is obtained:

$$\bar{S}_{al} = \bar{\sigma}_{ap} + t_{z=0} \cdot \rho_{ap}$$

In this way, we are already in position to calculate the allowable strength (\bar{S}_{al}), which will be the stress value we are looking for in our test application on the wheel. Therefore, with a fixed applied stress ($\bar{\sigma}_{ap}$) of 145 MPa, a value $t_{z=0}$ associated with a 99.7% reliability and a reasonable standard deviation of 20 MPa for the applied stress (ρ_{ap}) we obtain:

$$\bar{S}_{al} = 145 \text{ MPa} + 2.75 \cdot 20 \text{ MPa} = 200 \text{ MPa}$$

11.3 Conclusion

In order to achieve always an applied stress of 145 MPa on the component that ensures us to be working under a safer lower stress level, we must apply for our test 200 MPa

Chapter 12

12. SUMMARY AND CONCLUSIONS

12.1. ADI as general alternative engineering material

There is no doubt that ADI is a unique engineering material. It is produced by giving conventional ductile iron a special isothermal heat treatment known as austempering which provides it with an excellent combination of strength and ductility, together with good fatigue and wear properties.

While the steps for ADI are essentially the same as those for steel, the resultant microstructure is different. It is called Ausferrite and consists of a mixture of high carbon Austenite and ferrite.

The great combination of properties in ADI has therefore opened new horizons for cast irons to replace steel castings and forgings in many engineering applications with important cost benefits.

➤ *What ADI is not*

- It is not a remedy for casting defects. It does not weld cracked castings, nor does it fill shrinkage holes. It does not eliminate eutectic carbides. Austempering is therefore not the cure for poor quality as it will make bad iron even worse.
- It is not a substitute for process control. On the contrary, it requires tight and strict process control. Any discrepancy in the casting process will be amplified by the subsequent heat treating.
- Although ADI has a broad range of applications, it is not a solution to every engineering problem.

➤ *What ADI is*

- ADI is a material which is strong, light, wear resistant, fatigue resistance and better damper of vibration than steel. In addition, ADI provides high design and manufacturing flexibility, and is relatively inexpensive.
- ADI is stronger per unit weight than aluminum, as wear resistant as steel and has potential for up to 50% cost savings.
- In general, ADI may be characterized as an alloyed and heat treated ductile cast iron with properties that are highly versatile. Its Ausferritic matrix is unique to cast irons, and it should not be viewed as special steel with graphite particles dispersed within it.

12.2. ADI as potential rail wheel material

Within the railway sector, the remarkable properties of ADI are able to meet the demands for quieter and lighter wheels while at the same time reducing life-cycle costs. When compared to steel, ADI shows three times more damping capacity, promising in consequence a remarkable decrease concerning the travelling noise problem. Regarding its maintenance, ADI is also superior to steel due to its self-lubricating behavior on the rail to wheel contact. An additional important advantage of ADI over steel is its 10% lower density, allowing this for a substantial weight reduction due to the presence of graphite nodules in the matrix structure.

➤ *Current wheel materials*

As a proper response to the known mechanisms of damage, the materials employed in wheels and rails all around Europe are basically steels whose predominantly pearlitic structures guarantee a high resistance to wear.

Although UIC Leaflet 812-3 for solid wheels lists seven types of steel, which differ significantly in carbon content, heat treatment state and strength, the EN 13262 contains only four types of them: ER6, ER7, ER8 and ER9. From all them, it could be said that presently, ER7 steel represents the most used and reliable technology in Europe.

➤ *Current demands and problems*

Nowadays, the demands placed on materials used for wheels and rails have grown. The drive and breaking performance of new locomotives and multiple units has risen considerably and wheel-slide regulated traction controllers often operate at the limits of adhesion to achieve continuous transmission of maximum tractive effort and performance.

Such problems can be found in underground rapid transit units, where although speeds are not so demanding, too high breaking forces in relation to the available wheel/rail adhesion create irregularities on the wheel and rail running surfaces. This is the case of the Nürnberg's Metro in Germany, where the new train units are designed to operate controlled by an ATC system instead of a driver. Most common irregularities in this case seem to be the so-called wheel flats, which basically are flat spots on the rolling surface of the wheel that have been caused by its unintentional sliding on the rail.

➤ *Comparison of ADI with ER7 steel wheels*

Rolling-wear tests were already conducted by the Deutsche Bahn AG with different loads on ADI wheels for its later comparison with other tests already published for conventional wheel/rail steel pairings under the same conditions. It was clear that an ADI/steel pairing for wheel and rail had the most beneficial wear characteristics.

Mass loss at higher contact forces was reduced remarkably with the ADI wheel. The lubrication effect of the spheroidal graphite contained within the material structure of ADI was responsible for the remarkable reduction of friction and the wear on the wheel and rail. In contrast with the R7 wheels, the ADI wheels showed no signs of tread checks in the tests performed. There was virtually no evidence of wear in the cross-section of the wheel and the cross section of the rail hoops.

12.3. Possible problems in the ADI wheel

➤ *Corrosion problems in an ADI wheel*

An unusual environmental assisted embrittlement (EAE) effect has been reported to affect ADI when it is tested in tension with its surface in contact with water and other fluids during slow monotonic tensile load applications. As a consequence, ADI suffers significant reductions in UTS and elongation that can reach up to 30% and 70% respectively.

EAE takes place almost instantaneously when in contact with liquids and it reverses immediately when the surface of the sample is dried again, showing therefore no dependency with the time of exposition to liquid.

Another important characteristic of EAE is that it is unnoticed at high loading rates. As a result, failure in service requires a relatively slow overloading when the part is in contact with the liquids, which usually does not occur so frequent.

It is possible to conclude then on the basis of all this that despite the excellent properties of ADI, the material is subjected to EAE failure in presence of three conditions:

1. High constant stress near the yield stress and/or plastic deformation;
2. Any liquid presence;
3. A slow strain rate.

Therefore as a recommendation for the ADI wheels, apart from a corrosion resistance coating such as the current H-Epoxy, would be an additional surface protection with WD40 (Water Displacement, 40th) in order to isolate the material.

It is also recommended the supervision of the wheels in those days where due to intense rains, the contact with the water is especially important.

➤ ***Too high operating temperature in service***

Although the Austenite in the Ausferrite structure is thermally stable to very low temperatures, it can happen that the Austenite breaks down into ferrite and carbide when exposed to elevated, long-term service temperatures. Direct consequences of this would be gradual degradation of tensile strength together with the toughness.

Previous research has demonstrated that the ADI microstructure is long-term stable as long as operating temperatures did not exceed about 60°C less than the Austempering temperature. For this reason, since these wheels were casted with an ADI, the maximum operating temperature for them would be around 315°C.

It is recommended therefore to have in mind this aspect in those special situations such emergency brake stops, where wheel to rail contact could experience extreme high temperatures. In this way, and due to the impossibility of monitoring such temperatures, periodic inspection of the treads seems desirable.

12.4. Important calculations for the ADI wheel

➤ ***Considering the Mean Stress Sensitivity of ADI***

After the calculation of the mean stress sensitivity for ductile iron and ER7 steel according to the FKM guideline, it was clear that sensitivity factor for ductile iron – and hence for ADI – was almost the double of that in ER7 steel.

Consideration of this fact remains therefore important and should be taken into account for the finite element analysis.

➤ *Minimum Fatigue Strength for accepting track service of the wheels*

For this particular task, the factor of safety (FS) was used as a comparison between the ratio of the allowable strength and the applied stress as follows:

$$FS = \frac{\text{allowable strength}}{\text{applied stress}} = \frac{S_{al}}{\sigma_{ap}}$$

By considering both the allowable strength and the applied stress as normal distributions that can be represented about their mean, it was proved by how the factor of safety was directly related to the reliability or probability of not failure.

Following then with this concept, another important consideration was that for this particular case, the applied stress ($\bar{\sigma}_{ap}$) was going to be a fixed value, since it must be set on 145 MPa according with the standard DIN EN 13979. Reason behind considering always those 145 MPa of load, is that of guarantee that such a stress level will never be reached and in consequence working always on a lower and safer stress level.

Then, after some statistical transformations, and with the use of the cumulative probabilities of a standard normal distribution table, it was possible to calculate the allowable strength (\bar{S}_{al}) with a reliability of 99.7%.

It was concluded then that, in order to achieve always an applied stress of 145 MPa on the component that ensures us to be working under a safer lower stress level, we must apply for our test 200 MPa.

12.5. NDT In-Service inspection of the wheels

➤ *Inspection of the rolling surface*

The Fraunhofer Institute for Nondestructive Testing (IZFP) in Germany has already developed in co-operation with the Deutsche Bahn interesting methods and equipment for in-service inspection of wheel-sets in maintenance stations without dismounting the wheel sets.

The proposed system detects critical defects whilst the vehicle passes over ultrasonic transducers embedded in the rail heads. Four couplant-free operating EMAT transducers are applied for the inspection, two per rail. The wheel is circulated several times by the ultrasonic pulse and, consequently, a series of repetition echoes (round-trip signals) is detected by the receiver if the rolling surface is undamaged.

➤ *Inspection of the spokes*

Due to the complex geometry that a spoke wheel represents, the performance of the current nondestructive inspection techniques is not sufficient in terms of detection sensitivity, quantitative evaluation and field applicability. For that reason, alternative nondestructive testing and evaluation techniques based on electrical potential application has been suggested and presented.

Potential drop (PD) methods in this way can detect and size defects with high sensitivity, and also can monitor them under on-line condition. They are divided in two groups: Direct Current Potential Drop (DCPD) technique and Alternative Current Potential Drop (ACPD) technique.

Testing is performed using a pair of measurement terminals and a pair of current terminals which are attached to the specimen. Any method of them is based on the change of the electrical resistance with the change of the specimen cross section area. For a constant current flow, the electric potential or voltage difference across the crack plane will increase with increasing crack size due to modification of the electrical field and associated perturbation of the current lines.

It can be concluded then that both DC and AC potential drop techniques can be used to monitor initiation and propagation of defects in electrically conducting materials. ACPD offers the highest sensitivity with the minimum detrimental electrochemical interaction, whilst DCPD equipment tends to be cheaper and still maintains a popular following.

12.6. Future work

There are several lines of research arising from this work which should be pursued.

Firstly, the so-called Environmental Assisted Embrittlement effects on ADI in contact with liquids came about through the research conducted by Dr. Ricardo Martinez et al., at the Metallurgic Division of the Universidad Nacional de Mar del Plata in Argentina. In view of this, and because the study was conducted only under tensile loads, it would be interesting to evaluate the same effect but for compressive loads instead. Such results would contribute to a better understanding of the phenomenon in the rolling contact surface of the wheels.

Secondly, after the successful in-service operation of the wheels and their proper inspection after certain amount of kilometers on the track, conclusions regarding the material performance could be analyzed. In view of this additional alloys could be produced and tested in the same manner for the wheel improvement. By changing the base chemistry, it could be possible to either thermodynamically stabilize the austenite (increasing equilibrium transformation temperature) or to suppress the transformation kinetics sufficiently to slow the transformation beyond expected operating times.

LIST OF FIGURES

- Figure 2.1** – Approximate ranges of carbon and silicon for steel and various common cast irons ^[6].
- Figure 2.2** – Effect of cooling rate and chemical composition on the microstructure of cast iron ^[8].
- Figure 2.3** – The Iron-Carbon phase diagram.
- Figure 2.4** – Micrograph of Grey Iron showing the crack-like behavior of the graphite flakes ^[6].
- Figure 2.5** – Micrograph of Ductile iron showing graphite spheroids acting as "crack-arresters" ^[6].
- Figure 2.6** – Micrograph of a grey cast iron ^[9].
- Figure 2.7** – Micrograph of a white cast iron ^[9].
- Figure 2.8** – Micrograph of a mottled cast iron ^[9].
- Figure 2.9** – Micrograph of malleable cast iron ^[9].
- Figure 2.10** – Micrograph of a ferritic ductile (nodular) cast iron ^[9].
- Figure 2.11** – Micrograph of Compacted Graphite Iron.
- Figure 3.1** – Micrograph of an Austempered ductile cast iron ^[9].
- Figure 3.2** – ADI 900 with 371°C quench ^[13].
- Figure 3.3** – ADI 1600 with 260°C quench ^[13].
- Figure 3.4** – ADI 750 showing mixed proeutectoid ferrite (light) and Ausferrite microstructure ^[15].
- Figure 3.5** – Relationship between Yield Strength and Elongation for ADI and other common engineering materials ^[13].
- Figure 3.6** – Young's Modulus (Stiffness) for several materials ^[14].
- Figure 4.1** – Typical Austempering cycle according time and temperature ^[23].
- Figure 4.3** – Schematic of an equilibrium phase diagram of graphitic ductile iron.
- Figure 4.2** – Pearlite in Ausferrite on an ADI grade 2 micrograph (1050-750-07) ^[23].
- Figure 5.1** – Mass loss after 140.000 cycles for various wheel/rail material combinations. ^[4].
- Figure 5.2** – Depth of the transformed layer in ADI after the exposure to high normal force ^[38].
- Figure 5.3** – Comparison of pin abrasion test results for different ADI microstructures compared to competitive materials as a function of matrix hardness ^[39].
- Figure 5.4** – Comparison of carburized & hardened and carbo-Austempered steels to ADI 900 and ADI 1600 in a step load galling test ^[15].
- Figure 5.5** – The fatigue process: crack initiation (I), crack propagation (II), failure (III).

- Figure 5.6** – Constant amplitude fatigue loading with identical loading cycles and relevant parameters.
- Figure 5.7** – Typical S/N curve for different materials.
- Figure 5.8** – Extended service life of a cracked component.
- Figure 5.9** – Constant amplitude crack growth data.
- Figure 5.10** – Fatigue crack growth rate, da/dN.
- Figure 5.11** – Three regions of crack growth rate curve.
- Figure 5.12** – Categories of fatigue.
- Figure 5.13** – Example of S/N curves for high cycle fatigue (HCF) obtained for as-cast iron and ADI treated at two different temperatures. Adapted ^[51].
- Figure 5.14** – Comparison of S/N curves between irons A and B Austempered 300 °C. Adapted ^[51].
- Figure 5.15** – comparison of S/N curves between irons B and D Austempered 360 °C. Adapted ^[51].
- Figure 5.16** – Brittle Fracture of Steel broken at -190°C.
- Figure 5.17** – Ductile Fracture of Steel broken at -20°C.
- Figure 5.18** – Charpy impact test ^[56].
- Figure 5.19** – Izod impact test ^[56].
- Figure 5.20** – Necking leading to fracture in a typical tensile test with steel or aluminum.
- Figure 6.1** – Relative damping behaviors of steel, ductile and malleable iron and grey iron compared to ADI ^[59].
- Figure 6.2** – Comparison of noise in hypoid gears during vehicle road tests ^[61].
- Figure 6.3** – Plot of amplitude Vs time for Steel ^[64].
- Figure 6.4** – Plot of amplitude Vs time for SGI, Austempered at 640°C ^[64].
- Figure 6.5** – Plot of amplitude Vs time for ADI, Austempered at 300°C ^[64].
- Figure 6.6** – Plot of amplitude Vs time for ADI, Austempered at 340°C ^[64].
- Figure 6.7** – Comparison of typical densities for various material/process combinations ^[13].
- Figure 6.8** – Comparison of the weight per unit of yield strength for different materials/process.
- Figure 6.9** – Change in Ultimate Tensile Strength (UTS) and Elongation as a result of tensile testing of ADI grades 1, 2 and 3 (900, 1050 and 1200 respectively) in contact with water ^[73].
- Figure 6.10** – Change of Ultimate Tensile Strength (UTS) and Elongation caused by the contact with lubricant oil and isopropyl alcohol ^[73].
- Figure 6.11** – The FCC structure.

- Figure 7.1** – Relative cost per unit of yield strength for various material/process combinations.
- Figure 7.2** – Options for integrating casting, machining and heat treatment of ADI components.
- Figure 8.1** – Syntegra bogie for metro and suburban.
- Figure 8.2** – The three conventional loading cases.
- Figure 9.1** – Mean stress effect in the S-N diagram (schematic) ^[95]
- Figure 9.2** – Definition of the stress ratio R and stress amplitude at various mean stresses ^[95].
- Figure 9.3** – Mean stress effect for endurance limits in non-dimensional form of the amplitude versus mean stress plot according to Haigh and general description models ^[95].
- Figure 9.4** – Goodman and Morrow models to take into consideration the mean stress effect. Adapted ^[102].
- Figure 9.5** – Haigh diagram showing the mean stress sensitivity factor M and its dependence on the mean stress. Adapted ^[102].
- Figure 10.1** – Complexity of the task behind a non-destructive examination ^[129].
- Figure 10.2** – Testing principle ^[113].
- Figure 10.3** – Construction of the EMAT transducer ^[113].
- Figure 10.4** – Schematic A-scan for undamaged and damaged tread of wheel ^[113].
- Figure 10.5** – Principle of the testing method ^[113].
- Figure 10.6** – Construction principle of the EMAT probe ^[113]
- Figure 10.7** – Front side of the wheel with one of the many spokes for inspection highlighted.
- Figure 10.8** – Implementation of the potential drop method.
- Figure 10.9** – Figure 10.9 - Current flow lines in a typical CT specimen ^[123].
- Figure 10.10**– Schematic of a DCPD test configuration for spoke inspection.
- Figure 11.1** – Distribution of applied stress & allowable strength. Adapted ^[116].
- Figure 11.2** – Distribution of z. Adapted ^[116].

LIST OF TABLES

- Table 2.1** – Chemical composition limits for Ductile irons ^[9]
- Table 3.1** – Comparison ADI standards (Tensile strength - Yield strength - Elongation) ^[15]
- Table 3.2** – The European Standard Grades of ADI as designated by DIN EN1564:2012 at a relevant wall thickness of $t \leq 30$ mm ^[16]
- Table 3.3** – The American Standard Grades of ADI as designated by ASTM A897M-06 ^[17]
- Table 4.1** – Carbon Equivalent Guidelines for the Production of ADI ^[23].
- Table 5.1** – Chemical composition (%wt) and nodule data of the ductile irons used in Lin 's fatigue Study. Adapted from ^[50].
- Table 5.1** – Threshold stress intensity ranges for different heat treatment, adapted from ^[54].
- Table 5.2** – Values of C and m for different heat treatment, adapted from ^[54].
- Table 6.1** – Relative Damping Capacity for various materials. Adapted ^[13].
- Table 6.2** – Noise level recorded ^[64]
- Table 6.3** – The (Relative) Galvanic Series for selected metal alloys. Adapted from ^[13].
- Table 6.4** – Mechanical properties of ADI using different protective coating layers. Adapted ^[72].
- Table 6.5** – Estimated maximum operating temperature for the various grades of ADI ^[13].
- Table 8.1** – Wheel steel requirements according to UIC 812-3 and EN 13262. Adapted ^[94].
- Table 9.1** – Constants a_M and b_M for the different materials ^[98]
- Table 11.1** – Standard normal distribution table. Cumulative probabilities for positive z-values.

REFERENCES

- [1] Dittrich, M. G., and X. Zhang. "The Harmonoise/IMAGINE model for traction noise of powered railway vehicles." *Journal of sound and vibration* 293.3 (2006): 986-994.
- [2] Thompson, David. *Railway noise and vibration: mechanisms, modelling and means of control*. Elsevier, 2008.
- [3] Schulte-Werning, Burkhard, et al. "Noise and Vibration Mitigation for Rail Transportation, Systems." *Proceedings of the 9th International Workshop on Railway Noise, Munich, Germany*. Vol. 4. No. 8. 2007.
- [4] Mädler, Katrin, and Deutsche Bahn. "On the Suitability of ADI as an Alternative Material for (Railcar) Wheels." *English Translation, GIFA* (1999)
- [5] Jokipi, K. "Kymenite in railway applications." *Conference Group of the ADI-Seminar, Technical University Helsinki*. 1991.
- [6] Mullins, James D. "Ductile iron data for design engineers." *Rio Tinto Iron & Titanium Inc* (1990).
- [7] Rollason, Ernest Clarence. *Metallurgy for engineers*. London: Edward Arnold, 1973.
- [8] Yescas-González, Miguel Angel. *Modelling the microstructure and mechanical properties of Austempered ductile irons*. Diss. University of Cambridge, 2002.
- [9] Bramfitt, Bruce L. *Metallographer's guide: practice and procedures for irons and steels*. ASM International, 2001.
- [10] Chakrabarti, A. K. *Casting Technology and Cast Alloys*. PHI Learning Pvt. Ltd., 2005.
- [11] Dorn, T., et al. "The current state of worldwide standards for ductile iron." (2003)
- [12] Ihm, Mark, and T. R. W. Automotive. "Introduction to gray cast iron brake rotor metallurgy." *TRW Automotive, Seminar*. 2003.
- [13] J.R. Keough, K.L. Hayrynen and G. L. Pioszak. "Designing with Austempered Ductile iron *Applied Process Inc. Technologies Division, Livonia & University of Michigan.AFS Proceedings* 2010
- [14] Keough, J. R. "Austempered Ductile iron (ADI) - A Green Alternative." *AFS Transactions- American Foundry Society* , 2011.
- [15] J. R. Keough, K. L. Hayrynen, V. M. Popovski. "Continuing Developments in the Science and Application of Austempered Ductile Iron (ADI)" *Applied Process Inc. Technologies Division Livonia & University of Michigan, USA* (2012).

- [16] DIN EN 1564:2012-01, Founding, Austempered Ductile Cast Irons, Berlin, Germany, www.din.de
- [17] ASTM A897/A 897M-06, Standard Specification for Austempered Ductile Iron Castings, ASTM International, West Conshohocken, PA, www.astm.org.
- [18] SAE J2477:2004, Automotive Austempered Ductile (Nodular) Iron Castings (ADI), SAE International, Warrendale, PA, www.sae.org.
- [19] ISO 17804:2005, Founding Ausferritic Spheroidal Graphite Cast Irons – Classification, ISO, Switzerland, www.iso.org or www.ansi.org.
- [20] Davenport, E.S., Bain, E.C.: *Trans.AIMME, IronandSteelDivision*, 1930,p.117.
- [21] Flinn, R.: In: *Proceedings 2nd Int. Conf. on Austempered Ductile Iron*. Ohio, ASME-Gear Research Institute 1986, p.1.
- [22] Harding, R. A. "The production, properties and automotive applications of Austempered ductile iron." *Kovové materiály* 45.1 (2007): 1-16.
- [23] Hayrynen, Kathy L. "The production of Austempered ductile iron (ADI)." *World Conference on ADI*. 2002.
- [24] Rabinowicz, E. (1995). *Friction and Wear of Materials*. New York, John Wiley and Sons.
- [25] Williams, J. A. (2005). "Wear and wear particles - Some fundamentals." *Tribology International* 38(10): 863-870
- [26] Jones, M., H., and D. Scott, Eds. (1983). *Industrial Tribology: the practical aspects of friction, lubrication, and wear*. New York, Elsevier Scientific Publishing Company.
- [27] Stachowiak, G. W., and A. W. Batchelor (2005). *Engineering Tribology*. Burlington, Elsevier Butterworth-Heinemann
- [28] *Standard Terminology Relating to Wear and Erosion, Annual Book of Standards, Vol 03.02, ASTM, 1987, p 243-250*
- [29] Mamata, K. P. (2008). "A review on silt erosion in hydro turbines." *Renewable & sustainable energy reviews* 12(7): 1974.
- [30] Prado JM, Pujol A, Cullel J, Tartera J (1995) *Mater Sci Technol* 11:294
- [31] Owhadi A, Hedjazi J, Davami P (1998) *Mater Sci Technol* 14:245
- [32] Ahmadabadi MN, Nategh S, Davami P (1992) *J Cast Metals* 4:188
- [33] Xue, L., M. U. Islam, and G. McGregor. "Dot matrix hardening of steels using a fiber optic coupled pulsed Nd: YAG laser." *Materials and manufacturing processes* 14.1 (1999): 53-65.
- [34] Straffelini, G., M. Pellizzari, and L. Maines. "Effect of sliding speed and contact pressure on the oxidative wear of Austempered ductile iron." *Wear* 270.9 (2011): 714-719.
- [35] Nasir, T., et al. "Heat treatment–microstructure–mechanical/tribological property relationships in Austempered ductile iron." *Surface Effects and Contact Mechanics X: Computational Methods and Experiments* 71 (2011): 159.

- [36] Bosnjak, B., Bert Verlinden, and B. Radulovic. "Dry sliding wear of low alloyed Austempered ductile iron." *Materials science and technology* 19.5 (2003): 650-656.
- [37] Harding, R. A., "The production, properties and automotive applications of Austempered ductile iron." *Kovové materiály* 45.1 (2007): 1-16.
- [38] Mullins, James D. "Ductile iron data for design engineers." *Rio Tinto Iron & Titanium Inc* (1990).
- [39] Laird, George, Richard Gundlach, and Klaus Rohrig. *Abrasion-resistant cast iron handbook*. Illinois: American Foundry Society, 2000.
- [40] Stephens, Ralph I., et al. *Metal fatigue in engineering*. John Wiley & Sons, second edition 2001.
- [41] ASTM Standard E 1823, 2010a, "Standard Terminology Relating to Fatigue and Fracture Testing," ASTM International, West Conshohocken, PA, 2010, DOI: 10.1520/E1823-10A, www.astm.org.
- [42] Pook, Les, ed. *Metal Fatigue: What it Is, Why it Matters. Solid Mechanics and Its Applications*. Springer, 2007.
- [43] Davis, Joseph R., ed. *ASM materials engineering dictionary*. ASM international, 1992.
- [44] Schijve, Jaap. *Fatigue of structures and materials*. Dordrecht: Kluwer Academic, 2001.
- [45] Bannantine, J.A., Comer, J. S., Hancock, J. L. "Fundamentals of Metal Fatigue Analysis," PrenticeHall, Inc., Upper Saddle River, NJ, 1990.
- [46] SAE Standard J1099, "Technical Report on Low Cycle Fatigue Properties Ferrous and Non-Ferrous Materials," SAE International, Warrendale, PA, August, 2002.
- [47] Lin, Chih-Kuang, and Chih-Wei Chang. "Influence of heat treatment on fatigue crack growth of Austempered ductile iron." *Journal of materials science* 37.4 (2002): 709-716.
- [48] Lin, Chih-Kuang, and Wen-Jeng Lee. "Effects of highly stressed volume on fatigue strength of Austempered ductile irons." *International journal of fatigue* 20.4 (1998): 301-307.
- [49] J.R. Keough, K.L. Hayrynen and G. L. Pioszak. *Designing with Austempered Ductile Iron (ADI)*. Applied Process Inc. Technologies Division, Livonia & University of Michigan. AFS Proceedings 2010.
- [50] Lin, C-K., P-K. Lai, and T-S. Shih. "Influence of microstructure on the fatigue properties of Austempered ductile irons—I. High-cycle fatigue." *International journal of fatigue* 18.5 (1996): 297-307.
- [51] Dal Carobbo, Marco and Arias Fernández, Sergio. "Evaluation of impact and fatigue properties on Austempered ductile iron." *Chalmers University of Technology* (2009).
- [52] Lin, C-K., and T-P. Hung. "Influence of microstructure on the fatigue properties of Austempered ductile irons—II. Low-cycle fatigue." *International journal of fatigue* 18.5 (1996): 309-320.
- [53] Chapetti, Mirco D. "High-cycle fatigue of Austempered ductile iron (ADI)." *International journal of fatigue* 29.5 (2007): 860-868.
- [54] Greno, G. L., J. L. Otegui, and R. E. Boeri. "Mechanisms of fatigue crack growth in Austempered Ductile Iron." *International Journal of Fatigue* 21.1 (1999): 35-43.

- [55] Hertzberg, Richard W. *Deformation and fracture mechanics of engineering materials*. Vol. 89. Wiley, 1996.
- [56] Callister, William D., and David G. Rethwisch. *Materials science and engineering: an introduction*. Vol. 7. New York: Wiley, 2007.
- [57] Zanardi, F. "Machinable ADI in Italy." *AFS Library copy* 20050990.
- [58] Wu, G. H., et al. "Damping properties of aluminum matrix-fly ash composites." *Materials letters* 60.24 (2006): 2945-2948.
- [59] O'Rourke, Robert. "Cast Iron: A Solid Choice for Reducing Gear Noise." *Gear Technology September* (1999).
- [60] DeGarmo, E. Paul, J. Temple Black, and Ronald A. Kohser. *DeGarmo's materials and processes in manufacturing*. John Wiley & Sons, 2011.
- [61] Austempered Ductile Iron Database, ASME Gear Research Institute, Final Report, June 1989.
- [62] Keough, J. "ADI-A Designer Gear Material." *Gear Technology-The Journal of Gear Manufacturing* (1995).
- [63] Tada, M., et al. "Development of high damping Austempering grey cast iron." *Proceeding of the Third International Conference on Austempered Ductile Iron, AFS, Bloomingdale, Chicago, USA*. 1991.
- [64] Jayamathy, M., and R. Vasanth. *Noise reduction in two wheeler gears using Austempered ductile iron*. No. 2003-32-0041. SAE Technical Paper, 2003.
- [65] Gagné, M., and K. L. Hayrynen. "Environmental Embrittlement of Ductile Iron." *A Review of Available Data', Ductile Iron News 2* (2005).
- [66] Shibutani, S., S. Komatsu, and Y. Tanaka. "Embrittlement of Austempered spheroidal graphite cast iron by contact with water and resulting preventive method." *International Journal of Cast Metals Research* 11.6 (1999): 579-585.
- [67] Komatsu, S., et al. "Embrittlement characteristics of fracture toughness in ductile iron by contact with water." *International Journal of Cast Metals Research (UK)* 11.6 (1998): 539-544.
- [68] Martinez, R. "Embrittlement of Austempered ductile iron caused by contact with water and other liquids." *International Journal of Cast Metals Research (UK)* 13.1 (2000): 9-15.
- [69] Matinez, R. "Environmentally assisted embrittlement of ADI by contact with liquids." *International Journal of Cast Metals Research* 16.1 (2003): 251-256.
- [70] Martinez, R. A., S. Simison, and R. E. Boeri. "Environmentally assisted embrittlement of ADI-current understanding." *Transactions of the 2002 World Conference on ADI, Louisville, KY*. 2002.
- [71] Komatsu, S., et al. "Influence of water embrittlement effect on mechanical properties of ADI." *International Journal of Cast Metals Research* 16.1 (2003): 209-214.
- [72] Boeri, R. E., and R. A. Martínez. "Embrittlement of ADI by contact with liquids: influence of alloy content and preventive methods." *Materials Science and Technology* 29.6 (2013): 665-671.

- [73] Martinez, R. A., S. Simison, and R. E. Boeri. "Environmentally assisted embrittlement of ADI—current understanding." *Transactions of the 2002 World Conference on ADI, Louisville, KY*. 2002.
- [74] Jokipii, Kalevi. "Kymenite, Austempered Ductile Iron as Material for Gears and Other Applications." *1 st International Conference on Austempered Ductile Iron: Your Means to Improved Performance, Productivity and Cost*. 1984.
- [75] Hayrynen, K.L., PhD, Keough, J.R., P.E., Kovacs, B.V., PhD, "Determination of Mechanical Properties in Various Ductile Irons after Subjecting Them to Long-Term Elevated Temperatures"; *Research Project No. 28, 1999, Ductile Iron Society, North Olmsted, Ohio, USA*.
- [76] DeGarmo, E. Paul, J. Temple Black, and Ronald A. Kohser. *DeGarmo's materials and processes in manufacturing*. John Wiley & Sons, 2011.
- [77] Klocke, F., & Klöpper, C. "Machining of ADI". *WZL-Laboratory of Machine Tools and Production Engineering, University of Technology, Aachen, Germany*.
- [78] Hayrynen, K. L., and J. R. Keough. "Austempered Ductile Iron-State of the Industry in 2003." *Keith Millis Symposium on Ductile Iron*. 2003.
- [79] Druschitz, Alan P., and David C. Fitzgerald. *MADI™: introducing a new, machinable, Austempered ductile iron*. No. 2003-01-0831. SAE Technical Paper, 2003.
- [80] J.R. Keough and K.L. Hayrymen, "Developments in the technology and engineering applications of austempered ductile iron (ADI)", *Proceedings of the 8th International Symposium on Science and Processing of Cast Iron, Beijing, China (2006)*, pp. 474-479.
- [81] M. Cemal Cakir, Ali Bayram, Yahya Isik and Baris Salar, "The effects of Austempering temperature and time onto machinability of Austempered ductile iron", *Materials Science and Engineering A407*, (2005), 147- 153.
- [82] H. Muhlberger, "Process in the production, understanding and applications of Germanite-Austempered ductile iron", *ASME and Amax Inc., 2nd Int. Conf. on Austempered Ductile Iron: Your Means to Improved Performance, University of Michigan, Ann Arbor, MI, 17-19 March 1986, Illinois, 1986*, 55-93.
- [83] A.P. Druschitz and D.C. Fitzgerald, "MADI™: Introducing a new machinable Austempered ductile iron", *Non-Ferrous Castings (SP-1734)*, SAE World Congress, Detroit, Michigan, 3-6, 2003 SAE Technical Paper 2003-01-0831.
- [84] A.P. Druschitz and D.C. Fitzgerald, "A machinable Austempered cast iron article having improved machinability, fatigue performance and resistance to environmental cracking and a method of making the same", *International Patent Application WO 2004/022792 A2*, 18 March 2004. Also US Patent Application: 2004112479, June 17, 2004.
- [85] T. Kobayashi and S. Yamada, "Effect of holding time in the ($\alpha+\gamma$) temperature range on toughness of specially Austempered ductile iron", *Metall. Mat. Trans. A*, (1996), 27A(7), pp. 1961-1971.
- [86] D. Rousiere and J. Aranazabal, "Development of mixed (ferritic + Ausferritic) structures for spheroidal graphite irons", *Metallurgical Science and Technology*, vol. 18(a), (2000), 24-29.

- [87] A.M. Rashidi and M. Moshrefi-Torbati, "Effect of tempering conditions on the mechanical properties of ductile cast iron with dual matrix structures (DMS)", *Materials Letter*, vol. 45, (2000), 203-207.
- [88] K. Kocatepe, M. Cerah and M. Erdogan, "The tensile fracture behavior of intercritically annealed and quenched + tempered ferritic ductile iron with dual matrix structure", *Materials and Design*, July (2005).
- [89] J. Aranzabal, G. Serramoglia, C.A. Gorla and D. Rousiere, "Development of a new mixed (ferritic- Ausferritic) ductile iron for automotive suspension parts", *Int. J. of Cast Metals Research*, 2003, 16 (1-3), 185-192.
- [90] Cocheteux, F., and T. Pouillart. "Design, Manufacture and Maintenance of Wheelset at SNCF." *International Journal of Railway 2.1* (2009): 8-17.
- [91] Cocheteux, F., et al. "Toward the wheels calculation and validation in multiaxial fatigue under service loads." *7th World congress on railway research*. 2006.
- [92] A. Yameogo, C. Prioul, Am. Marechal, F. Demilly, Jj. Viet: Fretting fatigue crack prediction by finite element modelling in a press fitted assembly. *14th International Wheelset Congress. Orlando-2004*.
- [93] P. Feraud, J. J. Viet, M. Diener, M. Grab: Influence of corrosion on the behaviour of wheelsets in service. *15th International Wheelset Congress. Prague-2007*.
- [94] Mädler, Katrin, and Manfred Bannasch. "Materials used for wheels on rolling stock." *Deutsche Bahn AG, Technical Centre, Brandenburg-Kirchmöser, Germany*.
- [95] F. Klubberg, I. Klopfer, C. Broeckmann, R. Berchtold, P. Beiss, "Fatigue testing of materials and components under mean load conditions", *Anales de Mecánica de la Fractura*, 28, (2011) 419-424
- [96] E. Haibach, "Betriebsfestigkeit", 2nd edition, Springer-Verlag, Berlin, 2002.
- [97] E. El-Magd, "Versagensbedingung bei mehrachsiger schwingender Beanspruchung metallischer Werkstoffe", *Habil.-thesis, RWTH Aachen*, 1974.
- [98] H.-P. Lüpfer, "Beurteilung der statischen Festigkeit und Dauerfestigkeit metallischer Werkstoffe bei mehrachsiger Beanspruchung", *Habil.-thesis, TU Bergakademie Freiberg*, 1994, *Freiberger Forschungshefte: A; 833: Maschinen und Energietechnik*
- [99] F. Klubberg, H.J. Schäfer, M. Hempen, P. Beiss, P., "Kennwertbeziehungen für die Normal- und Torsions-Mittelspannungsempfindlichkeit metallischer Werkstoffe", *Werkstoffprüfung 2002 – Kennwertermittlung für die Praxis*, 229-234, Wiley-VHC, 2003.
- [100] F. Klubberg, H.J. Schäfer, M. Hempen, P. Beiss, P., "Empirical Relationship between Pulsating and Fully Reversed Fatigue Strength", *Fatigue Damage of Materials – Experiment and Analysis*, 355-365, *WIT Press, Southamton, Boston*, 2003, s. a.: *Betriebsfestigkeit – Neue Entwicklungen bei der Lebensdauerberechnung von Bauteilen*, 51-60, *DVM-Rep. 802*, 2003.
- [101] Morrow, J., *Fatigue Design Handbook. Advances in Engineering 4*, SAE, Warrendale, PA, pp. 21–29 (1968)
- [102] Milella, Pietro Paolo. "Fatigue and corrosion in metals". Springer, 2012.

- [103] Peterson, R.E., Wahl, A.M.: Two and three dimensional cases of stress concentration and comparison with fatigue tests. *Trans. Am. Soc. Mech. Eng.* 15–22 (1936)
- [104] MIL-HDBK-5D, Military Standardization Handbook, Metallic Materials and Elements for Aerospace Vehicle Structures, pp. 5–87 (1983)
- [105] Hänel, B., et al. "FKM-Guideline–Analytical strength assessment of components in mechanical engineering." *Forschungskuratorium Maschinenbau eV (FKM), Research Association for Mechanical Engineering, Frankfurt* (2003).
- [106] Martin E. Über Schalluntersuchungen an Achsen von Schienen-fahrzeugen. In: *Stahl und Eisen* 72, Düsseldorf: Verlag Stahleisen GmbH; 1952.
- [107] Clark R. "Hopes and needs for the future of railway industry NDT". *Insight* 1995;37(4):274–7.
- [108] Grum J, Jemec V, Beci A. Experimental system for ultrasonic testing of axle sets of diesel-engine trains. *Insight* 2000;42(12):782–8.
- [109] Junger M, Thomas HM, Krull R. "Das Wirbelstrom-Verfahren auf die Schiene gebracht: Prüfung betriebsbedingter Schädigungen an Eisenbahnschienen mit Wirbelstrom-Verfahren". *Proceedings of the DGZfP Annual Conference on Non-Destructive Evaluation*, Celle, Germany; 1999.
- [110] Junger M, Thomas HM, Krull R. "Wirbelstromprüfung betriebsbedingter Schädigungen an Eisenbahnschienen. In: *Stahl und Eisen* 119, Düsseldorf: Verlag Stahleisen GmbH; 1999.
- [111] Thomas HM, Junger M, Hintze H, Krull R, Rühle S. "Pioneering inspection of railroad rails with eddy currents". *Proceedings of the 15th World Conference on Non-Destructive Testing*, Rome, Italy; 2000.
- [112] Pohl, Rainer, et al. "NDT techniques for railroad wheel and gauge corner inspection." *NDT & E International* 37.2 (2004): 89-94.
- [113] Kappes, W., et al. "Non-destructive testing of wheel-sets as a contribution to safety of rail traffic." *CORENDE 2000 Proceedings* (2000).
- [114] H.-J.Salzburger, W.Repplinger: Diagnoseverfahren zur zerstörungsfreien automatischen Erkennung von Schäden der Lauffläche. Fraunhofer IzfP report (1985).
- [115] H.-J.Salzburger, H. Hintze: Tiefenbestimmung von Laufflächenfehlern an Eisenbahnrädern unter Nutzung linear polarisierter Transversalwellen – Verfahrens-optimierung und Erprobung. *Proceedings of the Annual DGZfP-Meeting, Lindau* (1996) 183-190
- [116] Sato, Yasumoto, and Tetsuo Shoji. "Development of Remotely Induced Current Field Measurement Technique." *Studies in Applied Electromagnetics and Mechanics: Electromagnetic Nondestructive Evaluation (V)* 21 (2001): 159-65.
- [117] Rossendorf, Forschungszentrum."Crack initiation determination for Charpy size specimens."(2003).
- [118] Schwalbe, K. H., B. K. Neale, and J. Heerens. "The GKSS test procedure for determining the fracture behaviour of materials." *EFAM GTP* 94 (1994).
- [119] ISO, IS. "12135 Metallic materials–Unified method of test for the determination of quasi-static fracture toughness." *International Organization for Standardization, Geneva* (2007).

- [120] Huang, Frank H. "Fracture toughness evaluation for zircaloy-2 pressure tubes with the electric-potential method." *ASTM SPECIAL TECHNICAL PUBLICATION* 1204 (1993): 182-182.
- [121] Schwalbe, Karl-Heinz, et al. "Measurement of stable crack growth including detection of initiation of growth using the DC potential drop and the partial unloading methods." *ASTM STP* 856 (1985): 338-362.
- [122] Matelect LTD. "Use of the Potential Drop Technique to Monitor Stress Corrosion Cracking", *A short Applications Note*
- [123] Matelect LTD. "Practical Aspects of the ACPD Technique". *For use with Matelect ACPD products*
- [124] Ullman, David G. *The mechanical design process*. McGraw-Hill Science /Engineering /Math, 2009.
- [125] DIN EN 13979-1:2010-02. Railway applications-Wheelsets and bogies-Monobloc wheels- Technical approval procedure- *Part 1: Forged and rolled wheels*. Berlin, Germany, www.din.de.
- [126] DIN EN 1564: Gießereiwesen – Bainitisches Gusseisen; Deutsche Fassung EN 1564:1997 + A1:2006
- [127] DIN EN 1564: Gießereiwesen - Ausferritisches Gusseisen mit Kugelgraphit; Deutsche Fassung prEN 1564:2009
- [128] Röhrig, K.: Fehlermöglichkeiten bei der Erzeugung von ADI. *Gießerei-Praxis* 4/01, S. 153-162
- [129] Mook, G., F. Michel, and J. Simonin. "Zerstörungsfreie Charakterisierung von ADI-Guss."

Additional sources:

Technical Library at www.appliedprocess.com

ADI Treatments Ltd. (UK) www.aditreatments.com

Ductile Iron Society www.ductile.org/didata

International Union of Railways www.uic.org

Siemens Global www.siemens.com